International Scientific-Technical and Production Journal

The Paton WELDING JOURNAL

January 2009 # 1

English translation of the monthly «Avtomaticheskaya Svarka» (Automatic Welding) journal published in Russian since 1948

Founders: *E.O. Paton Electric Welding Institute of the NAS of Ukraine*
International Association «Welding»

Publisher: *International Association «Welding»*

Address:
E.O. Paton Electric Welding Institute,
International Association «Welding»,
11, Bozhenko str., 03680, Kyiv, Ukraine
Tel.: (38044) 287 67 57
Fax: (38044) 528 04 86
E-mail: journal@paton.kiev.ua
http://www.nas.gov.ua/pwj

State Registration Certificate
KV 4790 of 09.01.2001

Subscriptions:
$324, 12 issues per year,
postage and packaging included.
Back issues available.

CONTENTS

SCIENTIFIC AND TECHNICAL

Skulsky V.Yu., Tsaryuk A.K. and *Moravetsky S.I.* Evaluation of susceptibility of welded joints of heat-resistant chromium martensitic steel to cracking at heat treatment 2

Makhnenko O.V., Muzhichenko A.F. and *Seyffarth P.* Application of mathematical modelling in thermal straightening of shipbuilding panels 6

Ustinov A.I., Falchenko Yu.V., Ishchenko A.Ya., Kharchenko G.K., Melnichenko T.V. and *Muravejnik A.N.* Producing permanent joints of γ-TiAl based alloys using nanolayered Ti/Al interlayer by vacuum diffusion welding 12

Najdich Yu.V., Sidorenko T.V. and *Durov A.V.* Brazing of ferroelectric ceramics in air environment and pure oxygen atmosphere 16

Pismenny A.S., Pentegov I.V., Stemkovsky E.P., Shejkovsky D.A., Kislitsyn V.M. and *Lavrenyuk A.V.* Improved method for calculating magnetic-pulse welding conditions 18

Chigaryov V.V., Shchetinina V.I., Shchetinin S.V., Stepnov K.K., Zavarika N.G. and *Fedun V.I.* Increase of crack resistance of shrouded traveling rolls in high-speed hardfacing 22

INDUSTRIAL

Lobanov L.M., Timoshenko A.N. and *Goncharov P.V.* Arc spot welding of overlap joints in vertical position 26

Knysh V.V., Kuzmenko A.Z. and *Solovej A.S.* Increase of cyclic fatigue life of tee welded joints with surface cracks 29

Ishchenko A.Ya. and *Khokholova Yu.A.* Evaluation of mechanical properties of microstructural constituents of welded joints 34

Litvinov A.P. Trends in development of combined and hybrid welding and cladding technologies 37

BRIEF INFORMATION

Kharlamov M.Yu., Krivtsun I.V., Korzhik V.N., Petrov S.V. and *Demianov A.I.* Refined mathematical model of the electric arc burning in plasmatron with external current-conducting wire 42

New books 45

Kuskov Yu.M., Ryabtsev I.A., Demchenko Yu.V., Denisenko A.M., Dzhavelidze Z.Z., Kbiltsetsklashvili Kh.N. and *Khutsishvili A.A.* Hard-facing bay for repair of hydropower equipment parts in company «Sakenergoremonti» 46

News 48

NEWS

Branch meeting-conference of «Gazprom» specialists 49

Developed at PWI 41, 51

EVALUATION OF SUSCEPTIBILITY OF WELDED JOINTS OF HEAT-RESISTANT CHROMIUM MARTENSITIC STEEL TO CRACKING AT HEAT TREATMENT

V.Yu. SKULSKY, A.K. TSARYUK and **S.I. MORAVETSKY**
E.O. Paton Electric Welding Institute, NASU, Kiev, Ukraine

The mechanisms of cracking of welded joints in tempering used to relieve stresses are considered. It has been found that welded joints on steel 10Kh9MFB with a homogeneous martensitic structure are insensitive to temper cracking. Formation of δ-ferrite in the martensitic structure may lead to cracking of the weld metal. Cracks form in tempering in the range of about 450–550 °C as a result of concentrated deformation within the zone of soft ferrite interlayers in development of secondary hardening of the martensitic matrix. A probable cause of hardening is precipitation of chromium carbide M_7C_3.

Keywords: *arc welding, martensitic steel, welded joints, heat treatment, dispersion hardening, soft interlayers, temper cracking*

Manufacture of welded structures from hardening heat-resistant and high-temperature steels is related to the need to perform heat treatment of welded joints for tempering of quenching structures and lowering of the residual stress level. In some cases temper cracks can form in the welded joints during heating or soaking in certain temperature intervals. The risk of cracking increases at treatment of rigid joints, as well as in the presence of design stress raisers, lacks-of penetration, undercuts and extended inner defects in them.

Temper cracks (or reheating cracks) are defects forming as a result of a non-uniform plastic deformation under the conditions of high-temperature relaxation of inner stresses [1]. The non-uniform nature of relaxation creep of metal at tempering can be related to chemical microinhomogeneity (which is characteristic of weld metal) and development of dispersion hardening of grain bodies at certain temperatures as a result of precipitation of finely dispersed phases, namely carbides, intermetallics. Grain strengthening due to secondary hardening is a factor of «relative softening» of grain boundary regions. As a result, the deformation at relieving of inner stresses is concentrated in the grain boundary zone. A fast increase of density of crystalline structure defects at local deformation, as well as formation of interatomic discontinuities under the impact of embrittling impurities, leads to initiation of microdamage in the form of initial pores [2–4] and to crack propagation. A feature of temper cracks is their intergranular nature.

A susceptibility to hardening and, therefore, to formation of cracks at tempering is found in steels containing strong carbide-forming elements (titanium, vanadium, niobium) and elements strengthening the solid solution (molybdenum, chromium, which also belong to carbide-forming elements) [1, 5–9]. Depending on the alloying system, strengthening can be induced in structural and heat-resistant steels by Cr_7C_3, Mo_2C, V_3C_4 carbides, in austenitic steels ---- by NbC, TiC carbides, in nickel-based alloys ---- by intermetallics of Ni_3(Al, Ti) type [1, 3, 7, 10, 11]. Lowering of high-temperature ductility in the boundary zone and crack formation are caused by impurities of phosphorus, arsenic, antimony, tin and sulphur [1, 5, 12–16]. According to the data of [17], the embrittling action of such impurities as phosphorus and sulphur is due to weakening of the bonds between the metal atoms as a result of formation of electronic bonds on the levels of *s*-orbitals of metal atoms and *p*-orbitals of impurity atoms. Such elements as silicon, manganese, carbon, aluminium and copper [3, 5, 18] also increase the temper cracking susceptibility. They, however, have an indirect influence on embrittlement, for instance, by enhancing the grain-boundary segregation of phosphorus (silicon, carbon, manganese) [5], or ousting carbon from the zone of their clustering with formation of soft microstructural components (silicon, aluminium).

In welded joints the metal in the near-weld sections is more susceptible to cracking, these sections developing a coarse-grained structure as a result of heating to subsolidus temperatures and a high degree of hardening as a consequence of a more complete dissolution of the carbide precipitates and saturation of γ-solid solution by carbon and carbide-forming elements. In the welds cracks can form predominantly in the microsections, in which the solidification boundaries enriched in liquating impurities, coincide with the secondary boundaries ---- the austenite grain boundaries.

There is a sufficient number of publications devoted to studying the problem of temper brittleness of low-alloyed pearlitic and bainitic heat-resistant steels with up to 2–5 % Cr [2, 4–6]. Introduction of new complex-alloyed martensitic steels with increased chromium content leads to the need to study the properties of their welded joints, including temper crack sensitivity. Possible predisposition of such steels to development of processes usually accompanied by cracking, is associated with the presence of carbide-

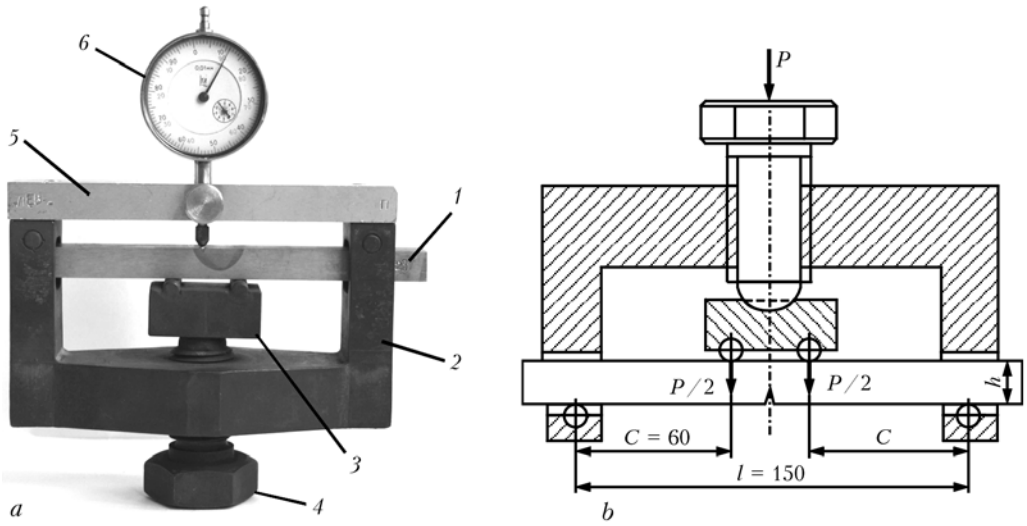

Figure 1. Appearance (*a*) (*1* — sample; *2* — welded bed; *3* — support; *4* — loading screw; *5* — removable plate for indicator fastening; *6* — indicator) and schematic for sample loading (*b*)

forming elements in their composition, as well as with martensite, the non-uniform decomposition of which at tempering (develops quickly at grain boundaries [19]) can be accompanied by non-uniform distribution of deformations and increase of the density of defects on grain boundaries.

The purpose of this work consisted in evaluation of the susceptibility of welded joints of martensitic steel with 9 % Cr to development of temper cracks.

Relaxation testing was conducted by the procedure of the I.I. Polzunov Central Institute for Boilers and Turbines [20], based on performance of heat treatment of welded joint samples loaded in a fixture of a high-temperature nickel alloy up to a certain stress level by four-point bending (Figure 1). Deflection f in the zone of a uniform bending moment (between the support contact points) was monitored by a removable indicator. Stresses s in the stretched zone on the surface of samples of a rectangular section were calculated using the following relationships:

$$\sigma = M/W, \quad f = \frac{M}{24EJ}(3l^2 - 4c^2),$$

where $M = (P/2)c$ is the bending moment, N·m; $W = bh^2/6$ is the axial moment of resistance of sample section, m^3; b, h is the section width and height; $J = bh^3/12$ is the axial moment of inertia of sample section, m^4; E is the modulus of elasticity equal to $218 \cdot 10^3$ MPa for steel.

Samples fastened in the fixture were placed into a cold furnace, heated up to the required temperature, soaked for the specified time, and then cooled in air. After heat treatment the visual and metallographic inspection of welded joints was conducted to find defects in them. Samples for testing were cut out across the weld made when filling the groove in the plate from 10Kh9MFB steel using automatic submerged-arc welding. A V-shaped stress raiser was made in the fusion zone in the samples. Welding was performed using test flux and flux-cored wire providing the following composition of the deposited metal, wt.%:

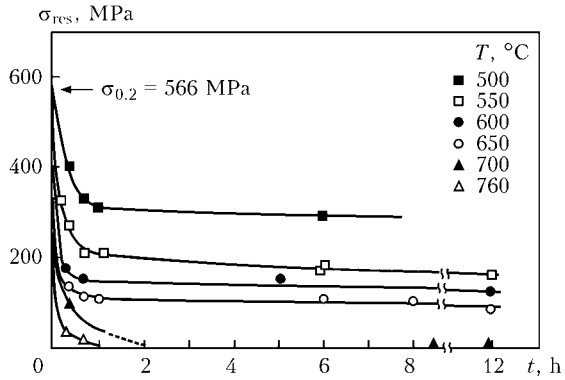

Figure 2. Nature of stress variation during tempering of pre-loaded samples

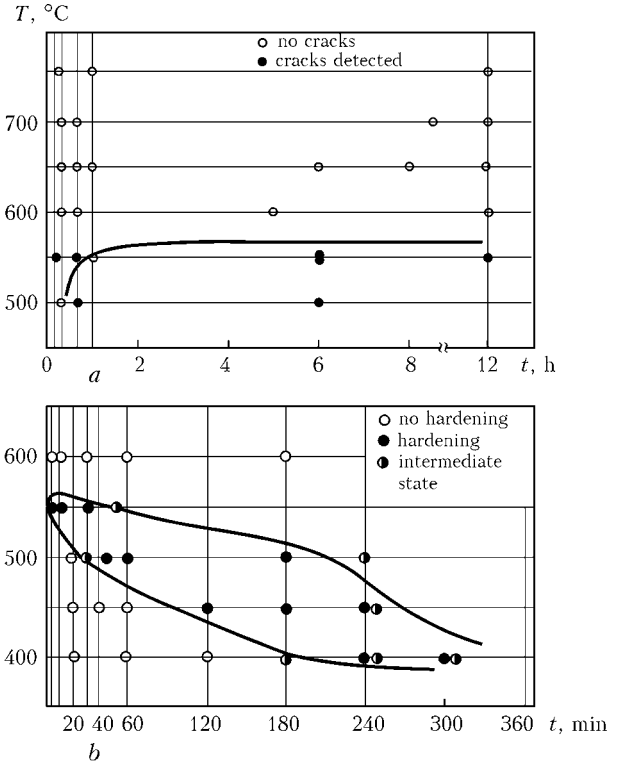

Figure 3. Regions of cracking (*a*) and development of secondary hardening (*b*) in the martensitic weld metal

0.098 C; 0.72 Mn; 0.13 Si; 1.0 Mo; 0.52 Ni; 0.27 V; 0.053 Nb; 0.048 N; 0.01 Al; 0.014 S; 0.015 P, similar to the steel to be welded. Welding was performed in the modes with the heat input of 16 and 23 kJ/cm.

Metallographic investigations showed that in as-welded condition the metal of the welds and HAZ had a predominantly quenched martensitic structure. However, in welding at higher currents (with increased heat input) overheating of weld pool melt and slowing down of the solidification rate lead to formation of a coarser crystalline structure, in which appearance of a small fraction of δ-ferrite is noted as a result of development of chemical inhomogeneity.

As follows from the test results (Figure 2), relaxation creep develops quite intensively in the first 40–50 min of tempering, which is indicated by the rate of lowering of stress in the loaded samples. The residual stress level determined by metal softening rate and its deformability, decreases with temperature increase. Complete removal of stresses during short soaking (from 2 to 1 h) is achieved at the temperature above 600 °C. It is established that under these conditions the metal with a purely martensitic structure features a high cracking resistance. No cracks were found in the base metal in the overheated section in the stress raiser vicinity. On the other hand, in the weld metal containing δ-ferrite, cracking was found at tempering at temperatures of 500 to 550 °C (Figure 3, *a*). No cracks were formed at temperatures above 550 °C.

In parallel with relaxation testing heat treatment of welded joint samples was conducted in a free (unloaded) state with subsequent measurement of hardness in the weld metal. It is established that in the temperature range of ~400–550 °C (Figure 3, *b*) metal of 10Kh9MFB type develops secondary hardening. Taking into account the data of [21], it can be assumed that the factor causing hardening in the weld metal

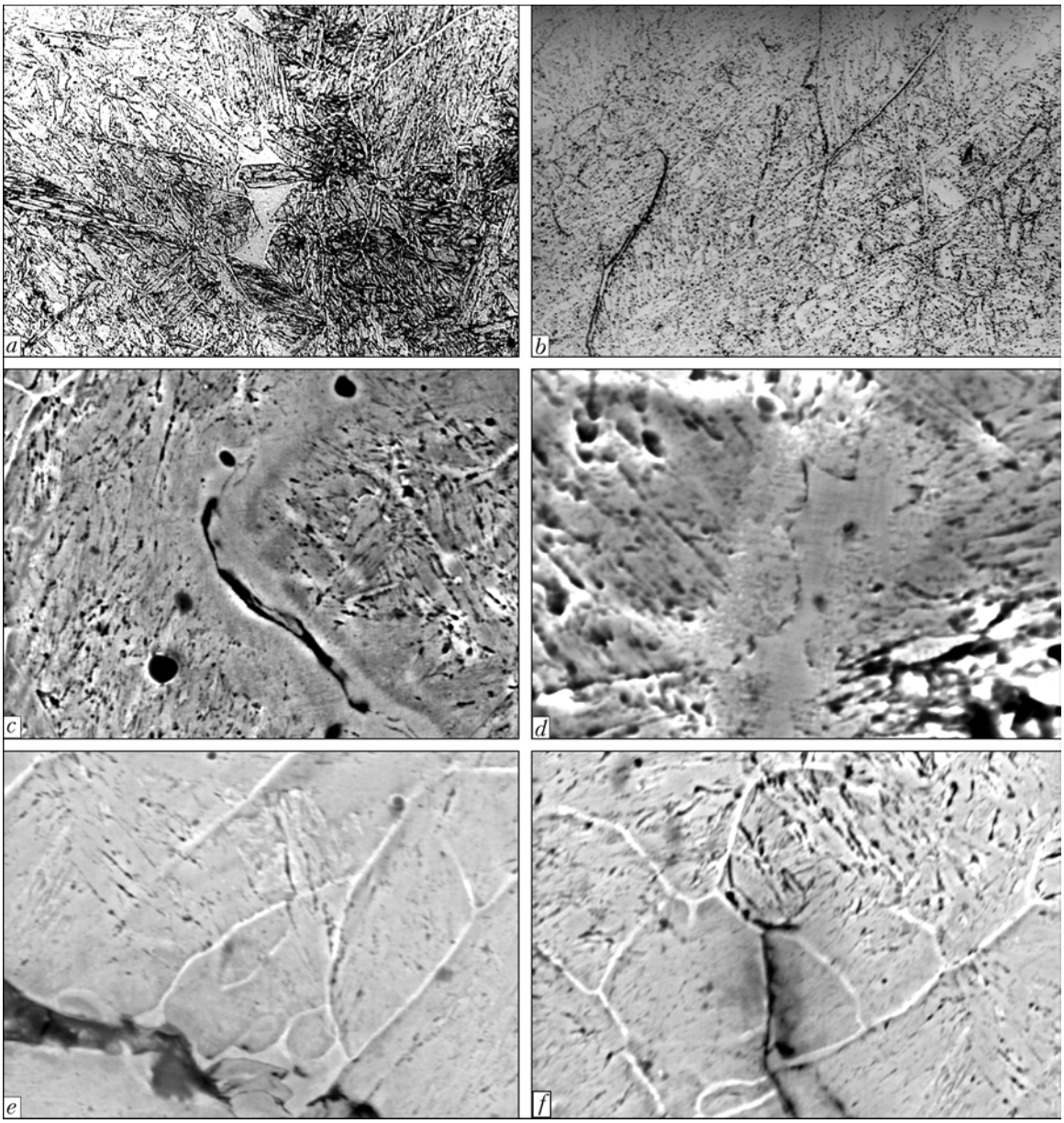

Figure 4. Microstructure of martensitic welds with δ-ferrite (*a*, *b*) and cracking in welds formed at relaxation testing (*c*–*f*): *a*, *b* — ×500; *c*, *e* — ×2020; *d* — ×4780; *f* — ×1690

of this type, is formation of alloyed carbide M_7C_3 ($(Fe, Cr)_7C_3$ type). This carbide can form in high-chromium steels both as a result of substitution of cementite ($Fe_3C \rightarrow (Fe, Cr)_7C_3$), and irrespective of cementite in the form of additional carbide.

Considered cracking in the welds is the consequence of deformation concentration in the zone of soft interlayers of δ-ferrite located in a more rigid (insufficiently tempered) martensite metal, further strengthened by chromium carbide precipitates. δ-ferrite proper features a high ductility and no cracks form in it. However, plastic flow of metal in δ-ferrite area leads to a higher density of dislocations along the boundary with the stronger martensite. As a result, cracks develop in the section of δ-ferrite–martensite transition, or along the thin solidification interlayers, which are a continuation of coarser sections of δ-ferrite (Figure 4). Interphases are a continuation of secondary boundaries of austenite grains, which could be detected by their decoration by dense carbide precipitates at tempering. Therefore, fracture in welds, similar to HAZ metal, develops along the grain boundaries.

Non-uniform distribution of chemical elements can be regarded as one of the possible metallurgical factors causing lowering of strength and ductility of the interphases. So, for instance, in the cracking zone in the section of δ-ferrite to martensite transition X-ray microprobe analysis recorded an increase of manganese concentration (~1.04–1.06 % at the interphase, 0.6–0.8 % in δ-ferrite zone, ~0.8 % in martensite). δ-ferrite usually contains more ferritizers (for instance, 1.23 % Mo; 10.15 % Cr) than the adjacent martensite (0.7 % Mo; 9.48 % Cr). In addition, δ-ferrite formation is associated with depletion of this phase in carbon, which accumulates on the interphases [22] and in the adjacent matrix microsections. Increased concentration of carbon near δ-ferrite is indicated by a denser arrangement of carbides after tempering, which was noted at metallographic examination of the structure of welds of this type. Carbide formation on the interphases and possible enhancement of impurity segregation (first of all phosphorus [5]) under the influence of local increased concentrations of alloying elements may cause boundary embrittlement. At fracture, carbides are the centers of dislocation accumulation and microcrack initiation [2]. However, on the whole, the mechanism of embrittlement of the studied metal with a multicomponent alloying system (Fe–9Cr–Mo–V–Nb–Ni–N taking into account manganese, silicon, aluminium, sulphur and phosphorus content) is quite complicated and requires a special study. In this case δ-ferrite may be regarded as the main structural factor causing cracking in the welds.

Thus, it is established that dispersion hardening develops in the martensitic metal of 10Kh9MFB type in the temperature range of ~450–550 °C, the probable cause of which is precipitation of Cr_7C_3 carbide. During tempering the welded joints with a martensitic structure do not demonstrate any susceptibility to cracking. However, as shown on the example of welds, cracking is possible only in the presence of soft δ-ferrite interlayers in rigid martensite. In this case cracks form at soaking of the hardened welded joints in the dispersion hardening temperature interval. A condition of high resistance of 10Kh9MFB steel welded joints to temper cracking is ensuring their uniform martensitic structure.

1. Zemzin, V.N., Shron, R.Z. (1978) *Heat treatment and properties of welded joints*. Moscow: Mashinostroenie.
2. Nawrocki, G.J. (2001) Stress-relief cracking of a ferritic alloy steel. *IIW Doc. IX-2001–01*.
3. Boniszewski, T., Eaton, N.F. (1969) Electron fractography of weld-reheat cracking in CrMoV steel. *Metal Sci. J.*, **3**, 103–110.
4. Gotoh, A., Nakagawa, T., Hatano, H. et al. (1999) The effects of vanadium on carbide precipitation in 1¼–3 % Cr–Mo steel weld metals. *IIW Doc. IX-708–99*.
5. Lundin, C.D., Khan, K.K. (1996) Fundamental studies of the metallurgical causes and mitigation of reheat cracking in 1¼ Cr–½ Mo and 2¼ Cr–1 Mo steels. *WRC Bulletin*, **409**, 117.
6. Tamaki, K., Suzuki, J., Nakaseko, Y. (1980) Effect of molybdenum carbide on reheat cracking sensitivity of Cr–Mo steels. *IIW Doc. IX-1159–80*.
7. Tamaki, K., Suzuki, J., Tajiri, M. (1984) Effect of vanadium and titanium on reheat cracking sensitivity. *Transact. of JWS*, **154**, 17–24.
8. Tamaki, K., Suzuki, J. (1983) Effect of chromium and molybdenum on reheat cracking sensitivity of steels. *Ibid.*, 14(**2**), 123–127.
9. Tamaki, K., Suzuki, J. (1983) Reheat cracking test on high strength steels by a modified implant test. *Ibid.*, 14(**2**), 117–122.
10. Tamaki, K., Suzuki, J., Nakaseko, Y. et al. (1984) Effect of carbides on reheat cracking sensitivity (Study on reheat cracking of Cr–Mo steels: Report 3). *Ibid.*, 15(**1**), 8–16.
11. Tamaki, K., Suzuki, J., Li, M.-L. (1993) Influence of vanadium carbide on reheat cracking of Cr–Mo steels — study on reheat cracking of Cr–Mo steels: Report 10. *Ibid.*, 24(**2**), 87–93.
12. Nawrocki, J.G., Dupont, J.N., Robino, C.V. et al. (2000) The stress-relief cracking susceptibility of a new ferritic steel. Pt 1: Single-pass heat affected zone simulation. *Welding J.*, 79(**12**), 355–362.
13. Tamaki, K., Suzuki, J., Tate, H. (1988) Combined influence of sulfur and manganese on reheat cracking of Cr–Mo steels. *Transact. of JWS*, 19(**1**), 46–52.
14. Tamaki, K., Suzuki, J. (1985) Combined influence of phosphorus, chromium and molybdenum on reheat cracking of steels. *Ibid.*, 16(**2**), 117–124.
15. Frumin, I.I. (1975) Surfacing in nuclear machine-building. *Avtomatich. Svarka*, **10**, 66–73.
16. Guo, A.-M., Wang, Y.-H., Shen, D.-D. et al. (2003) Influence of phosphorus on the ductility of 2.25Cr1Mo steel. *Mat. Sci. and Techn.*, **19**, 1553–1556.
17. Utevsky, L.M., Glikman, E.E., Kark, G.S. (1987) *Reversible temper brittleness of steel and iron alloys*. Moscow: Metallurgiya.
18. Ito, Y., Nakanishi, M. (1972) Study on stress relief cracking in welded low alloy steels: Report 2. *J. JWS*, 41(**1**), 59–64.
19. Sarrak, V.I., Entin, R.I. (1960) Irreversible brittleness in tempering. *Metallovedenie i Termich. Obrab. Metallov*, **10**, 14–19.
20. Demiantsevich, S.V., Zemzin, V.N. (1979) Procedure for evaluation of cracking sensitivity of welded joints in heat treatment. *Trudy TsKTI*, Issue 169, 22–27.
21. Lanskaya, K.A. (1976) *High-chromium heat-resistant steels*. Moscow: Metallurgiya.
22. Skulsky, V.Yu. (2006) Influence of alloying of filler material and welded steel on fusion zone structure. *The Paton Welding J.*, **1**, 9–15.

APPLICATION OF MATHEMATICAL MODELLING IN THERMAL STRAIGHTENING OF SHIPBUILDING PANELS

O.V. MAKHNENKO[1], **A.F. MUZHICHENKO**[1] and **P. SEYFFARTH**[2]
[1]E.O. Paton Electric Welding Institute, NASU, Kiev, Ukraine
[2]IMG GmbH, Rostock, Germany

Described is an example of application of mathematical modelling for investigation of the efficiency of the process of thermal straightening of shipbuilding panels, based on the approach of a combined use of the general thermoplasticity method and approximate shrinkage function method. It is shown that the approach suggested is particularly efficient for prediction of general distortions of large-size spatial structures in the case of a large number of welds contained in them or of local heatings used for straightening. The results of experiments on thermal straightening of shipbuilding panels with buckling distortions have been analysed, and objective factors limiting the efficiency of this technological operation, especially with large thicknesses of the panels, have been revealed.

Keywords: *thin-sheet welded structures, shipbuilding panels, welding distortions, thermal straightening, mathematical modelling, thermoplasticity method, shrinkage function method*

Modelling of the processes of welding or thermal straightening of large-size structures by the finite element and thermoplasticity methods involves problems associated with the required accuracy of solution. Firstly, a large-size structure has to be broken down into a large number of elements, compared with an individual piece, this requiring substantial computing resources and time for computation. Secondly, the problem becomes even more complicated when it is necessary to model a large number of welds or local heatings used for thermal straightening. All this makes finding a solution hardly possible.

General distortions of large-size structures can be determined by using the approximate shrinkage function method, which works within the ranges of the elasticity theory, as the general distortions or displacements of points of a welded structure are an integral characteristic, and just insignificantly depend upon the character of distribution of the shrinkage function (especially at some distance from its application). The study by E.O. Paton [1] can be considered the basic one dedicated to this subject. The study described a comprehensive investigation of residual welding stresses induced in cylindrical vessels by making of circumferential and longitudinal welds, as well as by welding of a bottom, welding-in of branch pipes, etc. Until now this study has not lost its scientific and practical interest. The idea suggested in it for estimation of residual welding stresses by the elasticity theory methods on the basis of a preset value of longitudinal shrinkage deformations, which are determined experimentally from simple tests, found application in a large number of studies [2–8]. The generalised description of the shrinkage function methods is given in study [2].

Figure 1. Sample of shipbuilding panel

A series of experiments was carried out to study the efficiency of thermal straightening of shipbuilding panels with buckling distortions on samples of a limited size (1300 × 1300 mm), prepared with allowance for design peculiarities, a technology and material identical to those of a real shipbuilding panel (Figure 1). A sample of the panel consisted of a skin sheet panel 6 mm thick with longitudinal and transverse frameworks welded in such a way that two buckling zones 600 × 1200 mm in size were formed between the frameworks. The value of buckling had a minus sign (deflection) in the majority of cases and was not in excess of 3–7 mm.

Thermal straightening was performed by heating of both round spots and strips 150 mm long using the indirect-action plasma heat source (effective power Q_{eff} = 1100 W, concentration coefficient K = = 0.004 l/mm^2), flame heat source (Q_{eff} = 2500 W, K = 0.005 l/mm^2) and laser source with a defocused beam (Q = 2800 W, uniform distribution of power in a round spot with diameter D_h = 24 mm).

Results of the experiments conducted on samples showed a very low efficiency of thermal straightening of buckling distortions. The effect of substantial local bending deformations with a minus sign (deflection) caused by non-uniform heating of the metal sheet through its thickness was observed for almost all heatings. This can explain the fact that the buckling distortions can be decreased only at a positive sign (flexure) of buckling. Therefore, the straightening process was performed not by tension of the skin sheet due to

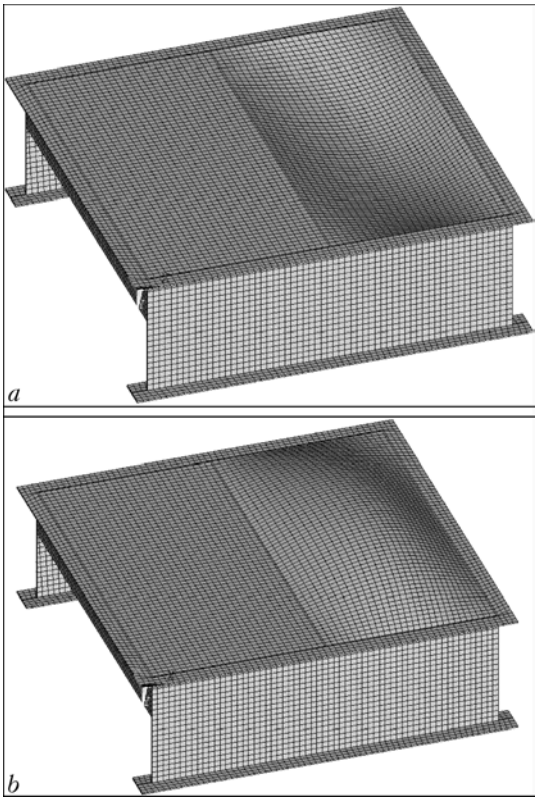

Figure 2. Finite element model of sample of a shipbuilding panel with buckling distortions of its skin: *a* — deflection; *b* — flexure

shrinkage in the sheet plane, but as a result of local bending deformations within the heating zone.

Modelling of the process of thermal straightening on the above experimental samples by using the ANSYS commercial software package was carried out to study this type of the problems. A model of the shipbuilding panel broken down into the finite elements (approximately 240,000 elements) is shown in Figure 2. Heatings were set in the form of additional shrinkage deformations in the skin sheet plane. A solution for general distortions and displacements of points of the skin sheet and stiffeners of a sample in a 3D statement of the problem was sought within the ranges of the elasticity theory by using the shrinkage function method, which is approximate and does not account for the history of formation and development of plastic deformations. Therefore, the developed model failed to determine the effect of a sequence of heatings on general distortions of a panel sample. Advantage of the shrinkage function method over the general thermoplasticity method is the possibility of obtaining a solution for general distortions of complex spatial structures with a large number of heatings.

Modelling of the process of thermal straightening on an experimental panel sample was performed when the skin of one panel had a buckling distortion, i.e. uniform deflection or flexure from the skin plane. Corresponding finite element models of a shipbuilding panel sample with buckling distortions are shown in Figure 3, *a, b*. Each model includes fixation of the sample at four points in corners along the contour against displacements from the skin sheet plane. Shrinkage deformations induced by heating of one strip 150 mm long were set equal to $\Delta_{tr} = 0.3$ mm and $\Delta_l = 0.1$ mm (in the transverse and longitudinal directions with respect to the heating strip), which approximately corresponded to real values in flame heating of such a strip [9, 10].

As shown by the calculation results, displacement of a skin sheet to 1.5 mm took place under the effect of shrinkage deformations induced by heating of one strip 150 mm long, located at the centre of a buckle

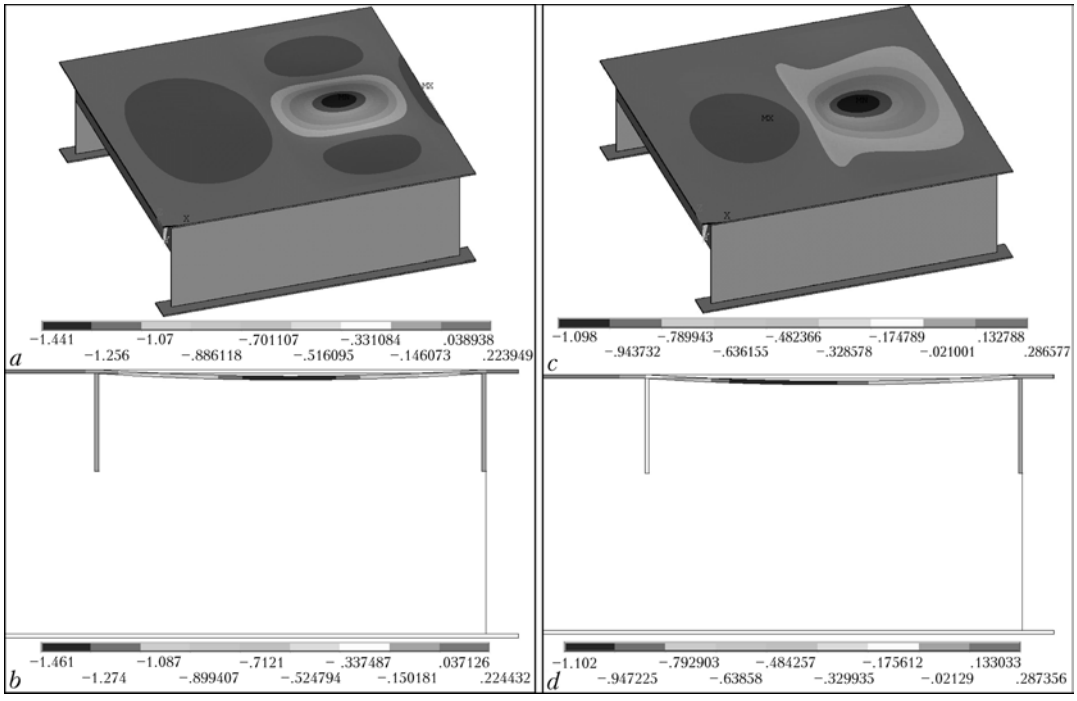

Figure 3. Displacements U_y (mm) from the skin sheet plane (decrease in buckling) under the effect of shrinkage deformations induced by heating of one strip 150 mm long: *a, b* — location at the centre of buckle; *c, d* — location at the end of buckle at a distance of 70 mm from stiffener; *a, c* — displacements on a general view of the panel sample; *b, d* — cross section at the centre of buckle

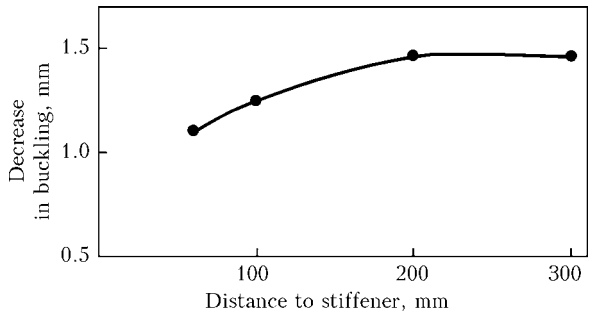

Figure 4. Decrease in the efficiency of straightening with displacement of a heating strip from the buckle centre to stiffener (framework)

(Figure 3, *a, b*), i.e. the buckling distortions decreased from 10 (initial value) to 8.5 mm. The calculations also showed that displacement of the heating strip from the centre of a buckle to a stiffener (to 70 mm from the framework) diminished the effect of straightening approximately by 25 % (Figure 3, *c, d*). Location of heating strips at the central part of a buckle is most efficient (Figure 4).

An important effect in terms of understanding of the thermal straightening process mechanism was revealed by calculation of decrease in buckling induced by one heating strip located at the centre of a buckle at different values of the initial buckling (2, 3, 5, 10, 15, 20 and 30 mm). The calculation results in Figure 5 show that the efficiency of straightening (decrease in buckling) first dramatically grows with increase in the initial value of buckling, then becomes constant, and further on decreases to some extent at high values of the buckling. At a zero buckling, i.e. in the absolutely plane sheet, the shrinkage due to heating in the sheet plane does not cause any displacement from the plane. This effect is in agreement with practical observations, i.e. it is more labour-consuming to straighten small buckles by the thermal method than big buckles. This effect can be explained by the fact that a decrease in buckling, i.e. bend of a sheet, depends upon the arm of application of shrinkage forces. The bigger the buckling, the higher the bending moment caused by shrinkage. At the same time, the skin sheet takes the spherical shape after the buckling reaches sufficiently high values, this leading to increase in bending resistance of the skin.

Therefore, as shown by the calculation results, straightening of buckling distortions under the effect of shrinkage deformations induced by heating of a strip features a marked efficiency for the shipbuilding panel sample under consideration. Moreover, this efficiency of straightening does not depend upon the sign (direction) of the initial buckling distortion. However, the calculations were made with no account for local bending deformations induced by non-uniformity of heating of the skin sheet. These bending deformations, which always cause deflection of the skin sheet, will contribute to decrease in buckling at the initial buckling distortion, while at the deflection buckling distortion they will partially or fully compensate for the effect of straightening due to shrinkage deformations. As bending deformations occur almost with any heat source, to ensure the efficiency of straightening it is necessary that the positive effect of shrinkage deformations in the sheet plane be much higher than the effect of bending deformations.

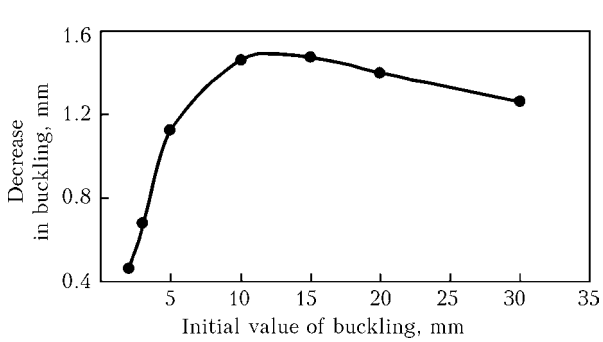

Figure 5. Dependence of the efficiency of straightening upon the value of buckling

The numerical algorithm based on the thermoplasticity method, i.e. on tracing of temperature fields and evolution of elasto-plastic deformations in a sheet sample with a size of 500 × 500 mm and 6 mm thick in the 3D statement of a problem was used to determine residual shrinkage deformations and local angular deformations for the case of heating of a strip with a moving heat source (material ---- low-carbon steel).

The data on temperature fields were obtained by using the numerical method for solving the thermal conductivity problem within the limits of the 3D model for a range of $0 \le x \le 500$ mm, $0 \le y \le 500$ mm and $-\delta/2 \le z \le \delta/2$ at initial temperature $T_0 = 20$ °C, where heat transfer with an environment having a temperature of 20 °C, following the Newton's law, is set for all the surfaces at surface heat transfer coefficient $\alpha_h = 0.00004$ W/(mm^2·°C). The surface heat source with power Q_{eff}, distributed over the surface following the normal circular law, with concentration coefficient K, acts on surface $z = -\delta/2$. The centre of the source at a moment of $0 < t < t_0$ is located at a point of $x = x_0$, $y = y_0$, then it moves at speed v along axis x at $t > t_0$. The movement ends at $t - t_0 = L/v$, and levelling of the temperature takes place.

Numerical experiments were conducted by using the indirect-action plasma source, flame (acetylene) heat source, which is widely applied now, and laser heat source holding promise for application in the near future. Experimentally measured effective power $Q_{eff} = 1100$ W and concentration coefficient $K = 0.004$–0.010 l/mm^2 were set in the calculations for the plasma heat source. $Q_{eff} = 2500$ W and $K = 0.004$ l/mm^2, corresponding to a torch employed for thermal straightening at a thickness of 6 mm, were set for flame heating. Effective power $Q_{eff} = 2800$ W and a uniform distribution of power in a round spot of the defocused laser beam with diameter $D_h = 24$ mm were set for the laser heat source.

The calculation results show that the temperature gradient through thickness of a sheet heated strongly depends upon power Q_{eff}, concentration coefficient K and the speed of movement of a heat source in heating of a strip with length $L = 150$ mm. For the plasma

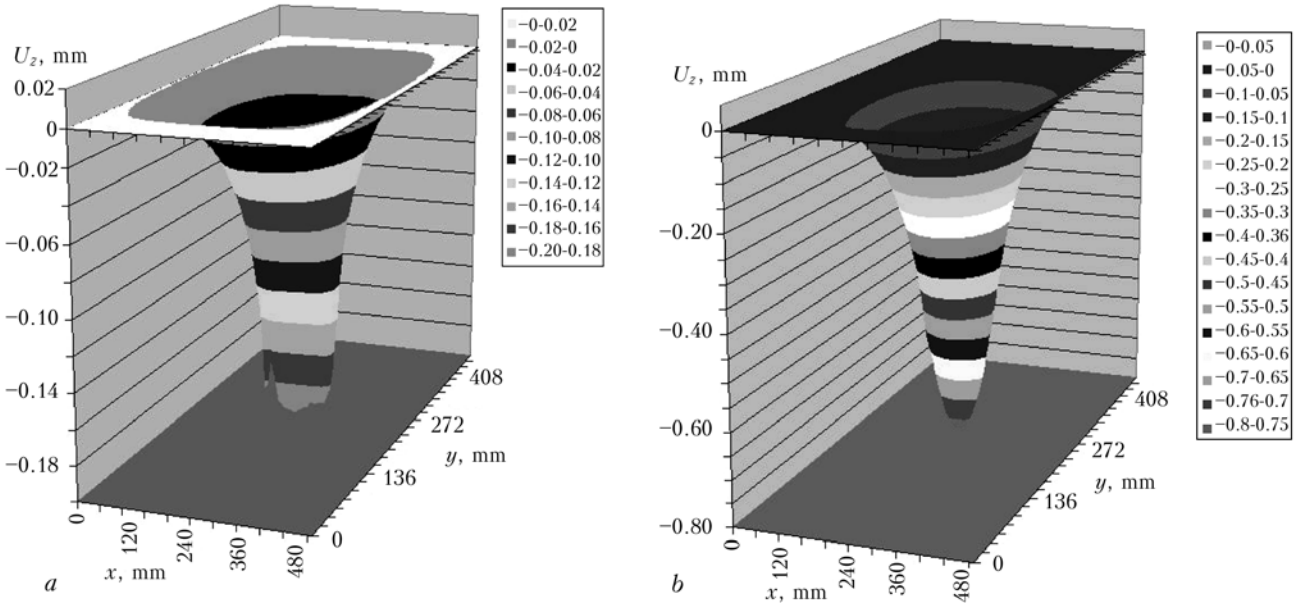

Figure 6. Distribution of residual deflections U_z (x, y) for flame (a) and laser (b) heat sources

heat source, the difference in heating temperatures at the upper and lower surfaces was approximately 40–60 °C, and maximal deflections were not in excess of 0.1 mm. The higher effective power (2–2.5 times) of the flame and laser heat sources, compared with the above plasma source, and, hence, the higher movement speeds of the sources cause a more substantial non-uniformity of distribution of temperature through thickness of the sheet. This explains the sufficiently high values of maximal deflections caused by local residual bending deformations. For the flame heat source, depending upon concentration coefficient K, the difference in heating temperatures on the upper and lower surfaces was approximately 100–160 °C, while for the laser heat source this difference amounted to 300 °C, depending upon its movement speed. Accordingly, maximal deflections U_z of local bending deformations were at a level of –0.2 mm (Figure 6, *a*) for flame heating, and –0.8 mm for laser heating (Figure 6, *b*).

Analysis of the calculation data given in the Table shows that flame heating is most efficient among the other heat sources under consideration for thermal straightening of buckling distortions in the proportions of values of the total volume of plastic shrinkage deformations V_p and maximal deflection U_z. The unexpectedly high values of bending deformations for the laser heat source, which is characterised by a uniform distribution of power in the spot with a diameter of 24 mm, might be explained by a sufficiently high reduced concentration coefficient K, obtained from a relatively small diameter of the heat input spot. When using the law of distribution of heating power from the formula

$$Q(r) = \frac{Q_{\text{eff}}}{\pi R^2} e^{-Kr^2}$$

and regarding coordinate r as a boundary of the heat spot, for which the $Q(r)/Q_{\text{eff}} = 0.1$ condition is met, the reduced concentration coefficient for the laser heat source at $R = 24/2$ mm will be $K = 0.009$ l/mm^2. To compare, with the flame heat source at $K = 0.003$ and 0.005 l/mm^2 the heating spot sizes will be 41 and 32 mm, respectively.

To allow for local bending deformations caused by non-uniformity of heating of the skin sheet during heating, different values of shrinkage deformation on the upper and lower surfaces of a sheet were set in the developed finite element model of heating of a strip, based on the use of the shrinkage function method. This difference in shrinkages should correspond to angular deformations α according to the following dependence:

$$\alpha = \frac{(\Delta_{\text{tr}}^{\text{up}} - \Delta_{\text{tr}}^{\text{low}})}{\delta},$$

where $\Delta_{\text{tr}}^{\text{up}}$ and $\Delta_{\text{tr}}^{\text{low}}$ are the shrinkages on the upper and lower surfaces of the sheet, and δ is the sheet thickness.

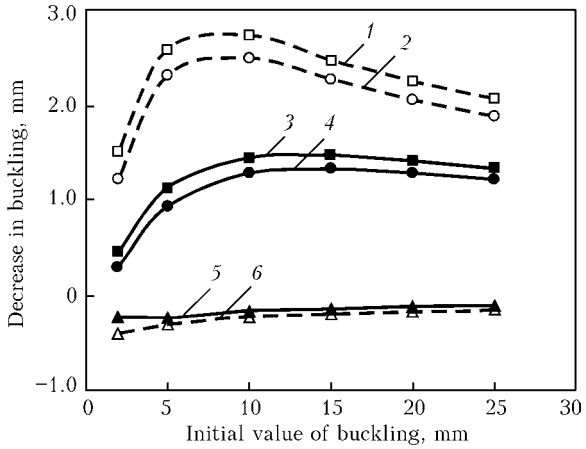

Figure 7. Dependence of the efficiency of straightening upon the initial buckling in heating of the 150 mm long strip at the centre of buckle of the skin sheet 6 mm (solid curve) and 3 mm thick (dashed curve), allowing for the effect of shrinkage in the sheet plane and angular deformations: *1, 3* — shrinkage; *2, 4* — shrinkage + angular deformations; *5, 6* — angular deformations

Calculation data on heating of strip with L = 150 mm for a sheet sample 500 × 500 mm in size and 6 mm thick

Heat source	Q_{eff}, W	K, 1/mm^2	D_h, mm	v, mm/s	V_p, mm^2	U_z, mm
Plasma	1100	0.004	--	1.0	--119	–0.08
	1100	0.007	--	1.0	--128.9	–0.09
	1100	0.010	--	1.0	--132	–0.07
Flame	2500	0.003	--	2.0	--631	–0.18
	2500	0.005	--	2.0	--669	–0.20
Laser	2800	N/D	24	4.0	--390	–0.55
	2800	Same	24	6.0	--269	–0.80

In the calculations, the difference in shrinkages was selected so that deflection of a sheet caused by angular deformation was approximately $U_x = 0.2$ mm, this corresponding to the results of numerical estimation of local angular deformations for a heating strip 150 mm long in flame heating. The mean value of shrinkage was set to be $\Delta_{tr} = 0.1$ mm and $\Delta_l = 0.1$ mm (in the transverse and longitudinal directions with respect to the heating strip).

Figure 7 shows the calculation data for displacements U_y from the skin sheet plane depending upon the initial value of buckling of the skin sheet 6 and 3 mm thick, allowing for a separate and combined effect of shrinkage in the sheet plane and angular deformations. The results were obtained for the deflection buckling distortion, where angular deformations partially compensate for the efficiency of straightening of shrinkage deformations. With this relationship of shrinkage and angular deformations the effect of the latter on the efficiency of straightening, i.e. decrease in buckling, is insignificant. At higher values of angular deformations the efficiency of straightening will dramatically decrease.

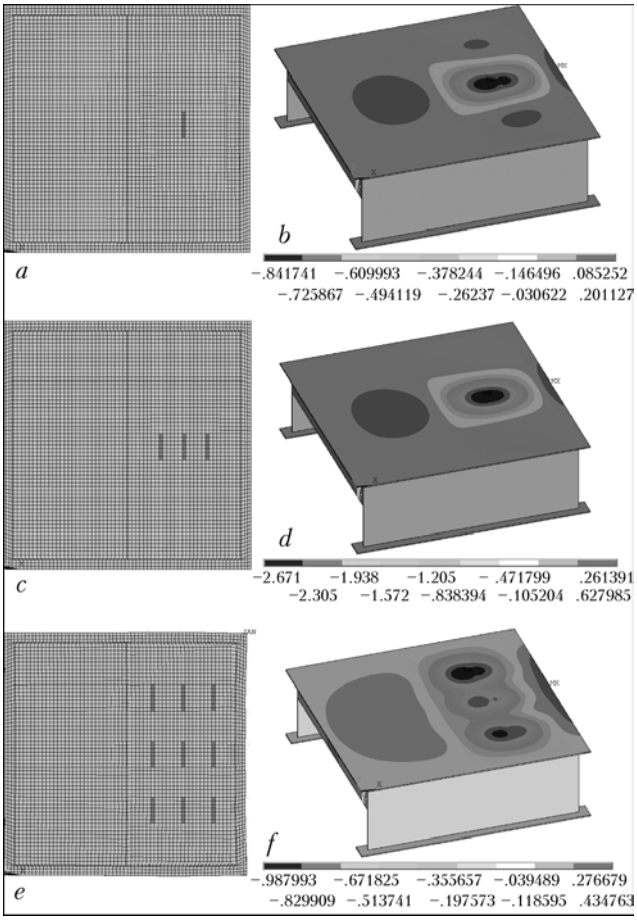

Figure 8. Decrease in buckling (displacement U_y) in heating of strips 150 mm long: *a, c, e* — scheme of heating of one, three and nine strips; *b, d, f* — corresponding distribution of displacements, mm

The results also show that the efficiency of straightening strongly depends upon the thickness of a skin sheet. Providing that the shrinkage characteristics are uniform at 3 mm thickness of the skin sheet, a decrease in buckling due to heating of a strip is 2 times as high as at 6 mm thickness. This is in good agreement with practical experience, where the application of thermal straightening of buckling distortions is most efficient at up to 4 mm thickness of the skin sheet.

The model developed made it possible to conduct numerical experiments to study the efficiency of straightening depending upon the quantity and arrangement of heatings. Figure 8 shows the calculation data on displacements U_y from the skin sheet plane for different variants of arrangement of the heating strips 150 mm long at a skin thickness of 6 mm. The initial values of buckling distortion was set equal to 5 mm. Displacements U_y under the combined effect of shrinkage deformations in plane and angular deformations were determined for each variant.

The results show (Figure 8, *a, b*) that a decrease of buckling in heating of a strip is of a local character and occurs in a zone limited by width of a buckle, and along the length of the buckle ---- approximately by two lengths of the heating strip. A small increase in this buckle, as well as in the neighbouring ones, takes place outside this zone. This effect is also confirmed by practical observations. Arrangement of several heating strips within one zone close to each other (Figure 8, *c, d*) provides a marked increase in the efficiency of straightening (decrease in buckling) within this zone. The uniform arrangement of the heating strips over the surface area of a buckle at a sufficient distance from each other (Figure 8, *e, f*) leads to a comparatively small decrease in buckling over the entire area of the buckle. This is attributable to

a mutual effect of the zones of increase and decrease in buckling due to different heating strips. Therefore, the results of straightening at a large number of heatings must not be considered to be a simple sum of decreases in buckling due to individual heatings.

As seen from comparison of heating of strips and round spots (Figure 9), even at a set value of shrinkage a decrease in buckling (the initial value of a buckling distortion is 5 mm) in heating of round spots has a much lower effect than in heating of strips. This is associated with a lower total volume of plastic deformations formed in heating of round spots. In addition, all of the above peculiarities related to a local character of the efficiency of straightening and mutual effect of heatings on each other persist in this case.

CONCLUSIONS

1. The efficiency of thermal straightening strongly depends upon the initial buckling, i.e. a decrease in buckling (in fact, bend of a sheet) depends upon the arm of application of shrinkage forces. At low initial values of buckling, or with decrease in buckling during the process of straightening its efficiency dramatically decreases.

2. The efficiency of thermal straightening is highly affected by thickness of a skin sheet. At a big thickness of the sheet (6 mm) the efficiency of straightening as a result of shrinkage deformation in the sheet plane greatly decreases. Additional bending deformations are formed at a big thickness, caused by non-uniformity of heating through thickness, which may substantially decrease the efficiency of straightening depending upon the sign (direction).

3. The result of thermal straightening depends to a considerably degree upon the quantity and location of heating spots and strips over the surface area of a buckle, and at their large quantity the efficiency of straightening cannot be considered to be a simple sum of decreases in buckling due to separate heatings. Decrease in buckling due to one heating is of a local character and occurs within the zone that is approximately equal in size to width of a buckle. Even a small increase in this buckle, as well as in the neighbouring ones takes place outside this zone. Therefore, thermal straightening should be performed by heating of spots or strips located within the zone of the maximal buckling.

4. The process of thermal straightening of buckling distortions has a number of objective factors that limit the efficiency of this technological operation, especially at big thicknesses of the skin sheets. The positive effect of straightening can be achieved only with the optimal selection of parameters and arrangement of heating spots.

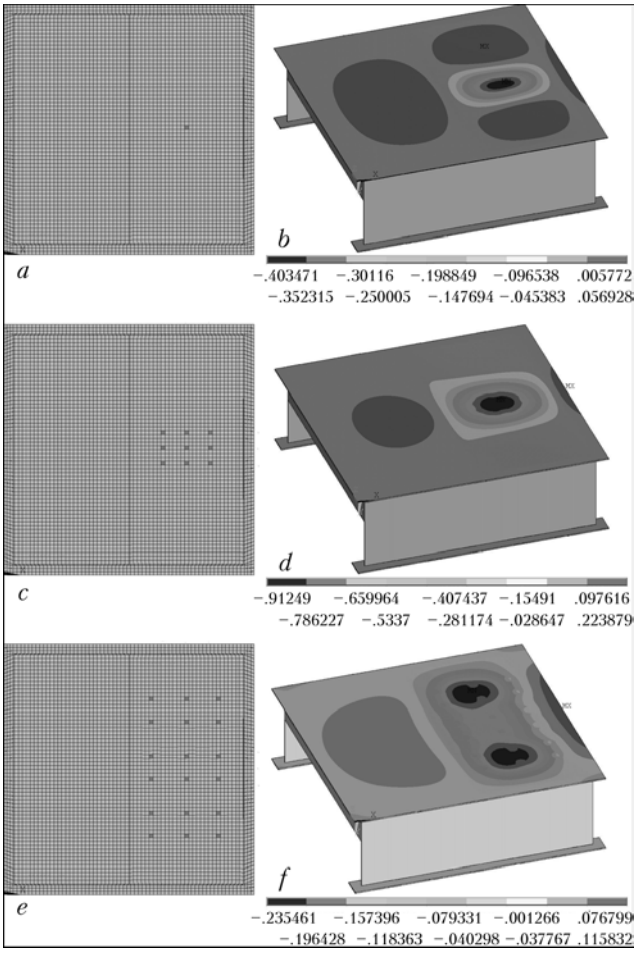

Figure 9. Decrease in buckling (displacement U_y) in heating of round spots: *a, c, e* — scheme of heating of one, nine and eighteen spots; *b, d, f* — corresponding distribution of displacements, mm

1. Paton, E.O., Gorbunov, B.N., Bernshtejn, D.I. et al. (1936) Shrinkage stresses in welding of cylindrical vessels. *Avtogennoe Delo*, **5/6**.
2. Podstrigach, Ya.S., Plyatsko, G.V., Osadchuk, V.A. (1971) On determination of welding residual stresses in cylindrical shells. *Avtomatich. Svarka*, **3**, 50–58.
3. Ueda, Y., Yuan, M.G. (1991) The characteristics of the source of welding residual stress (inherent strain) and its application to measurement and prediction. *Transact. of JWRI*, 20(**2**), 119–127.
4. Makhnenko, V.I., Lobanov, L.M., Makhnenko, O.V. et al. (1991) Prediction of general deformations of welded units by using the database on transverse and longitudinal shrinkage, and angular deformations of appropriate samples. *Avtomatich. Svarka*, **10**, 1–5.
5. Lobanov, L.M., Makhnenko, O.V., Sayfferth, P. (1997) Design prediction of welding deformations in production of flat sections with the purpose of decrease of fitting operations. *Ibid*., **1**, 21–24.
6. Makhnenko, V.I., Lobanov, L.M., Makhnenko, O.V. (1998) Problem-oriented software package for prediction of welding stresses and distortions with reference to the solution of various questions of formation. Weldability and accuracy of welded structures. *IIW Doc. X/XV-RSD*.
7. Luo, Y., Deng, D., Xie, L. et al. (2004) Prediction of deformation for large welded structures based on inherent strain. *Transact. of JWRI*, 33(**1**), 65–70.
8. Liang, W., Shinji, S., Tejima, M. et al. (2004) Measurement of inherent deformations in typical weld joints using inverse analysis. Pt 1: Inherent deformation of bead on welding. *Ibid*., 33(**1**), 45–51.
9. Kuzminov, S.A. (1974) *Welding deformations of ship hull structures*. Leningrad: Sudostroenie.
10. Vinokurov, V.A., Grigoriants, A.G. (1984) *Theory of welding strains and stresses*. Moscow: Mashinostroenie.

PRODUCING PERMANENT JOINTS OF γ-TiAl BASED ALLOYS USING NANOLAYERED Ti/Al INTERLAYER BY VACUUM DIFFUSION WELDING

A.I. USTINOV, Yu.V. FALCHENKO, A.Ya. ISHCHENKO, G.K. KHARCHENKO, T.V. MELNICHENKO and **A.N. MURAVEJNIK**
E.O. Paton Electric Welding Institute, NASU, Kiev, Ukraine

The possibility of producing diffusion bonds of γ-TiAl based alloys using nanolayered Ti/Al interlayer has been studied. It is shown that utilization of nanolayered foil as an intermediate element allows formation of sound joints in vacuum diffusion welding. Peculiarities of microstructure of the joint zone have been studied.

Keywords: *vacuum diffusion welding, titanium aluminide, structure, joint zone, nanolayered interlayer*

γ-TiAl based alloys are regarded as promising materials for manufacture of structural elements of aerospace system components operating at higher temperatures. The advantages of such alloys, compared to other high-temperature materials, mainly are their low (3.8--4.0 g/cm^3) density and high heat resistance [1].

The prospects of using γ-TiAl alloys in structural element design stimulated investigation and developments in the field of the technology of producing permanent joints of these alloys. A possibility of producing permanent joints by fusion [2] and diffusion [3--7] welding was considered.

Application of the traditional welding processes based on local melting of material in the joint zone showed that the quality of the produced welded joint depends essentially on phase transformations in the HAZ. At deviation of the welding mode from the optimum one, phase transformations accompanied by bulk effects occur in the joint zone, this leading to development of stresses in the HAZ and, as a result, to crack initiation near it [2]. In order to avoid it, welding has to be performed in strictly specified modes.

Use of vacuum diffusion welding is believed to be promising. Possible technological variants of this welding process for welding titanium aluminides are considered in [3--7]. Study [3] gives the results of vacuum diffusion welding of γ-TiAl alloy (49 % Ti, 47 % Al and 4 % Cr, Mn, Nb, Si, B) produced by the method of precision casting and hot pressing with subsequent homogenizing annealing in the following mode: welding temperature T = 950--1100 °C, welding time τ = 1--3 h, pressure P = 20--40 MPa, heat treatment at 1400 °C, 30 min. The authors determined the optimum welding mode: T = 1000--1100 °C, τ = 3 h, P = 20--40 MPa. Heat treatment ensures formation of the lamellar structure in the weld area. In [4] the possibility of pressure welding of Ti--Al--Nb alloy based on α_2-Ti_3Al (T = 900, 1000 and 1100 °C, τ = = 4--5 min, P = 200--300 MPa) was studied. Joints produced at T = 1000--1100 °C have equivalent strength with the base metal (σ_t = 800--820 MPa).

It is known that additional activation of the welded surfaces can be achieved when using interlayers, which are ductile or consist of two foils based on different elements, in which contact melting processes develop at temperature increase. So, [5] is a study of the possibility of using aluminium and titanium interlayers 0.15 and 0.20 mm thick, respectively, in pressure welding of γ-TiAl alloy (60.947 % Ti, 31.152 % Al, 4.65 % Nb, 2.73 % Mn. 0.31 % B). Welding was performed in the following mode: T = 750--850 °C, τ = = 10--20 min, P = 100 and 300 MPa with subsequent stabilizing annealing at 1000 °C, 50 h. The authors note that use of aluminium interlayers leads to formation of defects in the joint zone, namely microvoids and cracks. When titanium interlayers are used, a joint zone forms, which features a high strength, and considerable chemical and phase inhomogeneity.

In [6, 7] it is shown that deposition of thin nanolayered Ti/Al coatings on the surfaces of γ-TiAl alloy samples to be joined ensures a uniform structure in the joint zone in vacuum diffusion welding (T = = 1100 °C). The authors came to the conclusion that formation of a strong welded joint at 700--1100 °C is related to dynamic recrystallization of γ-TiAl alloy, thus promoting refinement of its structure and initiation of plastic deformation.

On the other hand, the process of deposition of such coatings on the part surfaces to be joined runs into certain technological difficulties in a number of cases. The technology of producing permanent joints is simplified when nanolayered materials in the form of foil are used. Such an approach was implemented by us, for instance, in welding of composite materials based on Al--Al_2O_3 using nanolayered Ni/Al foil [8]. The method of electron beam deposition enables producing nanolayered foil over a short enough period, owing to a high (up to 100 nm/s) rate of the deposition process. Conditions of formation of permanent joints using nanolayered Ti/Al foils as an interlayer were studied.

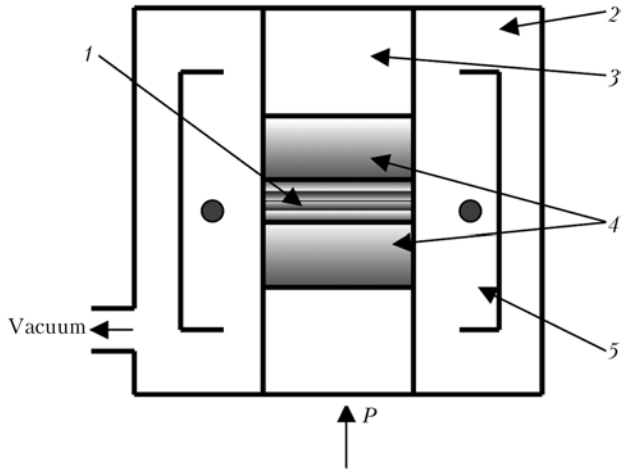

Figure 1. Schematic of the unit for vacuum diffusion welding: *1* — nanolayered interlayer; *2* — vacuum chamber; *3* — press-down rod; *4* — welded samples; *5* — electron beam gun

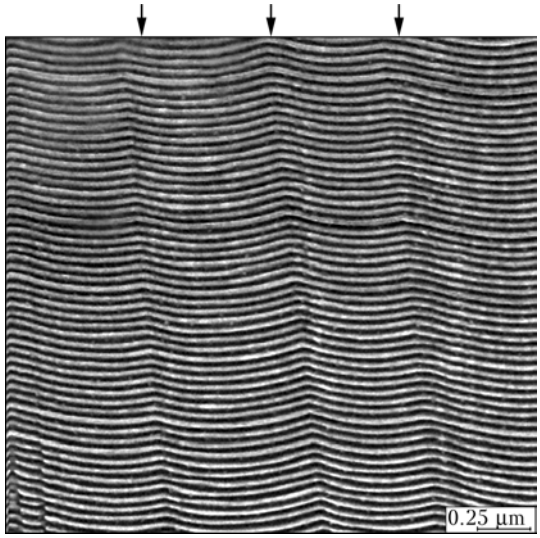

Figure 3. Cross-sectional microstructure of nanolayered foil in the initial condition: light layers correspond to titanium, dark ones — to aluminium; arrows show grain boundaries

Nanolayered Ti/Al foil was produced by layer-by-layer electron beam deposition of elements on a horizontal rotating substrate by a procedure described in several studies (see for instance [9]). Schematic of the process of foil formation is given in [10]. To perform layer-by-layer deposition of elements, the vacuum chamber was separated by a vertically located continuous screen into two equal parts, in each of which copper water-cooled crucibles were installed, one of them accommodating an ingot of titanium, and the other — an ingot of aluminium. The substrate was fastened on a vertical shaft located above the separating screen. Electron beam gun performed heating of the substrate up to the specified temperature, which was monitored during deposition by a thermocouple. Before deposition, a layer of CaF_2 was applied on the substrate, which promoted interlayer separation from the substrate. Then electron beam guns were used to induce a molten pool on the ingot surfaces, from which the elements were evaporated. Substrate rotation and presence of a separating screen allowed successive deposition of metal layers. The ratio of thickness of these layers was determined by the ratio of the ingot evaporation intensity, and their total thickness varied, depending on the substrate rotation speed. Total thickness of the interlayer at the set intensity of element evaporation depended on the duration of the deposition process.

Ti–48 at.% Al alloy with niobium and manganese additives was selected as the object of study. This alloy belongs to the group of titanium intermetallics, which are in the two-phase state ($\alpha_2 + \gamma$) with α_2-Ti_3Al and γ-TiAl (furtheron TiAl).

Welding was performed in a vacuum chamber fitted with a system of static loading of samples and their heating (Figure 1). Electron beam gun was used as the heat source. Welding process parameters were varied within the following ranges: T = 900–1200 °C, τ = 5–25 min, P = 10–70 МПа. Pressure in the working chamber was maintained on the level of $1.33.10^{-3}$ MPa.

Before welding sample surfaces were ground on a diamond wheel, and then degreased. Prepared samples of 10 × 10 × 4 mm size together with the interlayer were placed into the vacuum chamber. Uniform heating was ensured by a ring-shaped electron beam gun, installed on the butt level, and heating correction during welding was performed by heater displacement along the assembly of the samples being welded. Welding temperature was monitored by a thermocouple.

In order to conduct metallographic analysis welded joint samples were prepared by a standard procedure

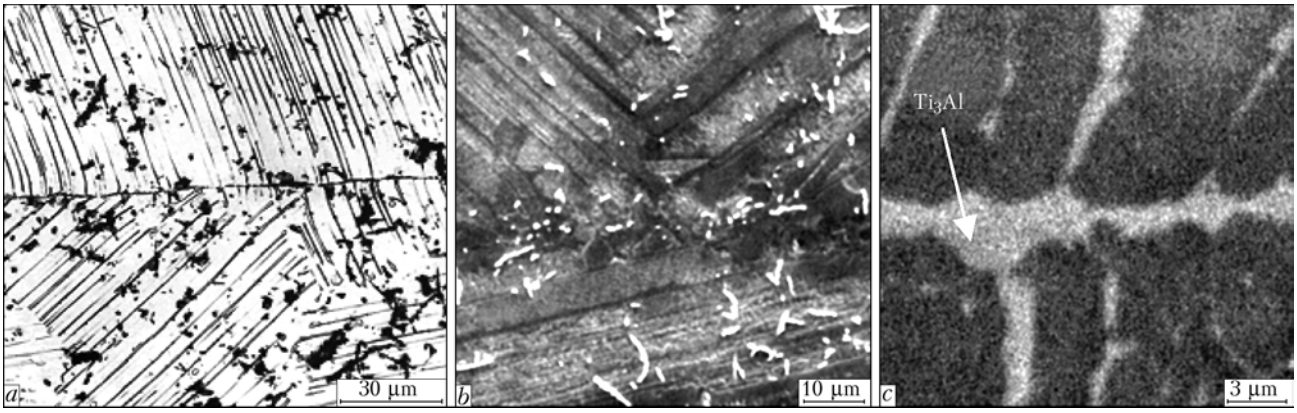

Figure 2. Microstructure of the zone of TiAl joint produced by vacuum diffusion welding without an interlayer: *a–c* — see the text

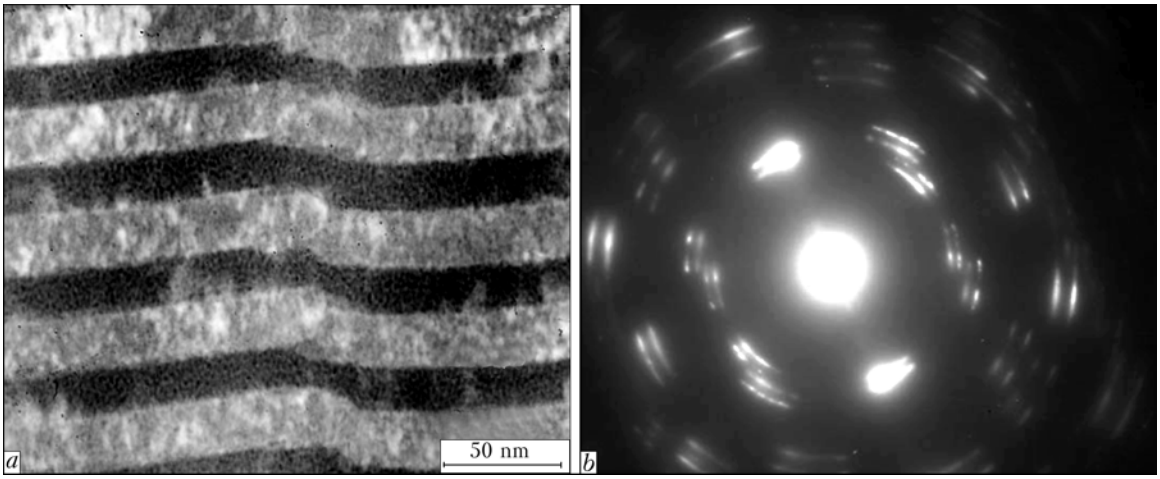

Figure 4. Microstructure (*a*) and microdiffraction pattern (*b*) of the nanolayered interlayer cross-section

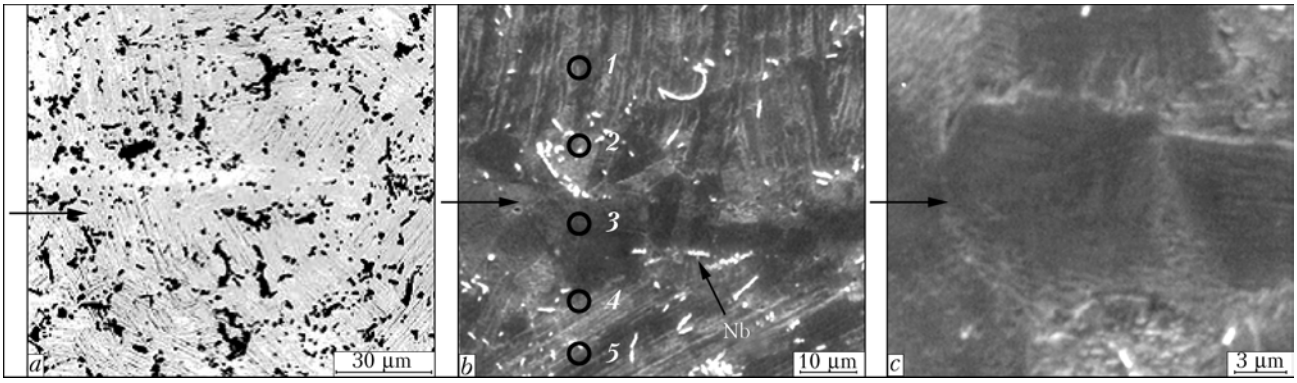

Figure 5. Microstructure of the zone of the joint of TiAl intermetallic samples produced by diffusion welding in vacuum using nanolayered Ti/Al foil: *a–c* ---- see the text; the arrows show the welding location; numbers are points in which the local composition and microhardness were studied; results of these measurements are given in the Table

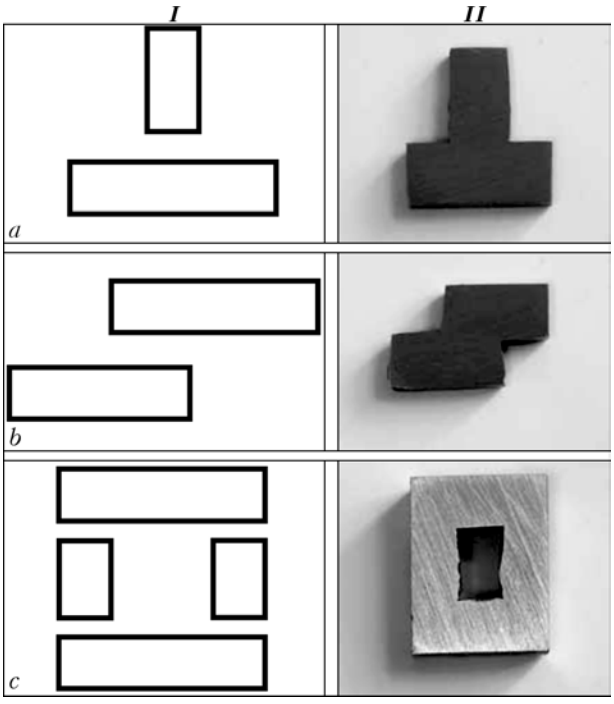

Figure 6. Schematic of sample assembly (*I*) and general view (*II*) of TiAl alloy welded joints of tee (*a*), overlap (*b*) and box-like (*c*) type made using nanolayered Ti/Al interlayer

in the Struers grinding-polishing machine tool Abramin. The condensate structure and chemical composition were analyzed using Neophot optical microscope and CamScan scanning microscope, fitted with an energy-dispersion system Energy 200 for local analysis. Chemical etching of the samples was conducted to reveal the weld metal structure. Condensate microhardness was measured by a micorhardness attachment to Polyvar-Met optical microscope at the load of 0.098–0.196 N by Vickers. The structure of nanolayered foil on transverse sections was analyzed using Hitachi transmission electron microscope H-800 at 200 kV accelerating voltage. The thin foil cross-section was first prepared by mechanical thinning, and then polished in Gatan 656 unit with subsequent thinning and bombardment of the surface at 3° angle by argon ions with 5 keV energy at ion gun current of 20 μA in PIPS 691 unit.

TiAl joints were produced by vacuum diffusion welding without an interlayer at T = 1200 °C and P = = 70 MPa with subsequent soaking for 20 min. Joint zone microstructure is shown in Figure 2. It is seen in the Figure that an interface is revealed in the above zone (Figure 2, *a*) without any pores in the joint (Figure 2, *b*). Structure analysis in phase contrast mode revealed that the interface is an intermetallic interlayer, the composition of which, by the data of local chemical analysis, is close to that of Ti_3Al in-

termetallic. Presence of a brittle intermetallic interlayer lowers the welded joint strength, thus leading to a degradation of its surface properties.

Nanolayered Ti--52 at.% Al foil 20 μm thick with 50 nm period of layer alternation (titanium and aluminium) was used in this study for diffusion welding of TiAl intermetallic samples. Its cross-sectional microstructure (Figure 3) shows that it is divided into individual grains. Within one grain a striated contrast is observed, which corresponds to alternation of titanium and aluminium layers. Transmission electron microscopy investigations were conducted to determine the characteristics of the laminated grain structure. Figure 4 gives the microstructure and microdiffraction pattern of the cross-section of nanolayered Ti/Al foil. Absence of element mixing is indicated by microdiffraction of electrons on the studied section (Figure 4, *b*). Certain orientational relationships characteristic for laminated materials are found between the layers. From the light-field images it can be seen (Figure 4, *a*) that the period of alternation of titanium and aluminium layers is equal to 50 nm.

The regularities of the diffusion processes running in nanolayered foil at its heating are analyzed in [9]. It is established that heating promotes their intensive development, this leading to formation of a heterophase structure consisting of a mixture of TiAl and Ti_3Al intermetallics. On this basis it was assumed that during diffusion welding of titanium intermetallics phase transformations will run in the foil, which will ensure formation of a structure similar to that of the base metal, in the joint zone.

Investigations of the influence of diffusion welding parameters (pressure, heating temperature and soaking time) on welded joint quality were conducted to determine the conditions of joint formation using nanolayered foils. It is found that at lowering of welding temperature (below 1000 °C) the joint zone develops discontinuities, which considerably lower its mechanical strength. Microstructure of the zone of a welded joint made in the optimum welding mode (T = = 1200 °C, τ = 20 min, P = 10 MPa) is given in Figure 5. In Figure 5, *a* it is seen that a poorly distinguishable interlayer is present in the joint zone, the composition of which (49.4 Al; 49.8 Ti; 0.8 Mn) is close to that of the initial intermetallic, by the data of local chemical analysis.

The interlayer has a uniform structure (Figure 5, *b*) and consists of equiaxed grains of up to 10 μm size (Figure 5, *c*), in which a lamellar structure is discernible, which is characteristic of the initial intermetallic. Absence of pores and cracks, both in the joint zone and on the boundary with the welded samples, is indicative of a high quality of the produced welded joint. It should be noted that no degradation of the welded intermetallic structure occurs in the above welding mode. Element distribution in the joint zone and microhardness of different sections of the welding zone are given in the Table. From Figure 5, *b* and the Table it is seen that manganese is present and niobium

Composition (at.%) and HV microhardness of different sections of the welded joint zone

Studied points of the joint zone (see Figure 5, *b*)	Al	Ti	Mn	Nb	HV, GPa
1	43.9	52.9	1.3	1.9	4.6
2	47.3	50.1	0.9	1.7	4.8
3	49.4	49.8	0.8	--	4.0
4	47.4	49.9	1.0	1.7	4.3
5	44.1	52.6	1.5	1.8	4.4

is absent in point *3*. According to metallographic and local chemical analysis, niobium particles accumulate on the interlayer--intermetallic interface. Manganese presence in the interlayer is indicative of running of the diffusion processes in the joint zone during development of the solid-phase synthesis reaction, initiated in the nanolayered interlayer during welding.

Intensive development of the diffusion processes in the joint zone as a result of application of nanolayered interlayers promotes producing sound welded joints. As an example Figure 6 gives the general view of samples of welded joints of tee, overlap and box-like types.

Thus, during diffusion welding of intermetallic samples using nanolayered Ti/Al interlayer, the joint zone develops an intermetallic, the composition of which corresponds to the initial TiAl intermetallic (see the Table). Such changes of the metal composition and structure in the joint zone are indicative of the high diffusion mobility of the components, and can be due to the heat evolution processes accompanying the solid-phase reactions initiated in the nanolayered foil by heating [9].

1. Lasalmonie, A. (2006) Intermetallics: why is it so difficult to introduce them in gas turbine engines? *Intermetallics*, **14**, 1123--1129.
2. Chaturvedi, M.C., Xu, Q., Richards, N.L. (2001) Development of crack-free welds in a TiAl-based alloy. *J. Materials of Processing Techn.*, **118**, 174–178.
3. Cam, G., Bohm, K.-H., Kocak, M. (1999) Diffusionsschweissen feingegossener Titanaluminide. *Schweissen und Schneiden*, **8**, 470–475.
4. Zamkov, V.N., Markashova, L.I., Kireev, L.S. et al. (1992) Specifics of structural modifications of heat-resistant Ti_3Al-based alloy in pressure welding. *Avtomatich. Svarka*, **9/10**, 13–16.
5. Yushtin, A.N., Zamkov, V.N., Sabokar, V.K. et al. (2001) Pressure welding of intermetallic alloy γ-TiAl. *The Paton Welding J.*, **1**, 33–37.
6. Duarte, L.I., Ramos, A.S., Vieira, M.F. et al. (2006) Solid-state diffusion bonding of γ-TiAl alloys using Ti/Al thin films as interlayers. *Intermetallics*, **14**, 1151--1156.
7. Ramos, A.S., Vieira, M.F., Duarte, L.I. et al. (2006) Nanometric multilayers: a new approach for joining TiAl. *Ibid.*, **14**, 1157--1162.
8. Ishchenko, A.Ya., Falchenko, Yu.V., Ustinov, A.I. et al. (2007) Diffusion welding of microdispersed AMg5 + 27 % Al_2O_3 composite with application of nanolayered Ni/Al foil. *The Paton Welding J.*, **7**, 2–5.
9. Ustinov, A.I., Olikhovskaya, L.A., Melnichenko, T.V. et al. (2008) Solid-phase reactions in heating of multilayer Al/Ti foils produced by electron beam deposition method. *Advances in Electrometallurgy*, **2**, 19–26.
10. Paton, B.E., Ishchenko, A.Ya., Ustinov, A.I. (2008) Application of nanotechnology of permanent joining of advanced light-weight metallic materials for aerospace engineering. *The Paton Welding J.*, **12**, 2--8.

BRAZING OF FERROELECTRIC CERAMICS IN AIR ENVIRONMENT AND PURE OXYGEN ATMOSPHERE

Yu.V. NAJDICH, T.V. SIDORENKO and **A.V. DUROV**
I.M. Frantsevich Institute of Problems of Materials Science, NASU, Kiev, Ukraine

The technology for brazing in air environment and commercially pure oxygen atmosphere as well as method for deposition of coatings using metal melts with high degree of wettability of ceramics have been developed for the $BaTiO_3$-base ferroelectric ceramics. The technology developed makes it possible to substantially increase adhesion strength of coatings and brazed joints, widen existing and open new possibilities for manufacture of different instruments and devices.

Keywords: *brazing, metallization, ferroelectric ceramics, barium titanate, metal-oxygen technology*

Functional ceramic materials, composition of which includes compounds with structure of perovskite similar to barium titanate $BaTiO_3$ (such structure is based on ratio of three atoms of oxygen to each two atoms of the metal), occupy special position in state-of-the-art electrical engineering and electronics. These materials have rather wide range of applications, for example, development of multilayer capacitors with high capacity, electric field sensors, and great number of piezoelectric and ferroelectric instruments (sensors, drives) and thermistors.

Metal coatings on surface of the ceramics may act as electrodes for capacitors and an intermediate layer for joining the ceramics with a metal using brazing [1].

Perovskite titanium-base ceramics exists in two states: ferroelectric (stoichiometric $BaTiO_3$ compound) and a semiconductor (the $BaTiO_{3-x}$ structure with oxygen-related defects, which is formed, in particular, at annealing of the $BaTiO_3$ ceramics in high vacuum) [2]. Semiconductor ceramics is used in electronics and electrical engineering. We have developed technology for vacuum brazing of the $BaTiO_{3-x}$ perovskite semiconductor ceramics with application of braze alloys which contain adhesively active component, for example, titanium [3]. The brazing is performed in high vacuum at temperature 700–1000 °C, that's why it can not be used for joining the $BaTiO_3$ ferroelectric ceramics.

Barium titanate of stoichiometric composition, which has high ferro- and piezoelectric properties, may be heated without changes only in the environment containing oxygen (air). For joining such materials special braze alloys and technological processes are used. A favorable factor consists in the fact that oxygen, dissolved in certain metals, enables significant increase of wettability and adhesion of these metals to ceramics. Influence of oxygen on wettability and surface and interphase tension of the metal melts was investigated in [4–6]. It was established that oxygen effectively increases adhesion of copper, silver, nickel and some other metals to ion compounds, for example, oxides. The following systems were investigated in detail: Cu–O–Al_2O_3, Cu–O–MgO, Ni–O–Al_2O_3, Ag–O–Al_2O_3, Ag–Cu–O–Al_2O_3. Of special interest in this respect is the Ag–Cu–O system. We made assumption that metal-oxygen technology is also applicable for joining ferroelectric barium titanate.

According to [7], adhesively active action of oxygen is explained by the fact that addition into a molten metal of some metalloid, which has sufficient affinity to electrons, pulls back the latter from atoms of the metal. They transform into positive ions which are bound with the solid phase anions, that causes wetting of the ion crystal with a metal melt.

At present only one work [8] is known, which is devoted to brazing of the $Pb(Mg_{0.33}Nb_{0.67})O_3$ perovskite compound using alloys of the Ag–CuO system. Scientific basis of this process is not yet developed, and reasons of wetting action of oxygen are not explained. Unfortunately, the authors of [8] are not, evidently, aware of our works of 1960–1970s [4–6] which concern oxide materials.

Purpose of this work is investigation of wettability of the $BaTiO_3$-base ceramic ferroelectric materials with a metal melt, development of compositions of braze alloys and technological conditions for producing brazed joints of the $BaTiO_3$ ceramics for joining with each other parts of the ceramics and the ceramics with metals, and deposition of the adhesively strong metal coating on surface of the ferroelectric perovskite ceramics. As basis of the braze alloys the Ag–Cu–O system alloys were used.

Specimens of barium titanate-base ceramics were specially produced using solid phase synthesis in laboratory of M.D. Glinchuk (the I.M. Frantsevich IPMS, NAS of Ukraine). Used in the experiments disks from the $BaTiO_3$ ceramics had diameter 20 m and thickness 3 mm. Porosity of the specimens was not more than 3.5 %. Substrates from the $BaTiO_3$ ceramics were ground and polished. Roughness of the surface equaled 0.02. Degree of the $BaTiO_3$ ceramics wetting was investigated using the sitting-drop method.

Experiments and technological processes were performed in air environment (such investigations were

never carried out yet). A special installation was designed, in which experiments were carried out in flowing oxygen at insignificant back pressure. Temperature of the experiment was 980, 1050, 1100 °C. Commercially pure oxygen was used. It was assumed that insignificant impurities of nitrogen and some other elements would not exert significant influence on results of the experiments.

Change of the $BaTiO_3$ ceramics contact angle θ depending upon content of copper in the melt is presented in Figure 1. At temperature 980 °C under vacuum conditions contact wetting angle for pure silver equaled about 130°, in air ---- 96°, and in pure oxygen ---- 75°. Addition of about 10 at.% Cu into silver caused reduction of the contact wetting angle down to 45--47° (in air environment) and almost full spreading of the alloy ($\theta \approx 5$--10°) in pure oxygen.

Temperature increase intensifies wetting process ---- contact angle reduces up to 25--30° in air environment (at 10 at.% Cu in silver melt) [9]. In case of using pure oxygen full spreading may be achieved as soon as at 6--7 at.% Cu.

Reasons of high capillary activity of the alloys in pure oxygen consist in significant equilibrium concentration of oxygen in the melt at its high partial pressure in the environment (partial pressure of oxygen in air equals 21 kPa, pure oxygen ---- 100 kPa). According to Siverts law, concentration of oxygen, dissolved in solution of silver in air, equals

$$[O]^{Ag}_{air} = k\sqrt{0.21},$$

and in pure oxygen

$$[O]^{Ag}_{pure\ ox} = k\sqrt{1}.$$

As far as solubility of oxygen in silver in air at 980 °C equals 10.5 cm^3/g, one may calculate that in pure oxygen it will be 2.2 times higher, i.e. about 22.9 cm^3/g.

So, brazing of the $BaTiO_3$ ferroelectric ceramics may be performed in air environment, but it is better to perform it in pure oxygen.

In the ceramics/ceramics combination braze alloy of the Ag + 10--15 at.% Cu (in air environment) and Ag + 3--5 at.% Cu (in pure oxygen) compositions was used.

In joining of ferroelectric ceramics with a metal one has to use as the latter, as showed the practice, platinum which ensures strong similar brazed seams.

An option for applying a silver-copper coating was developed with subsequent brazing to it of a platinum conducting electrode, the function of which successfully fulfilled a silver wire.

Tear and shear strength of the brazed joints was determined. It is known that it depends upon strength of the ceramics itself. Strength of the specimens of produced by us brazed joints equaled from 20 to 50 MPa. It is possible to increase these values if one uses pore-free well sintered ceramics (strength of dense ceramics from aluminium oxide may constitute about 100 MPa). It should be noted that strength of

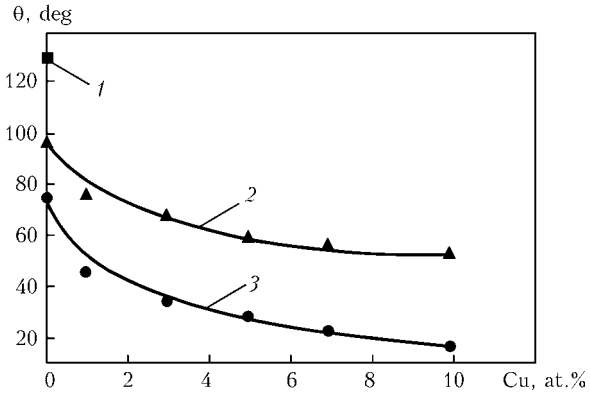

Figure 1. Dependence of contact wetting angle θ of $BaTiO_3$ ceramics by Ag--Cu--O system melts upon content of copper in them at 980 °C: *1* --- melt of pure silver in vacuum; *2, 3* ---- melt of Ag--Cu system in air environment and pure oxygen, respectively

brazed joints often is not a critical characteristic of the perovskite ceramics/metal melt contact, because in practical use of devices on basis of ferroelectric materials mechanical loads are not very significant.

An important task is application of a thin metal coating on the ferroelectric ceramics (for example, interlayers of a capacitor). This requires ensuring of high wetting with a metal of the ceramics surface. Theoretically for producing a continuous film from a molten metal it is necessary that spreading factor had a positive value:

$$K = W_a - W_c,$$

where W_a and W_c, are the works of adhesion and cohesion, respectively.

This may be implemented if pure oxygen is used as the atmosphere. In case of the air environment special methods were used: the CuO copper oxides were applied on the ceramics in the form of a powder and annealed in air for formation of a continuous layer, and then a mixture of silver and platinum powders was applied and annealed at 970 °C, whereby in the system were present a metal melt and a solid metal (platinum) in a highly dispersed state, due to which

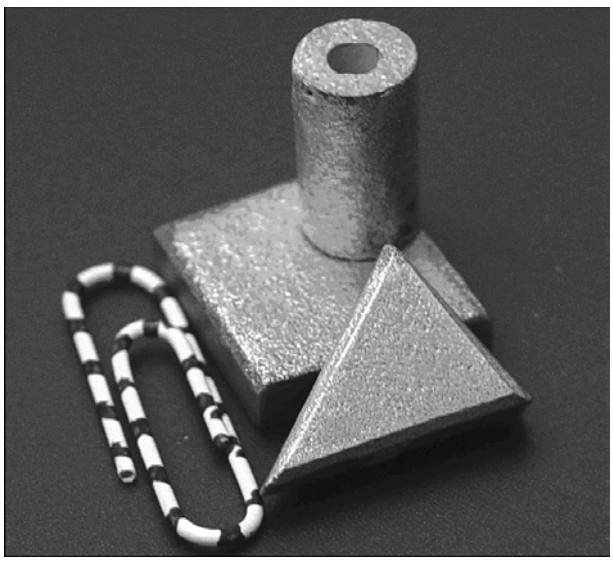

Figure 2. Specimens of $BaTiO_3$ ferroelectric ceramics metallized using metal-oxygen technology

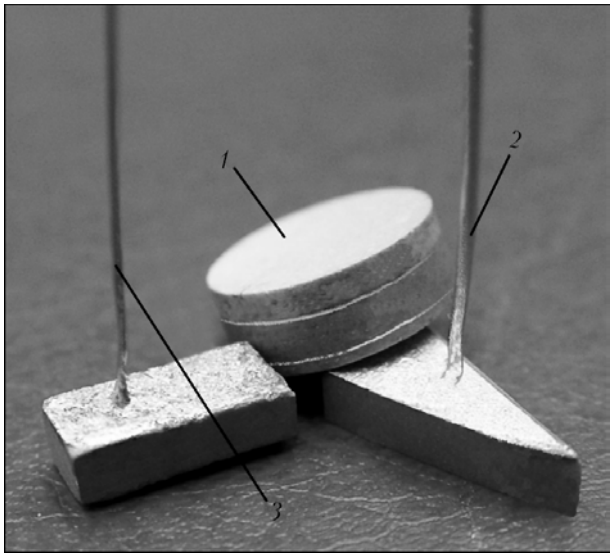

Figure 3. Brazing and metallization of $BaTiO_3$ ceramics using metal-oxygen technology: *1* ---- ceramics–ceramics joint; *2* ---- platinum wire–ceramics; *3* ---- silver wire--ceramics

homogeneity of the coating was preserved. Specimens of the metallized $BaTiO_3$ ferroelectric ceramics are presented in Figure 2.

Using the metal-oxygen technology brazed joints of the $BaTiO_3$ ferroelectric ceramics, brazed with each other and with metal electrodes, were produced (Figure 3).

So, for the first time wetting of the $BaTiO_3$ ceramics in pure oxygen was investigated. Application of oxygen environment at pressure 100 kPa intensifies capillary properties of the Ag--Cu--O system melts and reduce contact wetting angle up to full spreading at content 7--10 at.% Cu in the melt.

On basis of the data obtained the metal-oxide technology for metallization and brazing of the $BaTiO_3$ ceramics in air and pure oxygen was developed.

1. Rubashov, A.M., Berdov, G.I., Gavrilov, N.V. et al. (1980) *Heat-resistant dielectrics and their brazed joints with metals in new engineering*. Moscow: Atomizdat.
2. Bursian, E.V. (1974) *Nonlinear crystal (barium titanate)*. Moscow: Nauka.
3. Najdich, Yu.V., Sidorenko, T.V., Durov, A.V. (2007) Processes of metallization and brazing of perovskite ceramics on the base of barium titanate. *Adgeziya Rasplavov i Pajka Materialov*, **40**, 63--69.
4. Eremenko, V.N., Najdich, Yu.V. (1959) Wetting of oxide surfaces by metal-oxygen solutions. *Elektronika*, **4**, 136.
5. Eremenko, V.N., Najdich, Yu.V., Nosonovich, A.A. (1960) Surface activity of oxygen in copper-oxygen system. *Zhurnal Fiz. Khimii*, 34(**5**), 1018.
6. Najdich, Yu.V., Eremenko, V.N. *Method of brazing of ceramic parts*. USSR author's cert. 149020. Int. Cl. 49 H 25. Publ. 05.08.62.
7. Najdich, Yu.V. (1972) *Contact phenomena in metallic melts*. Kiev: Naukova Dumka.
8. Erskine, K.M., Meier, A.M., Pilgrim, S.M. (2002) Brazing perovskite ceramics with silver/copper oxide braze alloys. *J. Mater. Sci.*, **37**, 1705.
9. Najdich, Yu.V., Sidorenko, T.V. (2008) Processes of wetting of perovskite $BaTiO_3$-ceramics by metallic melts. *Dopovidi NAN Ukrainy*, **9**, 99--104.

IMPROVED METHOD FOR CALCULATING MAGNETIC-PULSE WELDING CONDITIONS

A.S. PISMENNY, I.V. PENTEGOV, E.P. STEMKOVSKY, D.A. SHEJKOVSKY, V.M. KISLITSYN and **A.V. LAVRENYUK**
E.O. Paton Electric Welding Institute, NASU, Kiev, Ukraine

The method for calculating magnetic-pulse welding conditions is suggested allowing for changes of inductivity of the parts being joined at their relative displacement. It is shown that it has to be used in those cases when energy necessary for processing of the metals constitutes a significant portion of the energy accumulated in the capacitor bank (for example, for joining parts of big diameter).

Keywords: *magnetic-pulse welding, inductivity of parts, method of calculation, optimum welding conditions*

In [1] a simplified method for calculating magnetic-pulse welding (MPW) conditions is suggested with complex application of analytical and numeric methods of calculation on a personal computer.

Below the attempt is made to develop an improved method for analysis of the processes occurring in MPW of cylindrical pipes with a single-turn inductor (Figure 1) which most fully correspond to the real processes. It is assumed that at a discharge of the capacitor bank on the inductor and in process of movement of the flyer part inductance of the discharge circuit increases, whereby movement of the pipe starts at the instant in which its material achieves state of plasticity.

Time of the capacitor bank discharge is divided into small sub-intervals of Δt duration, and all parameters of the discharge circuit in each such n-th time sub-interval are assumed invariable.

Values of all necessary parameters at the end of the first sub-interval Δt are initial conditions for the next time sub-interval. Indices of the parameters indicate their value in certain instants of time. Zero index indicates value of the parameter at the beginning of the first time sub-interval, index 1 ---- at the end of the first time sub-interval and beginning of the second time sub-interval, etc.

The whole process of the discharge is divided into three time intervals:

I ---- beginning of the discharge. Pressure on the flyer part is not yet equal to a certain limit value of

P_0. At such value yield strength of the material σ_y is not achieved yet, the flyer part is immovable, and current in each sub-interval is determined according to the formula for the fluctuation process of the capacitor bank discharge, whereby all parameters of the discharge circuit are invariable in the process of the discharge interval;

II ---- continuation of the capacitor bank discharge process at the pressure higher than P_0 from the instant of beginning of the flyer part motion till the instant of collision. The discharge current in each interval changes according to another law for which first of all non-zero initial conditions and change of inductivity of he flyer pipe are characteristic;

III ---- discharge process from the instant of collision of the parts till termination of the capacitor bank discharge. For the discharge current in each sub-interval of this interval constancy of the discharge circuit parameters is characteristic, whereby initial value of current and voltage in the capacitor bank corresponds to values of current and voltage at the end of the second time interval of the capacitor bank discharge.

Let us consider the processes which occur in I interval when the flyer part is still immovable. We will use the following dependence for the considered method of calculation [1]:

$$B(t) = \frac{\mu_0 K_R}{b_p} i(t), \qquad (1)$$

where $B(t)$ and $i(t)$ are respectively the magnetic induction in the working gap and the discharge current in I interval; μ_0 is the magnetic constant equal to $4\pi \cdot 10^{-7}$ H/m [2]; $K_R = 1 - \frac{\Delta_1}{\pi b_p}\left(1 - e^{-\pi \frac{b_p}{\Delta_1}}\right)$ is the Rogowski coefficient [3].

Pressure of the magnetic field on the flyer part is determined from the expression

$$P(t) = \frac{B^2(t)}{\mu_0}. \qquad (2)$$

Pressure on the flyer part, at which yield strength σ_y of the material is achieved and which depends only upon properties of the material and the geometrical dimensions, is determined from the expression which proceeds from the balance of forces acting on surface of the pipe and in its cross section:

$$P_0 = \frac{\Delta_p}{R_p}\sigma, \qquad (3)$$

where R_p is the mean radius of spread outward area of the flyer part in the welding zone.

Inductance of the discharge circuit L_0 consists of the constant within the capacitor bank discharge time inductance L, which is inductance of the external circuit, and invariable within the time of I interval inductance of the inductor--flyer part system L_{pt0}:

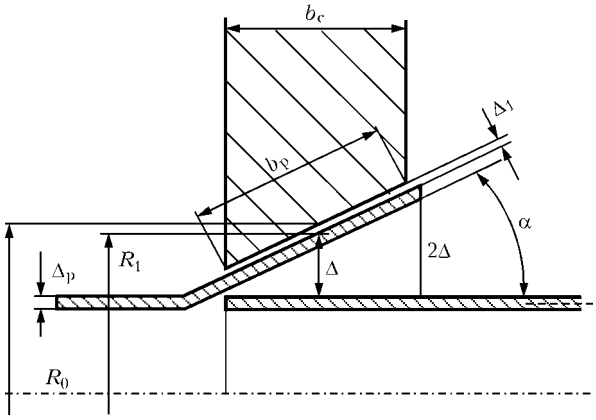

Figure 1. Scheme of MPW implementation at acceleration of pipe area to be deformed: R_0, R_1 ---- respectively internal diameter of inductor-concentrator and external diameter of flyer part in center of spread outward area; Δ_p ---- wall thickness of flyer pipe; Δ, Δ_1 ---- mean values of gap between pipes being joined, as well as between inductor-concentrator and pipe respectively; α ---- angle of pipe spreading outward; b_p ---- width of overlapping; b_c ---- width of working area of inductor-concentrator

$$L_0 = L + L_{pt0},$$

where

$$L_{pt0} = 2\pi \frac{\mu_0 K_R}{b_p} R_p \Delta_1.$$

Angular frequency of the discharge is found from the formula

$$\omega_0 = \sqrt{\frac{1}{CL_0} - \frac{R^2}{4L_0^2}}. \qquad (4)$$

Instant value of the discharge current in I interval is determined from expression [4]

$$i(t) = \frac{U_c}{\omega_0 L_0} e^{-\frac{R}{2L_0}t} \sin \omega_0 t, \qquad (5)$$

where U_c is the capacitor bank initial voltage; R is the discharge circuit active resistance.

By means of the discharge current passage, pressure on the flyer part increases till it gets equal to pressure P_0 determined from formula (3). By substitution in (2) of the expressions (1), (5) and equating $P(t)$ to P_0 value we get after transformations equation for determining t_0 ---- the time at which pressure on the flyer part achieves the P_0 value:

$$\sqrt{\frac{P_0}{\mu_0}} \frac{b_p}{K_R} = \frac{U_c}{\omega_0 L_0} e^{-R\frac{t_0}{2L_0}} \sin \omega_0 t_0. \qquad (6)$$

Transcendent equation relative t_0 (6) is solved by numeric methods using a personal computer.

In II time interval, inductance of the discharge circuit L_n consists of a constant inductance L during discharge of the capacitor bank and inductance of the inductor-- flyer part system L_{ptn}. Inductance L_{ptn} in process of the capacitor bank discharge changes in II interval thus changing conditions of the capacitor bank discharge, that's why in the index the interval number is present.

For calculating parameters of welding conditions on the personal computer we find initial conditions for II time interval of the capacitor bank discharge (current i_0, active losses within time of I time interval W_{R_0}, pressure on the flyer part p_0 and the capacitor bank voltage U_0):

$$i_0 = \frac{U_c}{\omega_0 L_0} e^{-\frac{R}{2L_0}t_0} \sin \omega_0 t_0, \quad (7)$$

$$W_{R_0} = \int_0^{t_0} i^2(t) R dt, \quad (8)$$

$$p_0 = \frac{\mu_0 K_R^2}{b_p^2} (i_0)^2, \quad (9)$$

$$U_0 = U_c - \frac{1}{C} \int_0^{t_0} i(t) dt. \quad (10)$$

Initial conditions of other parameters necessary for calculation in II interval equal zero.

In second area the flyer part starts to move. Movement of the part causes increase of the discharge circuit inductance thus changing conditions of the capacitor bank discharge.

When determining regularity of the discharge circuit inductance change, one has to take into account the fact that it consists of the inductance, which within the time of the capacitor bank discharge remains invariable, and the inductance, which increases within the time of the discharge. Constant inductance L is usually known, while variable part of the inductance $L_{pt(n+1)}$ for $(n + 1)$-th interval Δt is found from the expression

$$L_{pt(n+1)} = \pi \frac{\mu_0 K_{R_n}}{b_p} [R_0^2 - (R_1 - S_n)^2], \quad (11)$$

where S_n is the way passed by the flyer part in n-th interval; K_{R_n} is the Rogowski coefficient in n-th interval.

Value of current in II time interval for $(n + 1)$-th time interval is found from formula proceeding from Kirchhoff equation for a considered circuit in n-th time sub-interval:

$$i_{n+1} = i_n + \frac{U_n - i_n R}{L_n} \Delta t, \quad (12)$$

where U_n is the voltage in capacitors in n-th interval.

Pressure on the flyer part in $(n + 1)$-th sub-interval is determined from formula

$$p_{n+1} = \mu_0 \frac{K_{R_n}^2}{b_p^2} i_n^2. \quad (13)$$

Losses in active resistance of the machine discharge circuit in time interval $t = (n + 1)\Delta t$ equal

$$W_{R_{(n+1)}} = R i_n^2 \Delta t + W_{R_n}. \quad (14)$$

Increment of the flyer part velocity within time Δt in the n-th sub-interval is determined from formula

$$\Delta v_n = [p_n - P_0] \frac{\Delta t}{\Delta_p \gamma_p}. \quad (15)$$

Velocity of the flyer part at the end of the $(n + 1)$-th interval is

$$v_{n+1} = v_n + \Delta v_n, \quad v_0 = 0. \quad (16)$$

The way passed by the flyer part at the end of the first sub-interval in II interval is

$$S_{n+1} = S_n + v_n \Delta t, \quad S_0 = 0. \quad (17)$$

Time of the process is determined according to the expression

$$t_{n+1} = t_0 + \Delta t n. \quad (18)$$

Inductance of the discharge circuit at the end of $(i + 1)$-th time sub-interval is

$$L_{n+1} = L + L_{ptn}. \quad (19)$$

Using expressions (11)–(19) for $(n + 1)$-th time sub-interval we make a system of equations for calculating on a personal computer which has the form:

$$\begin{cases} i_{n+1} = i_n \dfrac{U_n - i_n R}{L_n} \Delta t, \\ K_{R_n} = 1 - \dfrac{\Delta_1 + S_n}{\pi b_p} (1 - e^{-\pi \frac{b_p}{\Delta_1 + S_n}}), \\ p_{n+1} = \mu_0 \dfrac{K_{R_n}^2}{b_p^2} i_n^2 n, \\ W_{R_{(n+1)}} = R i_n^2 \Delta t + W_{R_n}, \\ v_{n+1} = v_n + \left[\mu_0 \dfrac{K_{R_n}^2}{b_p^2} i_n^2 - P_0 \right] \dfrac{\Delta t}{\Delta_p \gamma_p}, \\ S_{n+1} = v_n \Delta t + S_n, \\ L_{n+1} = L + \pi \mu_0 \dfrac{K_{R_n}}{b_p} [R_0^2 - (R_1 - S_n)^2], \\ U_{n+1} = U_n - i_n \dfrac{\Delta t}{C}, \\ t_{n+1} = t_0 + \Delta t n. \end{cases} \quad (20)$$

II time interval finishes after the flyer part that passes the way S (mean value of the gap between the pipes being joined) touches the immovable part.

In Figures 2 and 3 the curves are built, from which it follows that the results obtained from the improved method differ approximately by 15 % from the results obtained according to the method that does not take into account change of the inductance, that proves the fact that by means of the pipe diameter increase one has to use the developed methodology.

For determining in a specific case necessary version of the calculation method (without allowing or allowing for inductance change of the parts during welding) it is necessary to calculate value of kinetic energy of the flyer part W_k using the given below formula:

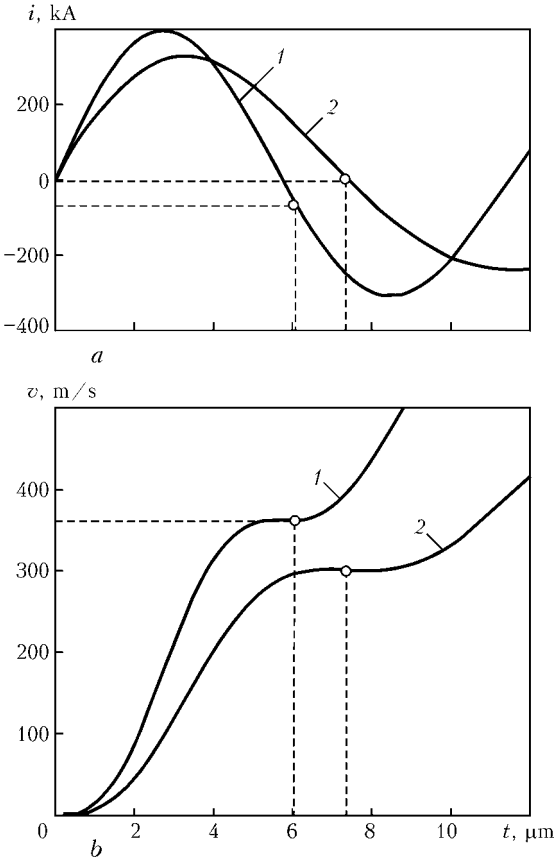

Figure 2. Curves of discharge current (*a*) and speed at acceleration of area to be deformed (*b*) of aluminium pipe of 80 mm diameter: *1* — simplified methodology of calculation [1]; *2* — developed methodology

$$W_k = \frac{m v^2}{2}, \tag{21}$$

where

$$m = 2\pi R_p \Delta_p \gamma_p b_p. \tag{22}$$

Comparison of this value with value of the whole accumulated in the capacitor bank energy $W = (C U_c^2)/2$, calculated using the simplified calculation, allows selecting the version of the calculation method. If difference of the energies does not exceed 10 %, one may use method of calculation described in [1]; if difference is more than 10 % it is necessary to use the method suggested in this work which takes into account change of inductance of the parts being joined.

It should be noted that when using considered method for producing quality welded joints, the time of the magnetic field penetration through the flyer pipe should be longer than flight time of the flyer pipe.

CONCLUSIONS

1. Calculation of the MPW conditions with a single-turn inductor in joining of cylindrical pipes of big diameter has to be carried out taking into account change of inductance of the parts being joined, that will allow ensuring high accuracy of calculations in comparison with the known methods and real reflecting processes occurring in the welding.

2. It was determined that the higher is kinetic energy acquired by the flyer part, the higher is amendment ensured by the suggested method of calculation. If amendment is less than 10 %, one may use a simplified method of calculation, if more ---- the improved one.

3. For ensuring high accuracy of the suggested method for calculating the MPW conditions it is necessary to take into account time when the part starts to move, within which the flyer part is in immovable state till pressure on it still has not yet achieved a certain boundary value, at which yield strength of the material of the parts is achieved.

4. The developed method is fit not just for calculating the MPW conditions, but also for application in related technologies (for example, in pressure processing of metals, etc.).

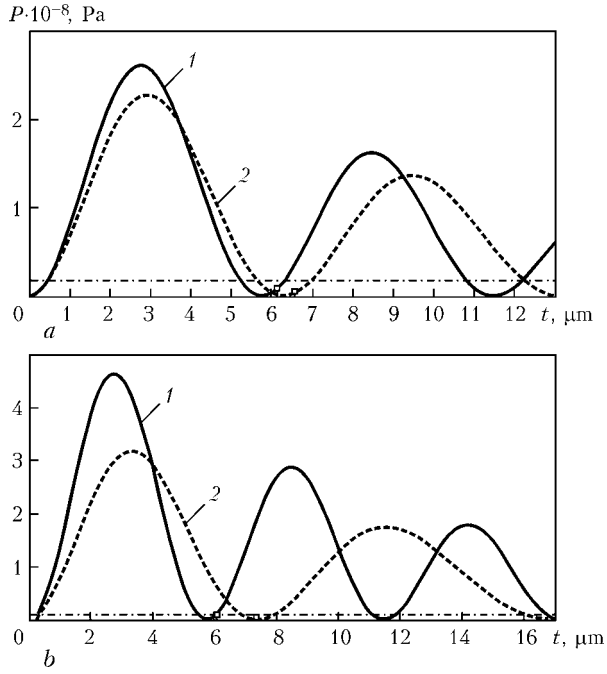

Figure 3. Calculated instant value of magnetic pressure $P(t)$ for pipes from aluminium alloy of 20 (*a*) and 80 (*b*) mm diameter: *1* — curve according to simplified methodology of calculation [1]; *2* — according to developed methodology; dash-dotted curve — according to given methodology

1. Pismenny, A.S., Pentegov, I.V., Stemkovsky, E.P. et al. (2004) Calculation of modes of magnetic-pulse welding. *The Paton Welding J.*, **11**, 13–16.
2. Key, D., Lebi, T. (1962) *Tables of physical and chemical constants*. Moscow: Fizmatgiz.
3. Vasyutinsky, S.B. (1970) *Problems of theory and calculation of transformers*. Leningrad: Energiya.
4. Paton, B.E., Lebedev, V.K. (1969) *Electric equipment for resistance welding. Theory elements*. Moscow: Mashinostroenie.

INCREASE OF CRACK RESISTANCE OF SHROUDED TRAVELING ROLLS IN HIGH-SPEED HARDFACING

V.V. CHIGARYOV, V.I. SHCHETININA, S.V. SHCHETININ, K.K. STEPNOV, N.G. ZAVARIKA and **V.I. FEDUN**
Priazovsky State Technical University, Mariupol, Ukraine

Regularities of influence of high-speed electric arc hardfacing with a low running energy on welding stresses and crack resistance of the deposited metal are established. Method for the high-speed hardfacing of shrouded traveling rolls has been developed.

Keywords: *electric arc hardfacing, shrouded traveling roll, carbon steel, running energy, strain, welding stresses, microstructure, impact toughness, cracks, wear resistance*

Main parts of metallurgical equipment include traveling rolls which are manufactured from high-carbon steels and operate under conditions of high specific pressure. This limits use of the hardfacing for shrouded traveling rolls which are manufactured by interference fit on an axle of the shroud. As a result stresses occur in the shroud which may cause damage of the equipment. Because of this reason hardfacing of shrouded traveling rolls usually is not performed.

Service life of the rolls is determined by their crack- and wear resistance, material consumption factor, specific consumption of materials in the process and production cost of the rolled metal. That's why increase of the service life is an important scientific-technical problem.

For the purpose of increasing crack resistance the high-speed electric arc hardfacing [1] with low running energy is used, characteristic for which are change of the arc existence conditions, reduction of heat input, increase of the rate of heating and cooling of the molten metal and heat-affected zone (HAZ) that causes change of conditions of the pool solidification [2, 3], level of strains, welding stresses and quality of the deposited metal.

This influence of running energy on crack resistance of the deposited metal is contradictory [2, 4, 5], and action of the electrode shape and running energy on strains, welding stresses and properties of the deposited metal was investigated not sufficiently yet.

The goal of this work is investigation of peculiarities of increasing crack resistance of the deposited metal and development of the method for high-speed hardfacing of shrouded traveling rolls at low running energy.

In electric arc hardfacing vacancies occur in structure of the deposited metal under action of heat. In zone of their formation occurs disturbance of static equilibrium of the interatomic interaction forces, which stipulates shift of the adjacent atoms from their equilibrium positions and microdistortion of the crystalline lattice [2].

As a result of heat input in process of hardfacing the metal is subjected to action of the heat strain cycle, upon which depend microdistortion of the crystalline lattice and microstresses. The heat strain cycle was determined using the strain gage, function of which performed an electron micrometer operating on basis of a movable-electrode tube. Observed strains ε_o and thermal cycle of heating of a point located between legs of the strain gage were measured using the strain gage on basis 0.01 m. Change of the strain level in process of hardfacing and thermal cycle of heating of the point were registered using the oscilloscope. Natural strains of the base metal located at distance $5 \cdot 10^{-3}$ m from the fusion zone were determined using the differential method [6–8]:

$$\varepsilon = \varepsilon_{elast} + \varepsilon_{pl} = \varepsilon_o - \varepsilon_w,$$

where ε_{elast}, ε_{pl}, ε_w are respectively elastic, plastic and welding strains.

Hardfacing of rib of a plate of approximately $(30 \times \times 125 \times 400) \cdot 10^{-3}$ m size was performed using a built-up electrode [9] consisting of two wires and an U-shape tape using the ZhSN-5 ceramic flux which ensured production of the deposited metal of the 25Kh5FMS type. Occurrence of the strains was registered in direction of hardfacing. As a result of measurement of heat strain cycles (Figure 1) it was established that in process of the hardfacing first at bringing nearer of the arc compression of the metal in area of the measurement under action of the expanding metal occurs, and when the arc is located in area of measurement of the heat strain cycle, expansion of the metal in the zone and its extension occur. By means of moving the arc away and cooling compression of the base metal occurs. Both at heating and at cooling instant values of ε_o and ε_w significantly differ which causes development of natural strains ε and welding stresses.

For investigation of the running energy influence on the base metal strains, welding of plates of $(8 \times \times 120 \times 900) \cdot 10^{-3}$ m size and hardfacing of plates of $(30 \times 120 \times 900) \cdot 10^{-3}$ m size were performed using a built-up electrode with different running energies. It was established that at increase of the welding speed and reduction of running energy because of reduction

of heat input, the base metal strains and welding stresses reduce (Figure 2).

Dependence of welding stresses upon efficient running energy is determined from the expression [8]

$$\sigma \geq \mu E \frac{q_e}{vF}, \quad (1)$$

where μ is the Poisson's ratio for carbon steel; E is the modulus of elasticity equal to $19.68 \cdot 10^4$ MPa; F is the plate cross section.

Strain of the plates depends upon welding stresses:

$$f = 0.613l \sqrt{\frac{\sigma - \sigma_{cr}}{E}}, \quad (2)$$

where l is the plate length; σ_{cr} is the critical value of welding stresses which are determined using formula

$$\sigma_{cr} = \frac{\pi^2 E}{12} \left(\frac{\delta}{l}\right)^2, \quad (3)$$

where δ is the plate thickness. At $\sigma > \sigma_{cr}$ deformation of the plate occurs.

It follows from the expressions presented above that welding stresses depend upon strain of the plate:

$$\sigma = \frac{f^2 E}{0.613^2 l^2} + \frac{\pi^2 E}{12} \left(\frac{\delta}{l}\right)^2. \quad (4)$$

By means of the running energy reduction at increase of the welding speed the welding stresses reduce (Figure 2) which significantly increases crack resistance and impact toughness of the welded joints that qualitatively characterizes crack resistance and depends upon structure of the deposited metal.

Influence of the electrode shape and running energy on structure of the deposited metal was established at five-layer hardfacing of plates of $(30 \times 300 \times 400) \cdot 10^{-3}$ m size using wire of $4 \cdot 10^{-3}$ m diameter and tape of $(0.5 \times 45) \cdot 10^{-3}$ m size, which was arranged in longitudinal and cross directions, and the built-up electrode. Hardfacing was carried out using the ZhSN-5 ceramic flux under optimum for each method conditions. Hardfacing using the Sv-08G2S wire electrode of 4 mm diameter was performed under the conditions: current ---- 650--750 A; arc voltage ---- 31--33 V; welding speed ---- $(0.56, 0.83$ and $1.10) \cdot 10^{-2}$ m/s. Hardfacing using the built-up electrode, consisting of the Sv-08G2S wire of 4 mm diameter and tape from the 08kp (rimmed) steel of 0.5445 mm^2 section, was performed under the conditions: current ---- 1950--2050 A, arc voltage ---- 29--31 V; welding speed ---- $(1.4, 2.1$ and $2.8) \cdot 10^{-2}$ m/s. Running energy for each method of welding varied within q_e/v = 1.8, 2.7 and 3.6 MJ/m.

Crack resistance of the deposited metal is determined to a great degree by welding stresses in it which are summed up at hardfacing. In connection with the fact that hardfacing of the wear-resistant layer is performed using five and more runs, welding stresses sharply increase. Due to summing of the welding stresses, thickness of the deposited layer is limited by 25 mm, while increase of these values causes significant increase of welding stresses and formation of spallings in zone of fusion with the base metal which was confirmed in hardfacing of traveling rolls of the mill 1700. The investigations were carried out at a five-layer hardfacing. Properties of the weld metal were determined by investigation of its structure and measurement of the tempering zone and impact toughness of the welded joints.

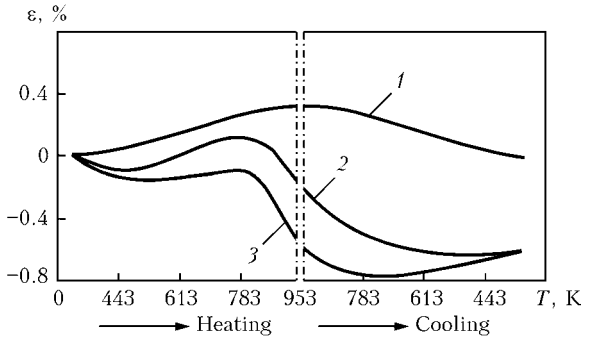

Figure 1. Curves of HAZ thermal strain cycle obtained in direction of hardfacing with application of built-up electrode (q_e/v = = 3.6 MJ/m) at distance $5 \cdot 10^{-3}$ m from fusion zone: *1* ---- free strains; *2* ---- observed strains; *3* ---- natural strains

It was established that at increase of the heating and cooling rates structure of the deposited metal gets refined, contact area and interatomic bond forces increase, and crack resistance gets higher. In hardfacing using the tape, arranged in longitudinal direction, structure of the deposited metal is coarse-grain and inhomogeneous, in case of perpendicular arrangement of the tape the structure gets refined insignificantly and remains the coarse-grain one. In hardfacing using wire and built-up electrodes also refining of the deposited metal structure occurs, it gets finely dispersed and homogeneous and represents a ferrite-cementite mixture.

In similar way gets refined structure of the deposited metal and HAZ in high-speed hardfacing at low running energy (Figure 3) because of increase of the

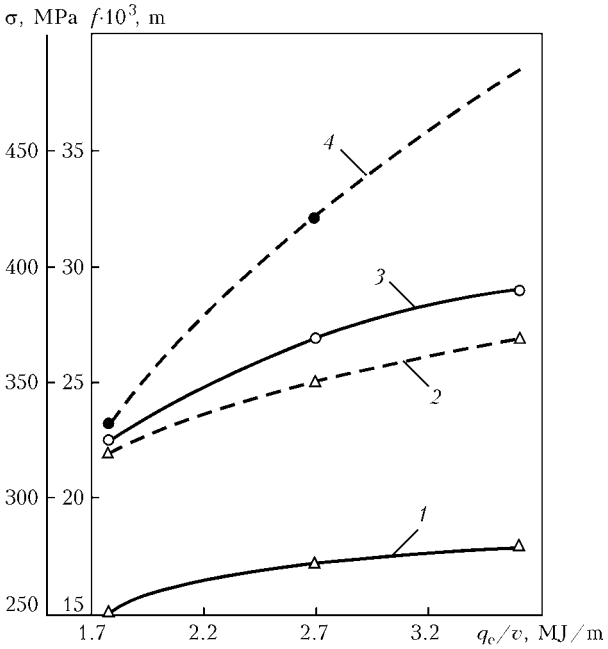

Figure 2. Dependence of welding stresses σ (*3, 4*) and strains f (*1, 2*) in plates of $(8 \times 120 \times 900) \cdot 10^{-3}$ m (dash curves) and $(30 \times 120 \times 900) \cdot 10^{-3}$ m (solid lines) size upon running energy of welding

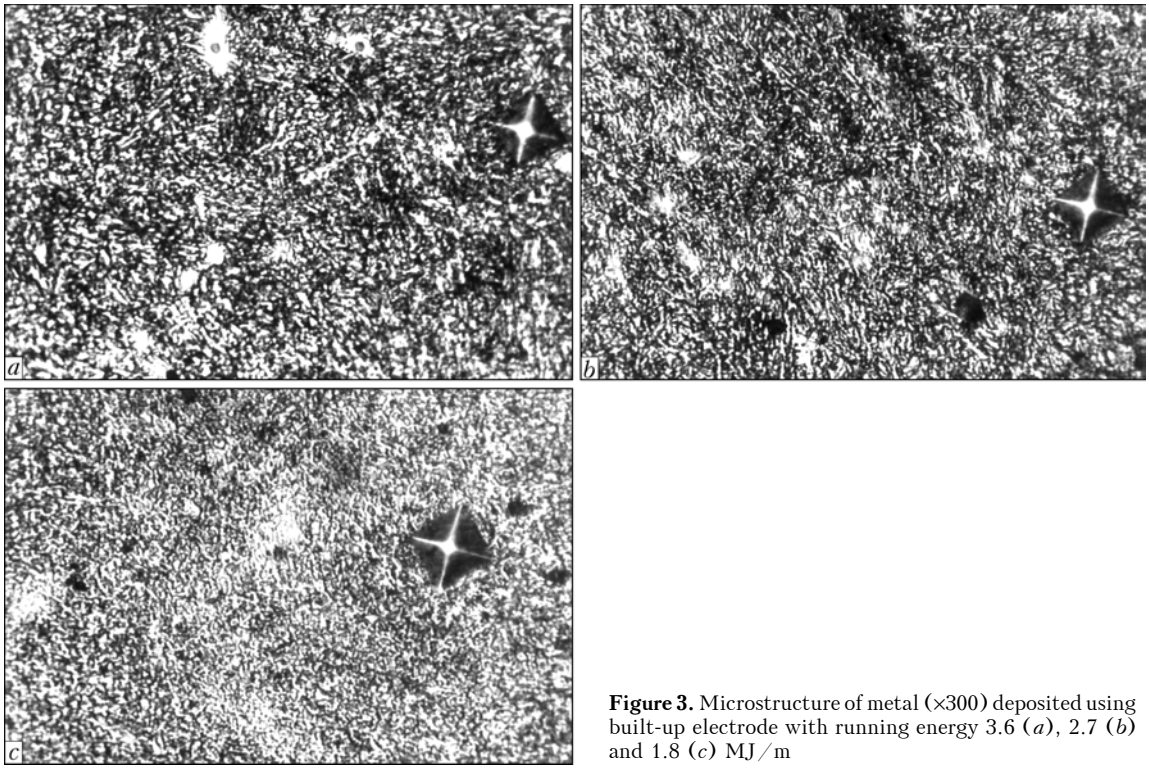

Figure 3. Microstructure of metal (×300) deposited using built-up electrode with running energy 3.6 (*a*), 2.7 (*b*) and 1.8 (*c*) MJ/m

heating, cooling and solidification rates in proportion to the hardfacing rate. Because of minimum microdistortions of the crystalline lattice, changes of microstresses, density of dislocations and fine-dispersed homogeneous structure, crack resistance increases, and joints, produced at low running energy, are characterized by high impact toughness and strength characteristics.

Measurements of impact toughness were performed on welded joints of the 09G2S steel. The 9KhF and 09G2S steels have different chemical composition and propensity to formation of hardening structures. As in hardfacing of the 9KhF high-carbon steels it is difficult to avoid cracks, so in welding of the 09G2S steel it is difficult to ensure impact toughness which would qualitatively characterize crack resistance.

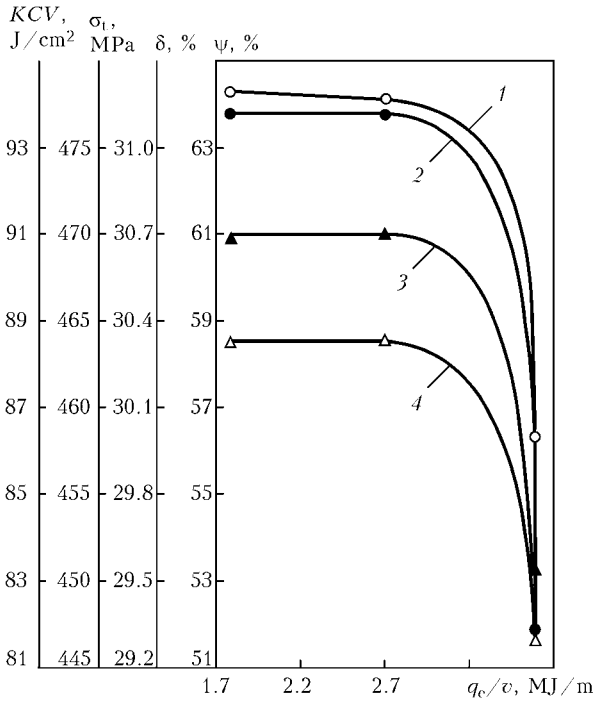

Figure 4. Mechanical properties of welded joints at one-sided welding using built-up electrode: *1* — tensile strength σ_t; *2* — impact toughness *KCV*; *3* — reduction in area ψ; *4* — relative elongation δ

At increase of the welding speed up to 0.021 m/s and reduction of running energy up to 2.7 MJ/m impact toughness first sharply increases and then remains practically invariable (Figure 4). At increase of the welding speed growth of the impact toughness occurs due to refining of the deposited metal structure and reduction of the crystalline lattice distortions, microstresses and density of dislocations, with which origination of the cracks is associated [10]. Similar to impact toughness, under the same conditions change ultimate strength, relative elongation and reduction in area. High values of impact toughness, relative elongation and reduction in area prove increased crack resistance of the deposited metal.

Tensile strength at increase of the welding speed and reduction of running energy gets higher. Its high values and high values of impact toughness and relative elongation are achieved at running energy 2.7 MJ/m and lower, which is confirmed by results of the experiments.

Similar data were obtained in investigation of the electrode shape and running energy influence on static fracture (Figure 5) on specimens of $(957 \times 5520) \cdot 10^{-3}$ m size with V-notch. It was determined that maximum value of static load is ensured at the running energy value 2.7 MJ/m and lower.

It was established in five-layer hardfacing using the ZhSN-5 flux that by means of increase of its rate due to increase of the cooling rate and dispersity of the deposited metal structure, microhardness of the metal gets higher. In HAZ microhardness, measured

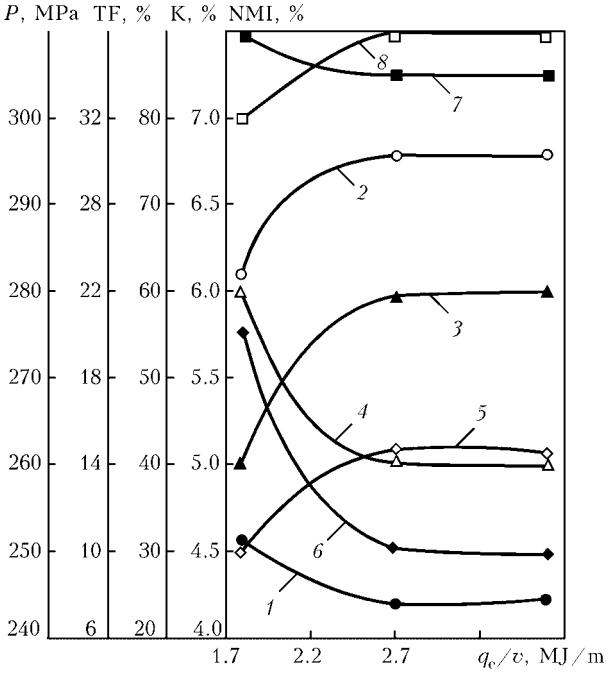

Figure 5. Influence of electrode shape and running energy on quality of welded joints produced with application of wire (*1, 3, 5, 7*) and built-up electrode (*2, 4, 6, 8*): *1, 2* — static load *P*; *3, 4* — non-metal inclusions (NMI); *5, 6* — tough fracture (TF); *7, 8* — quasi-spalling (K)

by the PMT-3 hardness gauge with automatic loading, reduces (Figure 6). Size of the tempering zone depends upon the electrode shape. Its minimum size is characteristic for hardfacing using the tape arranged perpendicularly, which is the result of minimum heat input into side edges of the pool. At longitudinal arrangement of the tape, tempered zone size increases. Use of wire and built-up electrode (Figure 6) increases of the tempered zone size due to increase in heat input into side edges of the pool.

At increase of the hardfacing rate size of the tempering zone reduces as a result of running energy lowering (see Figure 6) which matches available data [11]. Reduction of size of this zone increases resistance against lamination (because in this zone cold cracks may form), improves quality of the deposited metal, and reduces specific loads in rolling which increases wear resistance of the rolls.

At high-speed hardfacing in case of the running energy reduction, penetration depth and share of the base metal participation reduce, gradient of carbon concentrations increases and its diffusion in HAZ into the weld metal intensifies. As a result carbon equivalent in HAZ equals less than 0.45 and cracks do not form.

Despite the fact that the investigations were carried out only for the 09G2S steel, the data obtained were confirmed in hardfacing of the shrouded traveling rolls from the 9KhV steel, because in high-speed hardfacing at a low running energy welding stresses significantly reduce, structure of the deposited metal gets refiner, ductility increases, the HAZ size and specific pressure in rolling of the metal reduce, that excludes failure of the shrouds and increases crack resistance of the deposited shrouded traveling rolls.

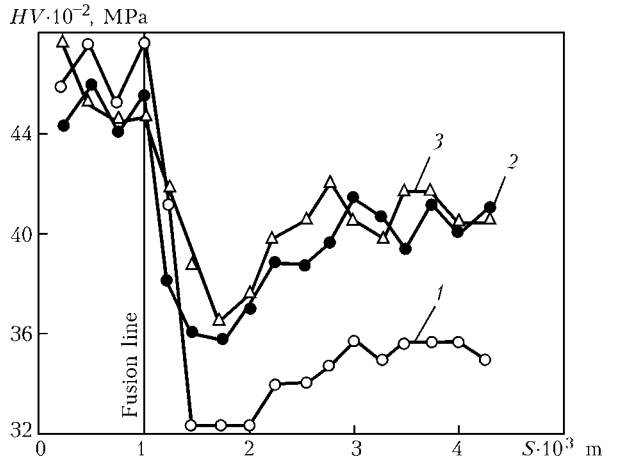

Figure 6. Influence of running energy on microhardness *HV* of deposited metal: *1* — q_e/v = 3.6; *2* — 2.7; *3* — 1.8 MJ/m; *S* — HAZ width

For increasing wear resistance of the shrouded traveling rolls, the energy conservation method of high-speed hardfacing at low running energy was developed [12]. High-speed hardfacing of the shrouded traveling rolls was performed with preliminary and accompanying heating up to 300–350 °C. First a buffer layer was deposited using the Sv-08G2S wire of 5 mm diameter and the AN-60 flux, and then — the wear-resistant layer. Its hardfacing was performed using the Sv-08G2S wire of 5 mm diameter and the ZhSN-5 ceramic flux at running energy 1.3 MJ/m under the following conditions: current — 750–800 A; arc voltage — 32–34 V; hardfacing rate — 75 m/h. After hardfacing heat treatment and slowed cooling were performed.

Energy conservation method of high-speed hardfacing at low running energy was developed which ensures minimum welding stresses, formation of a fine-dispersed homogeneous structure of the deposited metal and, as a result, high crack and wear resistances of the shrouded traveling rolls.

1. Frumin, I.I. (1961) *Automatic electric arc hardfacing*. Kharkov: Metallurgizdat.
2. Prokhorov, N.N. (1976) *Physical processes in metal during welding*. Moscow: Metallurgiya.
3. Shorshorov, M.Kh., Belov, V.V. (1972) *Phase transformations and variations of steel properties in welding*. Moscow: Nauka.
4. Kalensky, V.K., Chernyak, Ya.P., Vasiliev, V.G. et al. (2001) Heat input influence on formation of tears in high-carbon steel building-up with austenitic wires. *The Paton Welding J.*, **11**, 9–12.
5. Dragunov, V.K., Muraviova, T.P., Rodionov, Yu.P. (1990) Electron beam welding of dissimilar alloys applied in electromagnetic devices. *Svarochn. Proizvodstvo*, **4**, 2–4.
6. Okerblom, N.O. (1948) *Welding strains and stresses*. Moscow, Leningrad: Mashgiz.
7. Nikolaev, G.A., Kurkin, S.A., Vinokurov, V.A. (1982) *Strength of welded joints and deformations of structures*. Moscow: Vysshaya Shkola.
8. Vinokurov, V.A., Grigoriants, A.G. (1984) *Theory of welding strains and stresses*. Moscow: Mashinostroenie.
9. Shchetinina, V.I., Chigaryov, V.V., Shchetinin, S.V. *Method of arc welding*. USSR author's cert. 1407719. Int. Cl. B 23 K 9/00. Publ. 07.07.88.
10. Finkel, V.M. (1970) *Physics of fracture*. Moscow: Metallurgiya.
11. Gotalsky, Yu.N., Snisar, V.V., Novikov, D.P. (1981) Methods of narrowing of martensite interlayer in fusion zone of pearlitic steel with austenitic weld. *Svarochn. Proizvodstvo*, **6**, 7–9.
12. Bojko, V.S., Shchetinin, S.V., Klimanchuk, V.V. *Method of renovation and strengthening of cylindrical parts*. Pat. 65092 Ukraine. Int. Cl. B 23 K 9/04. Publ. 15.03.2004.

ARC SPOT WELDING OF OVERLAP JOINTS IN VERTICAL POSITION

L.M. LOBANOV, A.N. TIMOSHENKO and **P.V. GONCHAROV**
E.O. Paton Electric Welding Institute, NASU, Kiev, Ukraine

The technology for vertical spot metal-arc welding of sheet metal without preliminary piercing of holes in the external sheet was developed. Adjustment of parameters of the welding cycle allows producing the high-quality spot joints.

Keywords: *gas-shielded welding, spot overlap joints, structural steels, vertical position*

The arc spot welding (ASW) technology used to weld sheet metal finds application in car building, aircraft engineering, ship building, motor car industry and construction. The ASW technology provides high productivity and quality of operations, saves time and materials. The process is advantageous in the possibility of producing sound overlap joints both without and with holes made in workpieces, as well as fillet and T-joints [1–7].

The car building industry uses mainly semi-automatic CO_2 welding. This method allows making up to 80 % of all the welds, including the arc spot welds. In manufacture of railway cars, sometimes it is necessary to make spot joints in a vertical position. To reduce labour intensity, it is expedient to make some horizontal welds on a vertical plane by ASW.

In ASW of metal over 1.5 mm thick in the vertical and overhead position, it is recommended to make holes in the external sheet [1–3]. Given that ASW is performed with the semi-automatic device by switching on and off of feeding of the welding wire, the quality and consistency of sizes of the resulting spot welds are determined by the skill of a welder. In addition, when performing ASW on the vertical plane it is necessary to overcome difficulties associated with retention of the molten pool metal. Independently of the welder's skill, production of the sound welds can be achieved by programming parameters of the welding process. Existing equipment and technology do not always provide sufficient stability of the welding parameters and, as a consequence, preset sizes of the spot welds according to GOST 14776–79 [8]. Decrease in quality of the joints may be caused by probable deviations. Some welding power supplies have the possibility of programming time of the welding cycle (welding wire feed speed is usually not programmed).

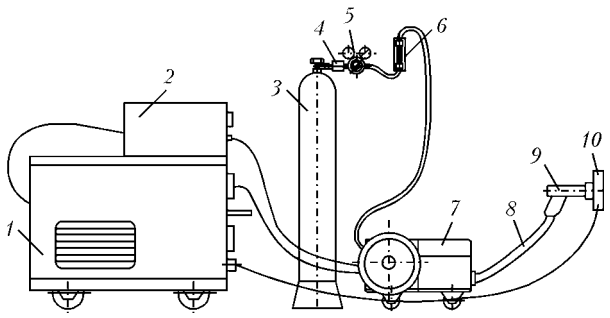

Figure 1. Flow diagram of ASW in vertical position: *1* — welding current source; *2* — control unit for ASW; *3* — carbon dioxide gas bottle; *4* — pre-reducer drier; *5* — reducer; *6* — gas flow rate meter; *7* — electrode wire feed mechanism; *8* — flexible hose cable; *9* — welding torch; *10* — workpiece

The task of this study was to provide the sound spot joints on the sheet metal in a vertical position without preliminary piercing of holes in the external sheet. Accomplishment of this task involves difficulties associated with retention of the molten pool metal, as well as with ensuring of reliable ignition of the arc in the initial period.

The experimental machine for CO_2 arc spot welding in a vertical position (Figure 1) was developed to fulfil the task posed. This machine consists of a welding current source of the VDUCh-500 type, welding wire feed mechanism PDG-500-4, specialised control unit, welding torch with a specialised nozzle, and a lever clamp providing elimination of a gap between the pieces joined.

Characteristic feature of the ASW process is separation of the welding cycles into stages, which differ in their technological purpose and welding parameters [3, 5]. The welding cycle without preliminary piercing of holes in the external sheet is performed in the following stages:

- heating of the surface of an external piece;
- burning through of the external piece and penetration of the second piece. A hole being formed in the external piece and partial penetration occurring in the internal one;
- filling up of the formed hole with molten electrode metal;
- welding up of the crater in the spot weld.

ASW in the vertical position performed under the conditions used for making spot joints in the flat position failed to give positive results. The weld spots had a number of essential defects, such as incomplete filling of the weld pool with electrode metal caused by its flowing down, formation of rolls of the flown-out metal, and undercuts (Figure 2).

Reproducibility of the weld spots was low, which was caused by a considerable effect of the following factors:

Figure 2. Spot joint made in vertical position under the conditions used for ASW in flat position

• different conditions of arc ignition caused by different sizes of the electrode metal drops solidified at the welding wire tip after each welding pulse;

• high heat input into a welded joint: molten metal flows out from the weld pool;

• effect of the gap between the pieces joined and shielding gas flow rate on the appearance and quality of a spot joint;

• shape of the welding torch tip;

• stability of the welding wire feed: the probability of slippage of the wire leads to inaccurate portioning of the depositing metal in formation of a weld spot;

• presence of various contaminants on the surfaces of the pieces joined.

While optimising the technology of ASW in the vertical position, the spots were made on experimental samples (Figure 3) using 1.6 mm diameter solid wire Sv-08G2S and CO_2 as a shielding gas.

To control heat input in making a spot joint, the time pauses between the welding pulses were added to the program of changing the process parameters of welding in the flat position. The program of changing the welding process parameters shown in Figure 4 provided the portioned addition of metal to the weld pool by alternating the welding cycles, as well as the reliable ignition of the welding arc. The need for the reliable arc ignition is attributable to the fact that in metal arc welding the arc does not always starts burning from the first touch, this having a significant effect on implementation of the programmed parameters of spot welding.

The stable arc ignition in ASW is achieved by decreasing the welding wire feed speed at the initial moment of welding (time period t_1). At the required wire feed speeds there is enough time for heating and

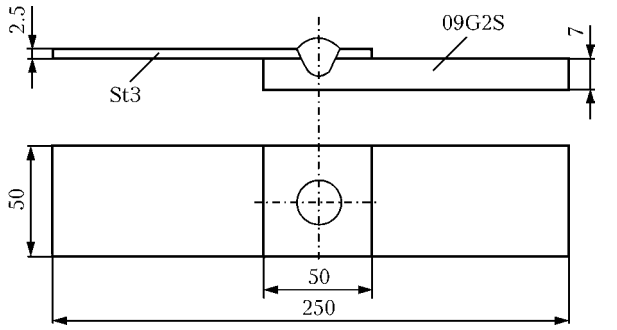

Figure 3. Schematic of experimental sample

melting of the electrode tip, which increases the probability of the arc ignition. At the high wire feed speeds the arc ignition stability decreases to a considerable degree.

The portioned heat input into the weld pool is ensured by alternating welding pulses and pauses, as well as by regulating their time, thus providing the optimal welding cycle, as well as more favourable structure and properties of the weld metal. Cooling of the weld takes place in intervals between the welding cycles, which prevents flowing of the molten metal from the weld pool and provides the satisfactory weld spot formation. Durations of pulses and pauses between the pulses, as well as the welding current are set, which makes it possible to form the final volume of the weld spot and its external surface. As noted in [4, 7], the stressed state in cyclic heat input into a welded joint is much lower than in welding performed under the conditions without pauses between the pulses, or under the conditions without pulses. The ASW parameters can be varied over a wide range, depending upon the ASW cycle, thickness of the pieces joined and diameter of the electrode wire.

Burning through of the first piece with formation of a hole, and partial penetration of the second piece are performed in cycle t_2. Welding in this period is performed under increased parameters.

Welding cycles in time periods t_4 and t_6 provide filling up of the formed hole after the welding cycle in time period t_2 and formation of the weld spot. The first cycle with duration t_4 is performed so that 50--60 % of volume of the deposited metal of the weld spot is provided. Completion of the second cycle (with

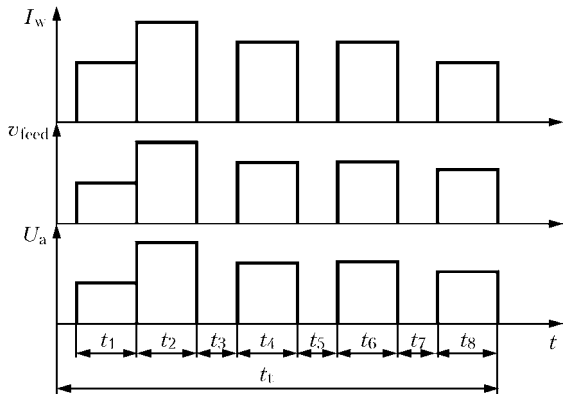

Figure 4. Program of changing of process parameters in ASW in vertical position: t_1–t_8 — duration of pulses and pauses; t_t — total time of the ASW cycle

Parameters of arc spot welding of sheets 2.5 + 7.0 mm thick

Welding cycles	U_w, V	I_w, A	v_w, m/h	t_w, s	t_{pause}, s
t_1	26–28	180–220	100–120	0.4–0.5	–
t_2	40–42	450–500	280–300	1.0–1.3	t_3 = 1.5–2.0
t_4	28–30	230–250	140–160	0.8–.1.0	t_5 = 1.0–1.5
t_6	28–30	230–250	140–160	0.8–1.0	t_7 = 0.5–1.0
t_8	24–.26	170–190	100–120	0.5	–

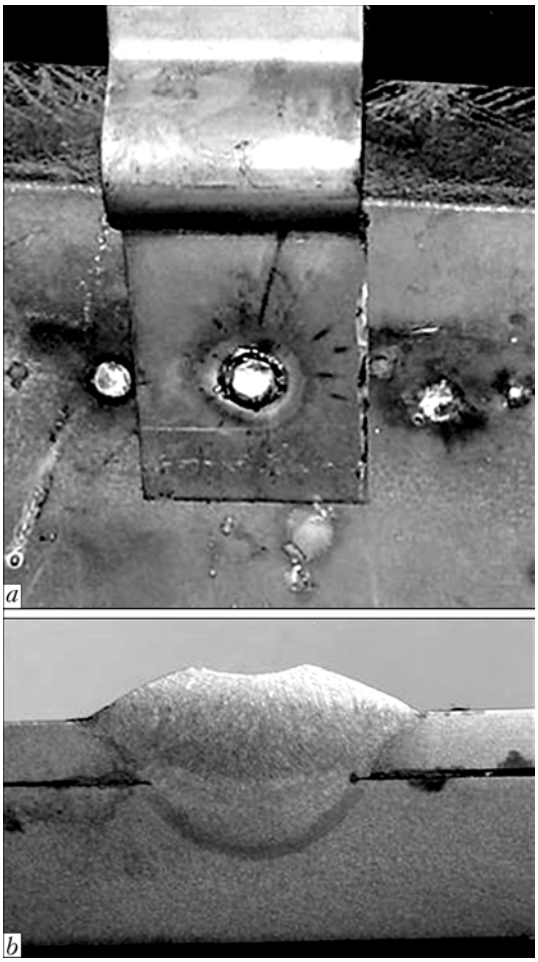

Figure 5. Appearance of spot welded joint produced by ASW in vertical position (*a*) and its macrosection (*b*)

time t_6) allows formation of the final volume of the weld spot. Cooling of the deposited weld metal takes place in time periods t_3, t_5 and t_7 (durations of pauses between the welding cycles). The durations of pauses are set so that the deposited metal volume could solidify during these time periods. Welding up of the crater and formation of the appearance occur in the last welding cycle (time interval t_8 according to the scheme of changing of the welding parameters).

Selection of optimal parameters of ASW was carried out on samples by changing the arc voltage, setting the optimal welding wire feed speed at each welding cycle, and by optimising the time of each welding cycle and pauses between them. The welding parameters are given in the Table.

The quality and size of the spot welds are strongly affected by the duration of each cycle and stability of the welding parameters. Parameters given in the Table provide the high-quality spot joints, which is confirmed by the results of metallographic examinations. As shown in Figure 5, the spot joint has a sound appearance, and rolls of the flown-out metal are absent. The macrosection confirms the absence of undercuts and defects of the type of pores, cracks and slag inclusions. The penetration depth in this case is 3.5 mm, and diameter of the weld spot nugget is 8 mm.

As proved by the investigation results, strength of the weld spot depends upon the metal thickness and diameter of the weld spot nugget, as well as upon the gap between the pieces welded. The presence of the gap in excess of 0.5 mm may cause flowing of the molten metal into the gap, and may lead, as a consequence, to production of a defective joint. In the cases where the gaps between the pieces joined were not in excess of 0.5 mm, shear tests of specimens with a weld spot nugget diameter of 7–9 mm showed that a fracture force was $\frac{19{,}000\text{–}32{,}000}{27{,}000}$ N, which is enough to provide sufficient performance of a spot joint.

Therefore, the high-quality spot joints are provided by regulating parameters of the welding cycles in ASW of the sheet metal in a vertical position. The joints can find application in manufacture of frame structures of modern freight and passenger cars.

1. Voropaj, N.M. (2004) Specifics of arc spot shielded-gas welding processes (Review). *The Paton Welding J.*, **7**, 26–31.
2. Potapievsky, A.G. (2007) *Gas-shielded metal arc welding*. Pt 1: Active-gas welding. Kiev: Ekotekhnologiya.
3. Tereshchenko, V.I., Sharovolsky, A.N., Sidorenko, K.A. et al. (1983) Peculiarities of consumable-electrode arc spot CO_2-welding. *Avtomatich. Svarka*, **9**, 51–53.
4. Asnis, A.E., Andrushchenko, S.V., Yushkevich, Z.V. (1986) Influence of stressed state on corrosion resistance of arc spot welded joints. *Ibid.*, **8**, 1–3.
5. Tkachenko, A.N., Voskresensky, A.S. (2005) Application of arc spot welding in fabrication of car bodies. *The Paton Welding J.*, **12**, 22–24.
6. Tatarinov, V.S., Tereshchenko, V.I., Iorsh, E.T. et al. (1986) Corrosion fatigue resistance of overlap joints made by arc spot welding. *Avtomatich. Svarka*, **7**, 46–48.
7. Krylov, S.V., Asnis, A.E. (1983) Increase in impact strength of arc spot welded joints. *Ibid.*, **7**, 17–18, 34.
8. *GOST 14776–79*: Arc welding. Spot welded joints. Main types, structural elements and sizes. Introd. 01.07.80.

INCREASE OF CYCLIC FATIGUE LIFE OF TEE WELDED JOINTS WITH SURFACE CRACKS

V.V. KNYSH, A.Z. KUZMENKO and **A.S. SOLOVEJ**
E.O. Paton Electric Welding Institute, NASU, Kiev, Ukraine

Investigation results on the efficiency of using high-frequency mechanical peening to increase the fatigue resistance of tee welded joints on low-alloy steels containing fatigue cracks on their surface are presented. Two approaches to strengthening tee joints damaged by fatigue cracks are considered.

Keywords: *welded structures, structural steels, tee welded joints, cyclic fatigue life, high-frequency mechanical peening, fatigue crack, strengthening technology*

At the stage of designing welded products or structures operating under the conditions of alternating loading, absence of fatigue damage in them is envisaged for the entire design service life. However, practical experience has shown that in welded structures for various applications, meeting the code requirements to their design and fabrication, fatigue cracks start appearing already at an early stage of operation of constructions or machines [1]. Being the most dangerous kind of defects, fatigue cracks essentially lower the cyclic fatigue life of the damaged elements and structure as a whole.

Replacement of damaged structures by new ones requires considerable expenditure and time, so that the damaged elements of large-sized structures are more and more often subjected to various repair-restoration operations, instead of replacing them. The following can be regarded as the most widely spread types of such repair operations: hole drilling in the crack tips with subsequent mounting of high-strength bolts with their tightening, repair welding with subsequent strengthening, redistribution of post-weld stresses and working loads, inducing favourable residual compressive stresses near the crack tips, etc. [2, 3]. These types of operations are mainly applied in large-sized welded structures, in which the presence of through-thickness fatigue cracks of 20 mm and greater length does not lead to any essential lowering of the load-carrying capacity.

On the other hand, we cannot limit ourselves to just the repair-restoration operations on the damaged parts, as cracks may develop with a high degree of probability in similar components and elements. Therefore, in repair of welded products and constructions their most loaded sound welded joints and joints with shallow surface fatigue cracks should be subjected to strengthening.

It is known that high-frequency mechanical peening (HFMP) of sound welded joints with 50 % and higher level of accumulated fatigue damage significantly improves their fatigue resistance characteristics [4].

Strengthening by other technologies of surface plastic deformation (SPD) of welded joints, containing surface semi-elliptical cracks of a small depth, improves the cyclic fatigue life up to 10 times, depending on the kind of strengthening treatment and crack depth. So, in [5] it is noted that shot blasting of Waspalloy samples with fatigue cracks of 0.67 mm and shorter length increases the sample fatigue resistance 3 times, and at treatment of more than 1 mm cracks no improvement of fatigue resistance is found. In [6] it is shown that peening of tee welded joints with fatigue cracks by a puncher promotes increase of cyclic fatigue life 1--10 times, depending on the crack size. At peening by a puncher of a crack of 1.0--1.5 mm depth, the cyclic fatigue life increases 10 times, at peening of a crack of about 3 mm depth ---- by 1--2.5 times, and at peening of a crack more than 5 mm deep no fatigue life improvement is found. Such a difference in the results is due to different depth of the zone of inducing residual compressive stresses of 0.33 and 2.5 mm at shot blasting and puncher treatment, respectively.

Improvement of fatigue life is observed also at application of strengthening treatments to samples with through-thickness fatigue cracks, and their effectiveness essentially depends on metal thickness [7, 8]. In [7] the results of studying the cyclic crack resistance produced on compact samples 12.5 mm thick with the initial 3 mm crack, point to a slight improvement of the sample fatigue life: after shot blasting ---- by 1.2 times, and after peening by single-pin puncher ---- by 2 times. At small metal thicknesses SPD technologies cause a more significant increase of cyclic fatigue life. In [8] after shot blasting of compact samples 4.2 mm thick with initial 4 mm crack an increase of their fatigue life 2--4 times is noted, depending on the location of the peening zone relative to the crack tip.

The above-mentioned publications demonstrate an increased interest to repair-restoration operations on welded joints with surface fatigue cracks by their strengthening by SPD technologies.

There are no published experimental data on improvement of cyclic fatigue life of welded joints with surface fatigue cracks by application of HFMP technology. On the other hand, in [9] it is noted that

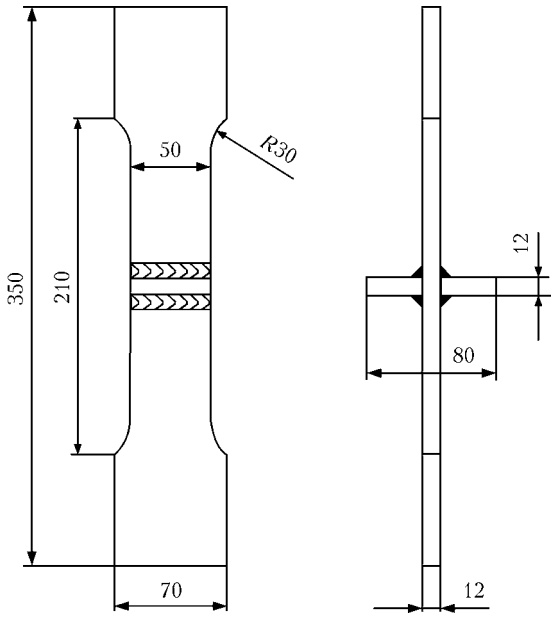

Figure 1. Schematic of a sample of tee welded joint with two transverse stiffeners

strengthening by HFMP technology results in inducing residual compressive stresses on the base metal surface down to 1.7 mm depth. For the case of welded joints (as a result of interaction with the residual tensile stresses) the layer of HFMP induced compressive stresses decreases to the depth of about 1 mm. On the other hand, a 2–3 times increase of the threshold stress intensity factor is noted at HFMP treatment of welded joints in as-welded condition. This leads us to believe that HFMP will turn out to be an effective technology for improvement of fatigue resistance of welded joints with shallow surface cracks.

The purpose of this work is determination of the effectiveness of HFMP technology application to improve the fatigue resistance of tee welded joints on low-alloyed steels with surface fatigue cracks and establishing the features of strengthening of such joints.

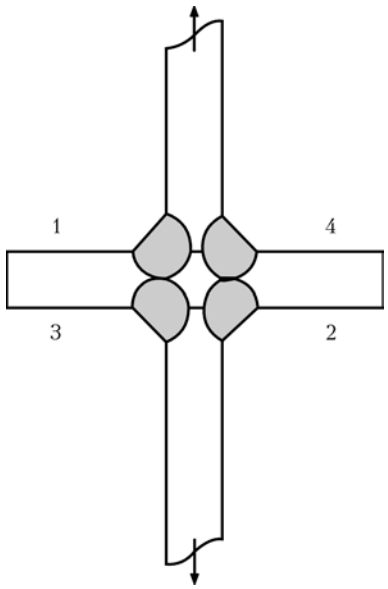

Figure 2. Schematic of a fragment of the tee welded joint with numbered near-weld zones

Experimental studies were conducted on samples of tee joints of steel 09G2S (σ_y = 370 MPa, σ_t = = 540 MPa) and 10KhSND (σ_y = 457 MPa, σ_t = = 565 MPa). Blanks for the samples were cut out of rolled sheets so that their long side was oriented along the rolling direction. Transverse stiffeners were welded by fillet welds from both sides by full-penetration manual arc welding by UONI-13/55 electrodes. The shape and geometrical dimensions of the sample were selected (Figure 1) proceeding from the testing equipment capacity. At joint strengthening by HFMP technology surface plastic deformation was applied to a narrow zone of weld metal transition to base metal. Fatigue testing of samples was conducted in URS 20 testing machine at zero-to-tension alternating cycle.

First the effectiveness of HFMP technology application to improve the cyclic fatigue life of the joints was established, depending on the crack depth. Welded sample of 10KhSND steel was tested at maximum cycle stresses σ_{max} = 280 MPa, and three samples of steel 09G2S were tested at σ_{max} = 180 MPa. After formation of a fatigue crack of the specified length in one of the zones of the weld-to-base metal transition in the tee joint sample, testing was interrupted and strengthening of all the four zones by HFMP technology was performed (Figure 2). After strengthening, testing was carried on up to complete failure of the sample or its withstanding $2 \cdot 10^6$ stress reversal cycles in the as-strengthened condition.

Determination of the parameters of non-through-thickness surface cracks was performed using fractographic and dye penetrant control techniques. Combination of both the methods allowed determination of parameters of non-through-thickness fatigue crack in the joint by sample fracture before its strengthening. A mixture of kerosene with synthetic oil was used as the penetrant. After strengthening by HFMP technology addition of penetrant into the cavity was stopped.

In the first sample a 5 mm fatigue crack developed after the sample has withstood 232,800 stress reversal cycles. After strengthening of all the four near-weld zones no new cracks initiated until the sample has withstood $2 \cdot 10^6$ stress reversal cycles in the as-strengthened condition.

In the second sample the fatigue crack 10 mm long initiated in one of the near-weld zones after 344,100 stress reversal cycles. After strengthening by HFMP no fatigue cracks initiated in other zones of the welded joint.

In the third sample about 23 mm long crack formed near one of the fillet welds after 428,600 stress reversal cycles. After strengthening by HFMP the sample failed along the damaged weld after 418,200 stress reversal cycles in as-strengthened condition.

In the welded joint of 10KhSND steel (fourth sample) a fatigue crack 7 mm long formed in the zone of

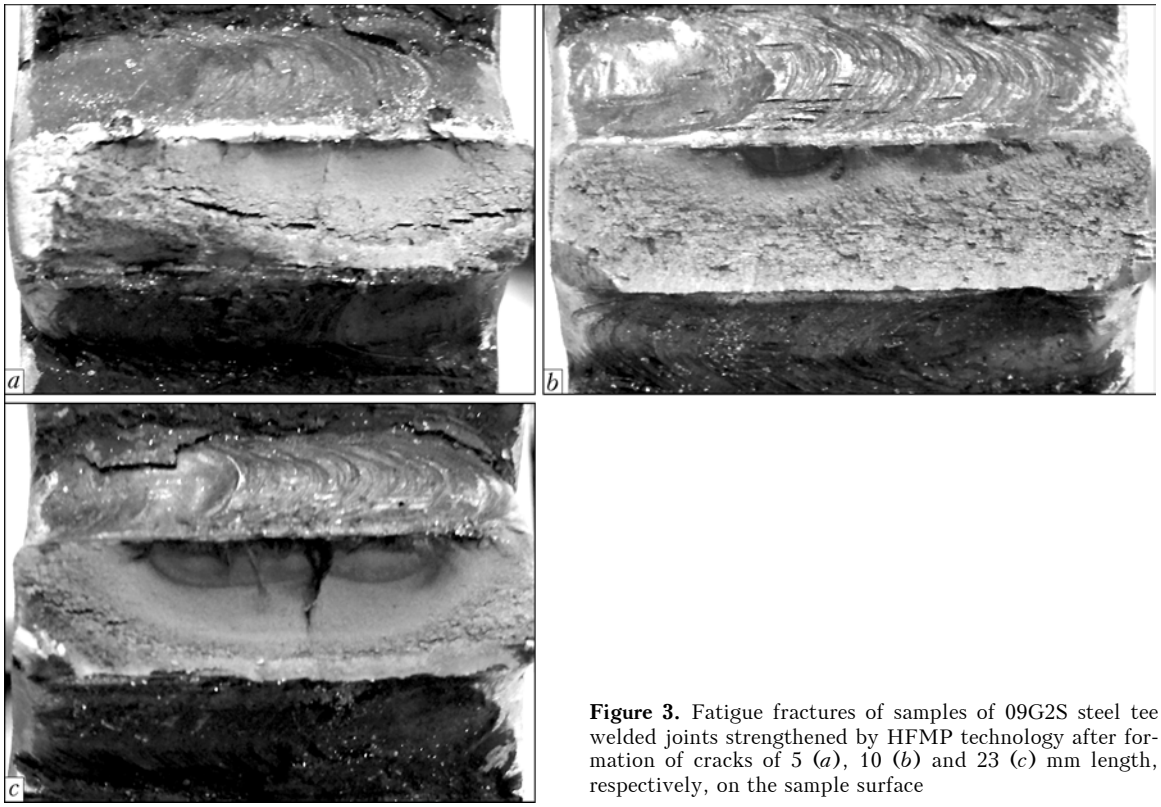

Figure 3. Fatigue fractures of samples of 09G2S steel tee welded joints strengthened by HFMP technology after formation of cracks of 5 (*a*), 10 (*b*) and 23 (*c*) mm length, respectively, on the sample surface

weld transition to the base metal after 178,400 stress reversal cycles. After strengthening by HFMP no fatigue crack formation in other zones was observed up to $2 \cdot 10^6$ stress reversal cycles.

To measure crack depth in those samples, which did not fail up to $2 \cdot 10^6$ stress reversal cycles in as-strengthened condition, sample complete breaking up was achieved by increasing the maximum cycle stresses up to 320 MPa. Figure 3 shows fractures of samples of 09G2S steel tee joints strengthened by HFMP technology after formation of cracks of different length on the sample surface. Fractographic analysis of fractures showed that the ratio of fatigue crack length on sample surface and its depth is equal to 5:1. Proceeding from the obtained results in further studies we will apply plastic deformation to surface fatigue cracks of approximately 1 mm depth (5 mm length of the crack on the surface).

To study the effectiveness of HFMP application to improve the fatigue resistance of welded structures, the elements of which have fatigue cracks of about 1 mm depth, fatigue testing of two tee welded joints from low-alloyed steel was conducted by the following procedure. One sample of 10KhSND steel in the initial condition was tested at uniaxial alternating tension with the constant maximum cycle stress, the second sample of 09G2S steel was tested at block loading (Figure 4). Samples were tested up to development of approximately 1 mm deep crack in one of the four zones of transition of the fillet weld metal to the base metal (see Figure 2). After that the zone damaged by the crack was strengthened by HFMP technology. Fatigue testing of the strengthened sample was continued up to appearance of the next crack approximately 1 mm deep in one of the fillet weld zones unstrengthened by HFMP. The zone damaged by fatigue crack was also strengthened by HFMP technology and sample fatigue testing was carried on. After similar testing of the third and fourth zones damaged by the fatigue crack, the strengthened sample was further tested at unchanged stress level up to fracture or up to $2 \cdot 10^6$ cycles.

Tested for fatigue by the above procedure the first welded sample of 10KhSND steel at maximum cycle stresses σ_{max} = 220 MPa demonstrated the following. The first fatigue crack developed in the zone of fillet weld-to-base metal transition (see Figure 2, zone 1) after 267,300 stress reversal cycles. As follows from the *S*–*N* curve of these samples given in [10], fatigue life of the sample up to formation of the first crack of approximately 1 mm depth is equal to 69 % of fatigue life of the sample to complete fracture. The second fatigue crack formed in the transition zone near the opposite stiffener (zone 2) after 587,200 stress reversal cycles, which is equal to 145 % of sample

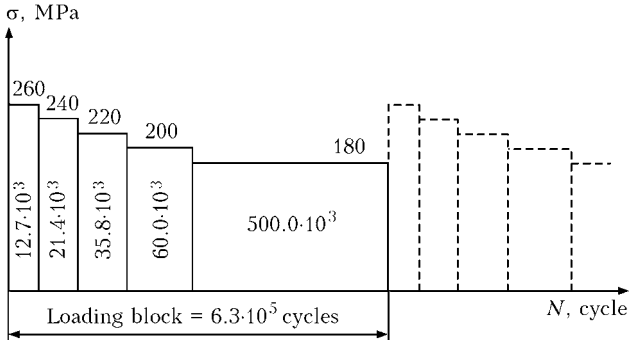

Figure 4. Schematic of block loading of tee welded joint of 09G2S steel

fatigue life up to compete fracture. The third crack developed after 1,318,300 stress reversal cycles (zone 3), which is equal to 330 % of fatigue life of the sample up to complete fracture. After HFMP treatment of three zones of fillet weld-to-base metal transition, where fatigue cracks formed successively, formation of the fourth crack in the fillet weld zone unstrengthened by HFMP (see Figure 2, zone 4) was not observed up to total fatigue life of the sample of 2,226,100 stress reversal cycles. After that fatigue testing of the sample was interrupted.

The second sample was tested at five-step block loading at the initial stress level of 260 MPa with subsequent decrease to 180 MPa with 20 MPa step. Number of cycles in each loading step is shown in the schematic given in Figure 4. After successive strengthening by HFMP of all the zones damaged by fatigue cracks testing was carried on under the specified block loading up to fracture. Testing results are given in the Table. Considering that before appearance of the third crack the total fatigue life of the sample was equal to approximately $2.6 \cdot 10^6$ stress reversal cycles (350 % of fatigue life of the sample in the initial condition to complete fracture), no strengthening of the third and fourth zone by HFMP technology was performed. Sample failure occurred in the unstrengethened zone after 2,723,200 stress reversal cycles in the second step of the fifth loading block (Table). The established values of cyclic fatigue life of the tee joint corresponding to formation of fatigue cracks of the specified length (depth) in four near-weld zones of fillet welds, point to a significant difference of fatigue resistance characteristics of these zones.

As is seen from the above results of tee sample testing, successive strengthening of the zones of fillet weld-to-base metal transition damaged by fatigue cracks of approximately 1 mm depth essentially improves the cyclic fatigue life of the joints. However, during performance of repair operations it is not rational to limit ourselves to strengthening of just the tee welded joint zone damaged by the fatigue crack, as furtheron cracks will initiate in the unstrengthened near-weld zones of the joint during their further operation. More effective is strengthening of all the four near-weld zones of the welded joint after formation in one of them of a fatigue crack of about 1 mm depth. This is confirmed by the results of fatigue testing given at the beginning of the article for samples of tee welded joints of 09G2S steel, which are shown in Figure 5 in the form of dark and light dots.

Figure 5 also gives the S–N curve of tee welded joints on 09G2S steel in the initial condition with 95 % confidence interval. Considering that the S–N curve is plotted from complete fracture of the samples, HFMP strengthening of the zone of transition of the weld metal-to-base metal with 4.5 mm deep fatigue crack does not lead to increase of cyclic fatigue life of the tee welded joint, as the fatigue life of the strengthened sample up to its fracture falls within the

Results of fatigue testing of a sample of 09G2S steel tee welded joint at block loading

Sample #	1st loading			2nd loading			3rd loading		
	$\sigma_{1\,max}$, MPa	n_1, thou cycles	n_1/N_1, %	$\sigma_{2\,max}$, MPa	n_2, thou cycles	n_2/N_2, %	$\sigma_{3\,max}$, MPa	n_3, thou cycles	n_3/N_3, %
1	260	12.7	10	240	21.4	10	220	35.8	10
2	260	12.7	10	240	21.4	10	220	35.8[2]	10
3	260	12.7	10	240	21.4	10	220	35.8	10
4	260	12.7	10	240	21.4	10	220	35.8	10
5	260	12.7	10	240	15.6[5]	7.3	–	–	–

Table (cont.)

Sample #	4th loading			5th loading			Testing features
	$\sigma_{4\,max}$, MPa	n_4, thou cycles	n_4/N_4, %	$\sigma_{5\,max}$, MPa	n_5, thou cycles	n_5/N_5, %	
1	200	60	10	180	500[1]	50	[1]HFMP of zone 1 (Figure 2) after 118,000 cycles
2	200	60	10	180	500	50	[2]HFMP of zone 2 (Figure 2) after 13,100 cycles
3	200	60	10	180	500	50	–
4	200	60	10	180	500[4]	50	[4]Crack 1 mm deep in zone 3 after 400,000 cycles
5	–	–	–	–	–	–	[5]Sample failure

Note. n_i ---- number of cycles withstood by unstrengthened sample at i-th stress level; N_i ---- number of cycles up to fracture of unstrengthened sample at i-th stress level.

95 % confidence interval of S–N curve for unstrengthened samples in the initial condition (Figure 5, points *3* and *3′*). Treatment of the near-weld zone at earlier stages of fatigue crack development (crack depth of 1 and 2 mm) essentially increases the cyclic fatigue life of the welded joint (points *1* and *1′*, *2* and *2′* in Figure 5). As shown above, after samples with fatigue cracks of 1 and 2 mm depth withstood $2 \cdot 10^6$ stress reversal cycles in as-strengthened condition, no propagation of the existing cracks or initiation of new cracks was observed. These samples failed at higher maximum cycle stresses equal to 320 MPa after another 35,100 and 37,200 stress reversal cycles, respectively, which was equal to about 130 % of the fatigue life of a welded sample in the initial condition corresponding to this loading level (see S–N curve in Figure 5).

Thus, strengthening of all the four near-weld zones of the welded joint after formation of a fatigue crack of approximately 1 mm depth in one of them allows not only restoring the fatigue life of the damaged sample to the initial level, but also significantly increasing its cyclic fatigue life.

CONCLUSIONS

1. An essential difference of fatigue resistance of four near-weld zones of fillet welds in tee joints of low-alloyed steels is established. The difference between the cyclic fatigue life of near-weld zones of fillet welds in these joints before formation of a fatigue crack approximately 1 mm deep can be more than 9 times.

2. Successive strengthening by HFMP technology of the near-weld zones with the formed fatigue cracks approximately 1 mm deep more than 3.5 times improves the cyclic fatigue life of the tee welded joint at constant or block loading compared to the initial condition.

3. In repair in order to achieve a maximum improvement of the cyclic fatigue life of tee welded joints it is rational to strengthen by HFMP technology all the four near-weld zones of such joints after formation of a fatigue crack approximately 1 mm deep in one of them. Three samples strengthened by such a procedure with the formed fatigue cracks after 178,400; 232,800 and 344,100 stress reversal cycles did not fail after $2 \cdot 10^6$ cycles in the as-strengthened condition.

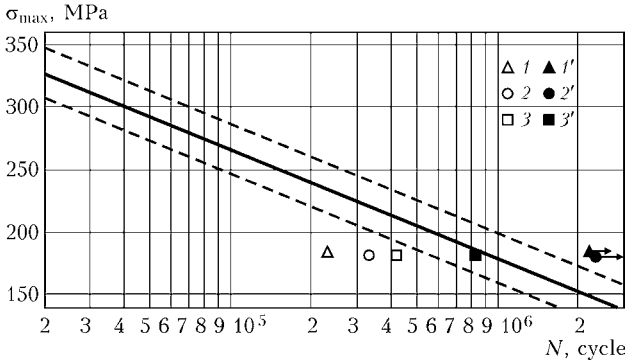

Figure 5. S–N curve of 09G2S steel tee joints in the initial condition with 95 % confidence interval and results of fatigue testing of three samples: *1–3* — up to formation of a crack 1, 2 and 4.5 mm deep, respectively; *1′–3′* — after HFMP strengthening

1. Trufyakov, V.I. (1998) Increase in fatigue resistance of welded joints and structures. *Avtomatich. Svarka*, **11**, 11–19.
2. Paton, B.E. (2000) Modern trends in increase in strength and life of welded structures. *The Paton Welding J.*, **9/10**, 2–8.
3. Knysh, V.V., Kovalchuk, V.S. (2007) Extension of service life of metal structures from low-alloy steels by high-frequency mechanical peening after repair welding. *Ibid.*, **11**, 31–33.
4. Knysh, V.V., Kuzmenko, A.Z., Vojtenko, O.V. (2006) Increasing fatigue resistance of welded joints by high-frequency mechanical peening. *Ibid.*, **1**, 30–33.
5. Turnbull, A., De Los Rios, E.R., Tait, R.B. et al. (1998) Improving the fatigue crack resistance of waspalloy by shot peening. *Fatigue & Fract. of Eng. Materials and Struct.*, **21**, 1513–1524.
6. Branko, C.M., Infante, V., Bartista, R. (2004) Fatigue behaviour of the welded joints with cracks, repaired by hammer peening. *Ibid.*, **27**, 785–798.
7. Farrahi, G.H., Majzoobi, G.H., Hosseinzadeh, F. et al. (2006) Experimental evaluation of the effect of residual stress field on crack growth behaviour in C(T) specimen. *Eng. Fract. Mechanics*, **73**, 1772–1782.
8. Song, P.S., Wen, C.C. (1999) Crack closure and growth behaviour in shot peened fatigue specimen. *Ibid.*, **63**, 295–304.
9. Xiaohua, C., Fisher, J.W., Prask, H.J. et al. (2003) Residual stress modification by post-weld treatment and its beneficial effect on fatigue strength of welded structures. *Int. J. Fatigue*, **25**, 1259–1269.
10. Knysh, V.V., Valteris, I.I., Kuzmenko, A.Z. et al. (2008) Corrosion fatigue resistance of welded joints strengthened by high-frequency mechanical peening. *The Paton Welding J.*, **4**, 2–4.

EVALUATION OF MECHANICAL PROPERTIES OF MICROSTRUCTURAL CONSTITUENTS OF WELDED JOINTS

A.Ya. ISHCHENKO and **Yu.A. KHOKHOLOVA**
E.O. Paton Electric Welding Institute, NASU, Kiev, Ukraine

Considered is the procedure for evaluation of mechanical properties of small-sized specimens based on determination of microhardness by the depth of penetration of Berkovich indenter in case of continuous indentation. Technical capabilities of this procedure have been assessed by evaluating the properties of γ-TiAl joints made by diffusion bonding. Statistical data on local distribution of microhardness were obtained, and values of Berkovich hardness, Young modulus and ductility coefficient of structural components within the zone of the diffusion bond have been determined.

Keywords: *diffusion welding, γ-TiAl alloy, titanium aluminide, foil, welded joint, mechanical testing, Berkovich indenter, microhardness, Young modulus, ductility coefficient*

Development of new processes of welding promising materials requires new approaches to evaluation of their mechanical properties. Produced welded joints are characterized by small dimensions and diversity of structural components. Strength testing of such objects by conventional destructive methods is highly problematic, which is associated with the influence of additional inner stresses induced during product fabrication, thus lowering the accuracy of testing results. In this connection a procedure is proposed for evaluation of mechanical properties of diffusion joints, which is based on microhardness determination by the depth of imprint of Berkovich indenter at continuous indentation [1–5]. The above procedure is applicable for non-destructive testing of products and allows studying local changes in material properties, including microhardness gradient in the HAZ of welded joints.

To determine mechanical properties of diffusion joints on the microstructural level, three-edge Berkovich indenter [6] was used. It is a diamond pyramid with the base in the form of an equilateral triangle; the pyramid ribs form a 76°54′ angle with the axis, and the faces form a 65° angle. The advantage of the indenter of such a shape is its pointedness, i.e. absence of a crest on the apex, inevitable for Vickers and Knoop pyramids. Presence of such a crest leads to violation of the geometrical similarity of the imprints and, in its turn, to microhardness deviation from its real values in the microindentation region. The main advantages of the trihedral pyramid are the simplicity of its fabrication and pointedness, allowing measurement of microhardness of such hard bodies as diamonds.

The imprints can have minimum dimensions. Berkovich indenter is standardized (ISO 14577–2) as an instrument for micro- and nanoindentation. By the data of [7] microhardness testing by such an indenter is the most widely used analytical method of monitoring the mechanical properties of modern materials with fine structures. The accuracy of digital instruments allows studying the mechanical properties of material structure microinhomogeneities.

During testing the depth of intender indentation on the load on it is recorded both at load increase and decrease. This yields the value of «unrecovered» hardness, thus eliminating the influence of the material elastic recovery on the actual microhardness value [8, 9].

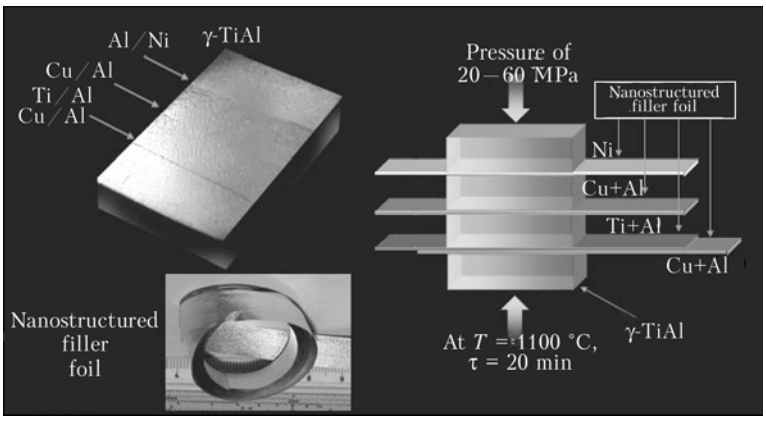

Figure 1. Mock up of a diffusion welded joint of γ-TiAl intermetallic alloy

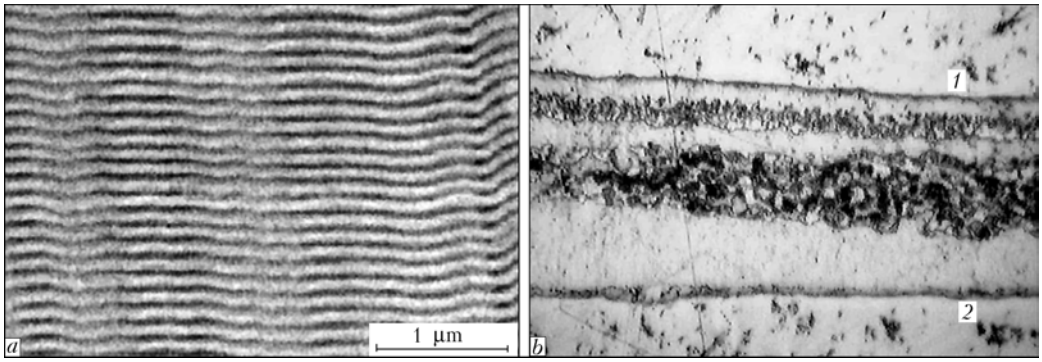

Figure 2. Laminated structure of filler nanostructured foil (scanning electron microscopy) (*a*) and microphotography (*b* — ×600) of Ti/Al (upper coarse-grained layer *1*) and Cu/Al (lower layer *2*) interlayers in a diffusion welded joint

The paper gives an evaluation of the technical capabilities of indentation for determination of the micromechanical properties of diffusion joints of γ-TiAl made with application of nanostructured metastable filler foils (Figure 1). γ-TiAl — a high-temperature material (fcc lattice is preserved at 1440 °C) with a high level of oxidation and combustion resistance at up to 900 °C temperature, low density (3.8–4.0 g/cm^3) and increased modulus of elasticity (160–175 GPa at room temperature and 150 GPa at 900–1000 °C) — is an advanced material for manufacturing aerospace systems and an alternative to titanium and nickel superalloys. However, its industrial application is restrained because of its brittleness, low ductility and high deformation resistance.

Cu/Al, Ni, Ti/Al filler foils used in the joint are multilayer metastable nanostructures [10], consisting of alternating nanolayers of various materials, with less than 100 nm layer thickness, their quantity being several thousands (Figure 2). Owing to the possibility of close contact of layers of various materials, such nanolaminates are unique materials, combining both the quality of laminated systems and specific properties of nanoobjects. Such multilayered metastable structures consist of components which may enter into exothermal interaction with each other [11]. At certain temperature conditions the process of self-propagating high-temperature synthesis (SPHTS) is initiated in such a system. As a result, the initial lamellar structure disappears, giving way to phases of new chemical compounds, formed as a result of interaction of synthesis products.

Multilayer metastable materials offer a number of advantages: monolithic nature of the initial structure and absence of pores in the reaction products; high uniformity of the reaction product composition; small thickness of the initial layers, which allows realization of SPHTS processes at a very high speed; absence of oxide films between the layers and good contact between the layers. The above features make their application promising in the technology of solid-phase joining of materials based on SPHTS.

The object of study is a four-layer welded joint of γ-TiAl alloy (4 mm sheet thickness) produced by vacuum diffusion welding (VDW) for 20 min at 600 °C with application of nanostructured metastable Cu/Al, Ni/Al filler foils and Cu/Al + Ti/Al double filler. Thickness of inner Ti/Al foil layers is equal to 23 nm for titanium, being 24 nm for aluminium. Thickness of filler foils in the joints is equal from 0.015 to 0.050 mm on average.

Investigations are performed using «Microngamma» instrument (Figure 4) designed for determination of mechanical properties of materials by the methods of continuous application of the indenter, indenter scanning (sclerometry), metallography and topography [12].

Computerized microprobe system of the instrument (Figure 3) includes Berkovich indenter, a rod with a sensor for recording the indentation depth, loading mechanism with a broad load range, videocamera with the resolution of 5 Mps and microscope (with 200–1200 magnification), automated system of sample positioning with the program of digital navigation over the studied object, which allows making a precise application to the selected structural microbject. To reduce vibration the instrument is mounted on a vibroinsulating support. Indenter displacement, measured with up to 1 nm accuracy, allows conducting testing at the load from 0.1 to 500 g and shallow depth

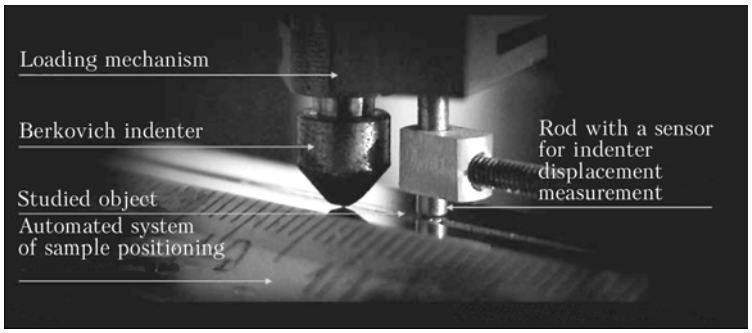

Figure 3. Computerized system with Berkovich intenter for testing the mechanical properties of diffusion welded joints

Figure 4. Instrument «Micron-gamma»

of the imprints. The derived loading–unloading diagram consists of 2000 dots (Figure 5, *a*). Processing of indentation results is performed by a specialized program, which allows automatic determination of the values of hardness and Young modulus at recording of the indenter tip displacement.

In this test hardness was determined by maximum depth of intender imprint at 20 g load. Each series of applications consisted of 16 successive imprints of the indenter with 20 μm step. Loading rate was 2 g/s without dwelling. Testing was conducted by the following schematic: loading/unloading without dwelling. Calculation data are summed up in an electronic table.

At metallographic analysis of a joint with a nanostructured interlayer of Cu/Al system a partial and in some places complete diffusion of the interlayer into the base material is found (Figure 5, *b*). Maximum value of microhardness of this joint was equal to 1.2 GPa at Young modulus E = 86.9 GPa and coefficient of ductility k_{duct} = 0.755, and minimum value was 0.536 GPa at E = 61.6 GPa and k_{duct} = = 0.853, respectively.

Metallographic examination of the joint with nanostructured Ni/Al interlayer did not reveal any visible diffusion (Figure 5, *c*). A precisely outlined recrystallization zone on the boundary of the base material and interlayer with higher microhardness values is visible. Maximum microhardness value of this zone is equal to 1.905 GPa at E = 121.9 GPa and k_{duct} = 0.705, and minimum microhardness value of 0.432 GPa is recorded in the central part of the interlayer at E = 89.8 GPa and k_{duct} = 0.938.

At metallographic analysis of the joint with two nanostructured interlayers of Cu/Al and Ti/Al systems a slight diffusion of Cu/Al interlayer is noted with development of coarse-grained dark-coloured intermetallic interlayer and formation of a homogeneous weld from Ti/Al interlayer (Figure 5, *d*). The gradient of variation of microhardness and modulus of elasticity for these interlayers is small. Average value of microhardness of the interlayer of Ti/Al system was equal to 1.972 GPa at averaged E = 159.8 GPa and k_{duct} = 0.781, and for interlayer of Cu/Al system it was 1.180 GPa at E = 120.3 GPa and k_{duct} = 0.823.

Thus, statistical data of local redistribution of microhardness in the HAZ of the diffusion welded joint of

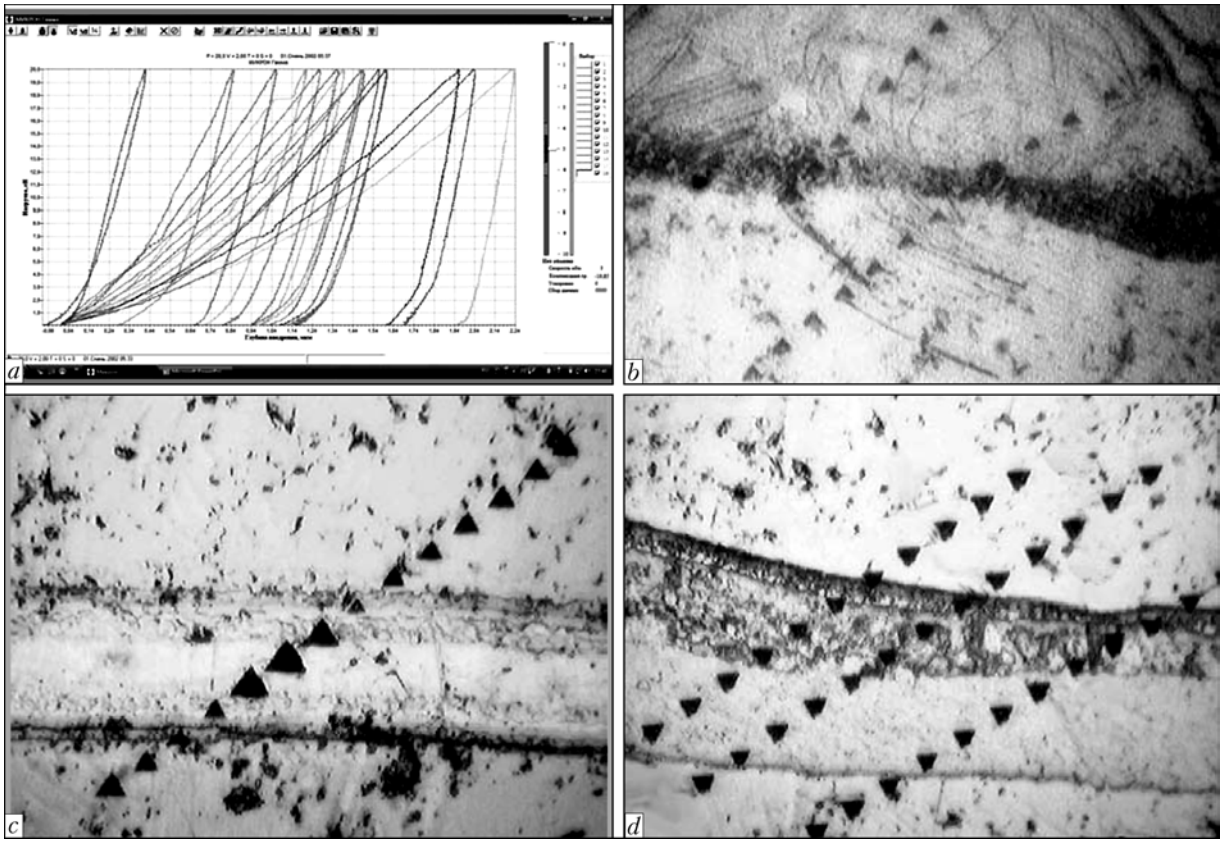

Figure 5. Loading–unloading diagram at indentation of a joint with Ni/Al interlayer (*a*) and microphotographs (×600) of nanostructured Cu/Al (*b*), Ni/Al (*c*) and Cu/Al with Ti/Al (*d*) interlayers with indenter imprints (▼)

γ-TiAl were derived. Accuracy of digital videonavigation and precise application of the indenter allowed revealing and getting imprints of structural microinhomogeneities in the form of individual intermetallic precipitates in the interlayer, as well as zones with different microhardness values. The undesirable change of microhardness should be regarded and taken into account simultaneously with the changes of Young modulus of elasticity and coefficient of ductility.

1. Oliver, W.C., Pharr, G.M. (1992) An improved technique for determining hardness and elastic modulus using load and displacement sensing indentation experiments. *J. Mater. Res.*, **7**, 1564–1570.
2. Glazov, V.M., Vigdorovich, V.N. (1969) *Microhardness of metals and semiconductors*. Moscow: Metallurgiya.
3. Grigorovich, V.K. (1976) *Hardness and microhardness of metals*. Moscow: Nauka.
4. Bulychev, S.I., Alyokhin, V.P. (1990) *Testing of materials by continuous indentation of indentor*. Moscow: Mashinostroenie.
5. Golovin, Yu.S., Tyurin, A.I., Ivolgin, V.I. et al. (2000) New principles, technique and results of investigation of dynamic characteristics of solids in microvolumes. *Zhurnal Tekhn. Fiziki*, 70, Issue 5, 82–83.
6. www/microstartech.com
7. *NASA/TM-2002-211497*: Surface characterization techniques. Glenn Res. Center.
8. Alyokhin, V.P. (1983) *Physics of strength and plasticity of surface layers of materials*. Moscow: Nauka.
9. Oliver, W.C., Pharr, G.M. (2004) Measurement of hardness and elastic modulus by instrumented indentation: Advances in understanding and refinements to methodology. *J. Mater. Res.*, **9**, 3–20.
10. Elistratov, N.G., Nosyrev, A.N., Khvesyuk, V.I. et al. *The experimental ion-assisted deposition equipment for producing the multilayers materials*: www:plasma-lab.ru//multilayers_r.html
11. www://vimi.ru/applphys/2001/2/f3-2/htm
12. Zaporozhets, V.V., Zakiev, I.M., Nikitin, Yu.A. *Device for macrohardness testing of materials*. USSR author's cert. 373581. Int. Cl. G 01 N 3/42. Publ. 07.02.93.

FROM HISTORY OF WELDING

TRENDS IN DEVELOPMENT OF COMBINED AND HYBRID WELDING AND CLADDING TECHNOLOGIES

A.P. LITVINOV
Priazovsky State Technical University, Mariupol, Ukraine

The history of development of the technologies based on the interrelated simultaneous action of two heat energy sources is considered. It is suggested that the combined and hybrid processes should be discriminated. The combined processes involve the action of several sources, which are either identical or of the same type, whereas with the hybrid processes the use is made of the sources differing in their physical characteristics, which impart new technological properties to a process.

Keywords: *fusion welding, cladding, arc welding, plasma welding, laser welding, combined welding, hybrid welding, history of technology*

Every welding method has certain advantages and disadvantages. Development of the combined and hybrid technologies involves integration of technological and other advantages of individual welding methods and minimisation of their drawbacks. Main challenges facing the welding industry include increase of the welding speed, decrease of the metal and power consumption, control of the weld shape, and improvement of the quality of welded joints. The problem of widening the range of thicknesses of pieces joined has been successfully tackled in the field of fusion welding for many years, while in the field of cladding such a problem consists in minimisation of penetration and decrease of the fusion zone between a workpiece and deposited layer (bead). These problems can be efficiently solved by distributing heat input, heating and melting between the two (or more) energy sources, which simultaneously act in the common welding/cladding zone. In this case, each of the sources can perform insignificantly or substantially different functions. It should be noted that such methods are sometimes termed «combined» or «hybrid» in corresponding publications, assuming that the new technological effect is a generalising attribute of these terms. To tell the difference, it is necessary to consider the history of development of the welding and cladding technologies using several energy sources.

According to study [1], the hybrid welding processes are a combination of two (or more) conventional (standard) processes, resulting in the effects which cannot be achieved by each of the processes taken separately. R.V. Messler dates emergence of the first hybrid technology back to 1972. He starts from the method developed by W.G. Essers and A.S. Lifken at a «Philips» (The Netherlands) laboratory [2]. In Ukraine the «plasma-MIG» term is already approved in the State Standard for terminology for this type of welding (cladding) [3].

Definition «hybrid welding» has not been officially approved as yet. Notion «hybrid» (from Latin «Hibreda» --- mixture) belonged, starting from the 18th century, to biology, i.e. cross breeding of animals or types of plants [4]. The combined or integrated processes, units, systems and devices with different properties and characteristics, resulting in achievement of a new technical effect (e.g. hybrid computer

systems, integrated circuits, interconnections of radio duct systems) were started to be referred to as the hybrid ones in the 20th century. R.V. Messler considers the action on a common weld pool by two laser beams going in series along the axis of a joint or on each side of the axis also to be among the hybrid welding processes. He thinks that this qualification of the «hybrid process» is grounded on the effect of improvement of weld formation, rather than on differences in technical characteristics of components. The definition he suggested is not clear enough, as in this case the submerged two- and three-arc welding methods should also be classed with the hybrid ones, as they make it possible to solve the problem of weld formation at a speed increased dozens of times and, thus, put off the date of emergence of the hybrid technologies by twenty years [5].

In multi-arc welding developed by the E.O. Paton Electric Welding Institute, each of the heat sources arranged in series performs a certain function: the first prepares (penetrates) the edges, the second fills up the gap between the edges (pool), and the third finally forms the weld [6].

Technologies for submerged-arc welding by using five electrodes simultaneously were developed abroad in the 1980s. Multi-electrode systems with parallel electrodes, i.e. direct current--direct current, direct current--alternating current and alternating current--alternating current systems, and a system of three AC sources, found the widest commercial application [7]. However, these technologies cannot be called the hybrid ones ---- they are the combined processes using similar sources.

The first process called the hybrid one was welding with the laser beam plus arc (arc plasma) [8]. For some time only this process was considered to be the hybrid one, until R.V. Messler classed the plasma-MIG process also with the hybrid processes [1]. Both processes have similar flow diagrams, i.e. with plasma-MIG there is another heat source, i.e. the metal-electrode arc, inside the circular arc (plasma). Moreover, these sources differ in physical and technological properties [9].

It should be noted that emergence of the plasma-MIG method was preceded by the development of other welding methods using two dissimilar heat sources.

The purpose of this study is to refine classification and range of the combined and hybrid processes allowing for the chronology of their development. Here the physical essence of energy sources (similar or dissimilar in their nature), their impact on a workpiece and interaction between them, resulting in formation of a new effect, should be used as a basis, like in the already standardised terminology [3]. It is suggested that welding and cladding processes based on interaction of the energy sources that are similar in their physical nature and technological properties should be considered the combined processes. The hybrid processes are an integration of two (or more) dissimilar (in terms of physical phenomena) heat sources, resulting in formation of a new technological effect.

The retrospective analysis shows that both types of the processes emerged almost at the same time. At the end of the 1880s N.N. Benardos introduced the combined two-arc welding technology. The point of the first hybrid technology was that a gas flame was burning around the carbon-electrode arc [10]. N.N. Benardos designed a special torch for this technology. A combination of the heating flame and melting action of the arc widened technological capabilities of the process both for welding and cladding. In the same years E. Thomson employed a concurrent spark and arc heating to increase the productivity of resistance butt welding [11].

Another method put forward by N.N. Benardos, i.e. welding, soldering and cladding with the arcs burning simultaneously from the consumable and non-consumable electrodes, also solves the problem of preheating, like its arc-gas process. However, it cannot be defined as the hybrid one. In 1930 H. Munter developed a method incorporating acetylene-oxygen welding and metal-arc welding, the so-called «arcogen» method. With this method the gas flame provided about 60 % of heat, and the AC arc ---- 40 %. The amperage was 2--3 times lower than in open-arc welding, thickness of metal welded being the same. However, voltage in this case amounted to 100 V. This is attributable to the fact that the flow of gases caused intensive ionisation of the arc column. The procedure of such a welding was complicated, as a welder had to perform both processes manually. This method could not compete with the simpler methods involving one heat source, which were widely applied at that time [12].

V.P. Nikitin was a supporter of the hybrid processes. He noted: «Fusion welding in the course of its development until the last years has been characterised by the permanent fundamental principle: one heat source is used for two different thermal operations (fusion of the base metal and melting of the filler metal). Strong, hardly controllable relationship between thermal preparation of the base and filler metals leads in many cases to reduction of the productivity and deterioration of the welding quality, thus limiting its application. With single-arc welding the basis for rise in the productivity is increase in the arc power. The productivity of welding with a high-power arc is determined, primarily, by the efficiency of penetration of the base metal, as the electrode metal constitutes 20--25 % of the weld. Deep penetration hampers achievement of the satisfactory quality of welding of steel to copper, brass, bronze and other alloys. Moreover, in some cases this leads to decrease in anticorrosion and antifrictional properties of alloys. The above limitation is equally applicable to cladding of high-speed steel and hard alloys on carbon steel at a high power of the arc and strong relationship between thermal preparation of the base and filler metals. Concentration of the alloying elements that determine

properties of the deposited layer decreases because of dilution with the base metal: composition of the weld metal in such cases differs from the preset one, and it is difficult to regulate it. All modern melting methods characterised by the strong relationship are totally irrational for application to cladding operations. So, the welding methods should be developed with allowance for their energy basis» [13, p. 234]. In 1941, V.P. Nikitin suggested a method providing for a separate control of heat input, i.e. an integration of the arc heating and melting by feeding a metal preliminarily melted (and overheated) in the furnace from a separate crucible to the welding zone. The low-current arc discharge in this hybrid process was required for surface preparation (cathodic cleaning and incipient melting), thus providing a high quality of cladding. Despite a high productivity of the device incorporating the arc torch and electric crucible, it found a limited application because of its complexity [14].

The method of gas-shielded fusion arc welding by feeding a filler metal to edges of the parts joined via a hollow electrode aligned with the arc to the arc zone is characterised by the fact that, to increase the productivity of the process and widen the range of thicknesses of the parts welded, the filler metal is fed via the hollow electrode to the arc zone in a molten state, melting of the filler metal being provided by its passing through a high-frequency inductor [15]. The E.O. Paton Electric Welding Institute returned back to the idea of a separate formation of the pool (penetration and filling) at the beginning of the 1960s, when developing technologies for plasma-arc welding. Through penetration was considered to be the main technological feature of the process. The weld pool with a hole (the process was termed «the keyhole» ---- effect) allowed the plasma-gas flow to go out from below of a welded joint [16]. However, intensification of the plasma-gas pressure to increase the welding speed and penetration depth leads to deterioration of the weld formation, formation of undercuts and even cuts. To achieve a satisfactory weld formation, the E.O. Paton Electric Welding Institute suggested filling the weld pool with a filler metal melted in a high-frequency inductor. Thus the welding speed was increased 4–5 times. The plasmatron and inductor were assembled in one welding head on a carriage. Nevertheless, it was difficult to control such a process because of substantial differences in principles of operation of the equipment.

To solve this problem in high-speed plasma welding, it was suggested at the end of the 1960s that the pool should be filled up with the electrode metal melted by the pulsed metal-electrode arc. In this case the arc crosses the plasma-gas flow. Part of the wire electrode at a short arc receives extra heat [17]. At the end of the 1960s, it was necessary to use two different current sources with a single control device to implement this method. Circuit of the control device was based on the electromagnetic relay, and was complicated and sluggish. Welding by using the plasmatron with a zirconium electrode pressed into a copper holder allowed using the carbon dioxide gas as a plasma gas, thus making it possible to joint steel plates of a comparatively big thickness in one pass. This process (which can be classed with the hybrid ones) turned out to be stable at a metal electrode current of only 20–40 A. The penetration depth in this case was less than 1 mm [18]. The Paton Institute returned back to improvement of this process and development of the specific technologies based on the combined action of metal- and tungsten-electrode constricted arcs in the 1990s [19]. Investigations of the process combining the tungsten electrode arc with the arc of a metal electrode fed to the same weld pool were conducted on samples of aluminium alloys 8 mm thick. The search for rational flow diagrams of metal- and tungsten-electrode welding processes, and spot plasma-arc welding, went on in the years that followed, and efforts were made to develop the equipment for implementation of these processes.

Among all TIG welding processes it is the tungsten-electrode helium-arc welding (HAW) method that features the highest penetrating capacity. The welding technology combing different heat sources, i.e. HAW and metal-electrode argon-arc welding, was developed to solve the problem of the satisfactory weld formation in making of long welds with a variable gap [20]. The process parameters can be rapidly and flexibly adjusted in automatic through-penetration butt welding without backing, thus providing a good quality of the weld metal and minimal weakening of aluminium alloys.

By the beginning of the 21st century the combined methods, featuring the use of two successively arranged electrode wires (tandem welding) and a strip electrode, as well as the spray or rotating arc, performed preferably under the pulsed welding conditions, were considered to be the most efficient versions of MAG welding [21].

The technologies based on the plasma-MIG process (known abroad as a «Philips-process») were applied to manufacture unique structures, including nuclear reactors [22]. At the end of the 1990s the plasma-MIG welding and cladding processes were studied at the E.O. Paton Electric Welding Institute and Priazovsky State Technical University. It was established that the current is flowing not only through the electrode wire, but also through the hollow-cylindrical arc plasma surrounding the wire. Separate heating of the surface and melting of the electrode showed good results in flux-cored wire cladding [23–25]. The presence of the plasma surrounding the metal electrode and arc provides a much wider range of currents in the electrode wire, within which the arcing process is stable, the efficiency of melting grows, and the critical current of transition to spray and spray-rotating transfer of the electrode metal decreases [26].

The technology for welding stainless steels, featuring the integrated use of the plasma arc and tung-

sten-electrode arc, thus providing the quality welds at an increased welding speed, was developed in France [27]. A similar hybrid scheme of integration of the plasma-arc and metal-electrode arc processes in one torch was applied at the E.O. Paton Electric Welding Institute for spot welding [28].

Two-sided welding with opposite heat sources, i.e. the plasma (constricted) arc and metal-electrode arc, plasma arcs, etc., can be qualified as a hybrid process. This type of welding was first put forward by the E.O. Paton Electric Welding Institute in 1966 for welding vertical welds [29], and covered by the State Standard of Ukraine under the term of «bipolar arc welding» [3]. The Department of Metallurgy and Materials of the College of Science and Technology (London, Great Britain) developed the technology for welding with the laser and arc arranged according to the same scheme [30]. Another technology for TIG welding of high-strength aluminium alloys in argon atmosphere by using two oppositely directed torches was developed in the USA [31]. At the end of the 20th century the laser-arc welding and cutting methods were started to be called the hybrid methods. V.Yu. Khaskin notes: «Discrimination is usually made between the hybrid and combined processes. The first provides for feed of the focused laser beam and electric arc to one point in the common pool, whereas the second is characterised by a common thermal cycle, although the heat sources involved act on a workpiece at different geometric points» [32, p. 18].

This classification of the methods based on the «common thermal cycle» using two or more energy sources is incorrect, as the thermal cycle is undetermined in space and time. The laser-arc welding processes [33--41] are characterised by one specific feature, which cannot be explained by simple superposition of properties of the employed heat sources taken separately. This feature consists in increase of the coefficient of utilisation of energy of both laser and arc heat sources. With such a hybrid process it is more efficient to use the constricted (plasma) arc combined with the laser beam, located at an angle to each other or coaxially. During the last decade the E.O. Paton Electric Welding Institute offered several schemes for the hybrid processes. Investigations are conducted under the leadership of Prof. B.E. Paton to study characteristics and technological capabilities of different combinations of laser, arc and other melting sources. In particular, peculiarities of thermal processes, efficiency and temperature fields were studied, and recommendations for selection of shielding gases, etc. were worked out [39, 41].

The development of the «hydra-process» based on the use of three or more heat sources, having different physical origin and application, was a new stage of progress in the field of the hybrid plasma-arc welding technologies [42]. They include the plasma-arc welding process, which provides for utilisation of two TIG torches with tungsten electrodes and a plasmatron located between them. The impact on a workpiece by the sources may be of different kinds. Company «Munchengladbach» in Germany applied a combination of three TIG welding processes and a plasma-arc process for high-speed welding. All electrodes, a plasmatron nozzle with electromagnetic and gas stabilisation, and a shielding gas nozzle are housed in one torch. Control of the processes is synchronised. It is noted in one of the latest studies [1] dedicated to development of welding with two or more energy sources that this area has the highest promise. The hybrid processes based on the integrated action of the fusion and pressure welding processes also show promise. One of the key problems in this case is complexity of the devices used to implement the processes. Most often the equipment for the hybrid processes is a sum of the basic units of each of the heat sources, as well as of separate or combined power supplies with electronic control of process parameters.

During the last decade the laser-arc and laser-plasma welding processes have been developed most intensively. On the basis of experimental data, I.V. Krivtsun from the E.O. Paton Electric Welding Institute developed the theory of physical phenomena occurring in interaction of the focused laser beam and plasma of the electric arc. It was established that a special type of the gas discharge, the properties of which differ from properties of the conventional arc and from properties of the optical beam, may form in this system. Mathematical models of such a discharge in laser-arc plasma torches were developed. The application showed certain advantages [43--45].

1. Messler, R.V. (2004) What's next for hybrid welding? *Welding J.*, **3**, 30–34.
2. Essers, W.G. (1980) Plasma-MIG lassem van aiuminium. *Lastechnik*, **8**, 187--193.
3. (1999) *Welding and related processes. Terms and definitions*. Kyiv: Derzhstandart.
4. Prokhorov, A.M. (1971) Hybrid. In: *B.S. Encyclopedia*, Vol. 6, 453.
5. Paton, B.E. (1952) Achievements and tasks in the field of submerged-arc welding. *Avtomatich. Svarka*, **5**, 18–19.
6. Paton, B.E., Mandelberg, S.L., Lashkevich, R.I. et al. (1960) About selection of scheme for production of large-diameter longitudinal welded pipes. *Ibid.*, **7**, 3–14.
7. Uttrachi, G.D. (1983) Multiple electrode systems for submerged arc welding: Pt 1. *Can. Weld. and Fabr.*, **8**.
8. Walduck, R.P., Biffin, J. (1994) Plasma arc augmented laser welding. *Welding and Metal Fabr.*, **4**, 172–176.
9. (1972) Plasma-MIG. En ny interessant svetsmetod. *Verkstadsinformation*, **12**, 365--367.
10. Benardos, N.N. (1982) *Scientific-technical inventions and projects*. Kiev: Naukova Dumka.
11. Thomson, E. (1887) Electric welding. *J. Franklin Institute*, 123(**737**), 245–247.
12. Munter, H. (1933) Der Einfluss von Schweiss- und Schutzgasflammen auf die Vorgange im Schweisslichtbogen. *Elektroschweissung*, **7**, 80–84.
13. Nikitin, V.P. (1956) Search for new methods based on the principle of separate control to increase productivity and quality of welding. In: *Problems of arc and resistance electric welding*. Kiev: Mashgiz.
14. Nikitin, V.P. (1947) Method of welding of metals using different fusion processes. *Doklady AN SSSR*, LVI(**5**), 45–57.
15. Lebedev, V.K., Dudko, D.A., Medvedenko, N.F. et al. *Shielded-gas fusion arc welding method*. USSR author's cert. 501850. Int. Cl. B 23 K 9/16. Appl. 14.08.72. Publ. 05.02.70.
16. Dudko, D.A., Lakiza, S.P. (1960) About new possibilities of high-temperature welding with the arc constricted by gas flow. *Avtomatich. Svarka*, **11**, 38--46.
17. Dudko, D.A., Kornienko, A.N., Esibyan, E.M. (1970) *Method of plasma-arc welding*. USSR author's cert. 294422. Int. Cl. B 23 K 17/00.
18. Vajnbojm, D.I., Brokhun, N.N., Ratmanova, Zh.V. (1976) Automatic thin-layer CO_2 cladding of steel by combined

method (with consumable and non-consumable electrode). *Svarochn. Proizvodstvo*, **8**, 23–24.
19. Kaika, V.I., Rabkin, D.M. (1984) Combined process of argon-arc non-consumable and consumable electrode welding of aluminium. *Avtomatich. Svarka*, **5**, 72–73.
20. Petrovanov, V.M., Bobrinsky, V.I., Tenebaum, F.E. et al. (1985) Peculiarities of the technology for welding large-sized structures from heat-hardened aluminium alloy 1201. In: *Paper coll. of All-Union Conf. on Current Problems of Welding of Non-Ferrous Metals*. Kiev: Naukova Dumka.
21. Miklos, E. (2001) Aktuelle Prozessvarianten des MAS-HL-schweissens. *Aachen Shaker*, **1**, 389–405.
22. Areskonq, M., Smarst, E. (1976) Application of the gas-metal — plasma-arc process for weld cladding in nuclear manufacturing. *Welding and Metal Fabr.*, **4**, 274–277.
23. Makarenko, N.A. (1998) Plasma surfacing with axial feed of flux-cored wire. *Avtomatich. Svarka*, **12**, 52–53.
24. Kornienko, A.N., Makarenko, N.A., Granovsky, A.V. (2001) Study of stabilising properties of the halogen type flux-cored wire charge for MIG-plasma processes. In: *Proc. of Int. Conf. on Welding Consumables* (18–20 June 2001, Oryol), 74–75.
25. Chygariov, V.V., Kornienko, O.M., Makarenko, N.O. et al. *Unit for plasma welding and surfacing*. Pat. 48383 Ukraine. Int. Cl. B 23 K 9/16. Appl. 28.05.01. Publ. 15.08.02.
26. Bozhenko, B.L., Ronsky, V.L. (1984) Technology of plasma-arc consumable electrode welding in argon atmosphere. *Svarochn. Proizvodstvo*, **6**, 17–18.
27. (1984) En visite a la soudure autogene francaise. *Souder*, **3**, 76–78.
28. Voropaj, N.M., Ilyushenko, V.M., Mishenkov, V.A. (2004) Combined process of spot plasma-arc welding. *Svarshchik*, **4**, 26–27.
29. Dudko, D.A., Kornienko, A.N., Vinogradsky, F.M. *Method for plasma welding and cutting of metals*. USSR author's cert. 237568. Int. Cl. B 23 K 35/02. Appl. 17.06.67. Publ. 19.04.68.
30. Steen, W.M., Eboo, M. (1979) Arc augmented laser welding. *Metal Construction*, **7**, 332–335.
31. Zhang, Y.M., Zhang, S.B. (1999) Welding aluminium alloy 6061 with the opposing dual-torch GTAW process. *Welding J.*, **6**, 202–206.
32. Khaskin, V.Yu. (2003) Combined laser-arc processes. *Svarshchik*, **3**, 18–19.
33. Steen, W.M. *Methods and apparatus for cutting, welding, drilling and surface treating*. Pat. 1547172 Great Britain. Int. Cl. B 23 K 26/00. Publ. 06.06.79.
34. Diebold, T.P., Albright, C.E. (1984) Laser-GTA welding of aluminium alloy 5052. *Welding J.*, 63(**6**), 18–24.
35. Gorny, S.G., Lopota, V.A., Redozubov, V.D. et al. (1989) Peculiarities of heating of metal in laser-arc welding. *Avtomatich. Svarka*, **1**, 73–74.
36. Walduck, R.P., Biffin, J. (1994) Plasma arc augmented laser welding. *Welding and Metal Fabr.*, 62(**4**), 172–176.
37. Paton, B.E. (1995) Improvement of welding methods — one of the ways to increase welded structure quality and efficiency. *Avtomatich. Svarka*, **11**, 3–11.
38. Krivtsun, I.V., Chizhenko, M.I. (1997) Bases for design of laser-arc plasmatrons. *Ibid.*, **1**, 16–23.
39. Paton, B.E., Gvozdetsky, V.S., Krivtsun, I.V. et al. (2002) Hybrid laser-microplasma welding of thin sections of metals. *The Paton Welding J.*, **3**, 2–6.
40. Krivtsun, I.V., Shelyagin, V.D., Khaskin, V.Yu. et al. (2007) Hybrid laser-plasma welding of aluminium alloys. *Ibid.*, **5**, 36–40.
41. Paton, B.E. (2003) Current trends in research and development in the field of welding and strength of structures. *Ibid.*, **10/11**, 5–11.
42. (2001) Welding and joining technologies in the 21st century. *J. JWS*, 70(**3**), 6–11.
43. Gvozdetsky, V.S., Krivtsun, I.V., Chizhenko, M.I. (1991) Interaction of laser beam with electric arc plasma. In: *Proc. of 8th All-Union Conf. on Physics of High-Temperature Plasma* (Minsk), Pt III.
44. Voropaj, N.M., Ilyushenko, V.M., Khaskin, V.Yu. (2006) Selection of shielding gas for hybrid process of laser-arc welding. *Svarshchik*, **4**, 20–22.
45. Krivtsun, I.V., Shelyagin, V.D., Khaskin, V.Yu. et al. (2007) Hybrid laser-plasma welding of aluminium alloys. *The Paton Welding J.*, **5**, 36–40.

REFINED MATHEMATICAL MODEL OF THE ELECTRIC ARC BURNING IN PLASMATRON WITH EXTERNAL CURRENT-CONDUCTING WIRE

M.Yu. KHARLAMOV[1], **I.V. KRIVTSUN**[2], **V.N. KORZHIK**[2], **S.V. PETROV**[2] and **A.I. DEMIANOV**[2]
[1]V. Dal East-Ukrainian National University, Lugansk, Ukraine
[2]E.O. Paton Electric Welding Institute, NASU, Kiev, Ukraine

Mathematical model of electromagnetic processes has been refined for the arc burning in plasmatron with an anode wire. Comparative numerical analysis of electric, thermal and gas-dynamic characteristics of the arc plasma has been conducted by using a boundary layer approximation and the refined model of the electromagnetic processes. It is shown that the method of description of the said processes has a substantial effect on calculated distributions of characteristics of the arc plasma generated by the plasmatron under consideration.

Keywords: *plasmatron with anode wire, electric arc, mathematical model, plasma flow characteristics*

Study [1] puts forward a mathematical model to describe a turbulent flow of the electric arc plasma generated by the plasmatron with an external current-conducting anode wire. An assumption of smallness of radial component j_r of density of the electric current in the arc, compared with axial component j_z ($j_r << j_z$), is made in this study within the framework of a boundary layer approximation. This approach fails to adequately describe electromagnetic characteristics of the arc burning in the plasmatron under consideration, as j_r has sufficiently high values, comparable with those of j_z, in the near-cathode region at exit from the plasma-shaping channel and in a region of cathode fixation of the arc. Therefore, the model of electromagnetic processes used in [1] needs to be refined, which is the purpose of this concise article.

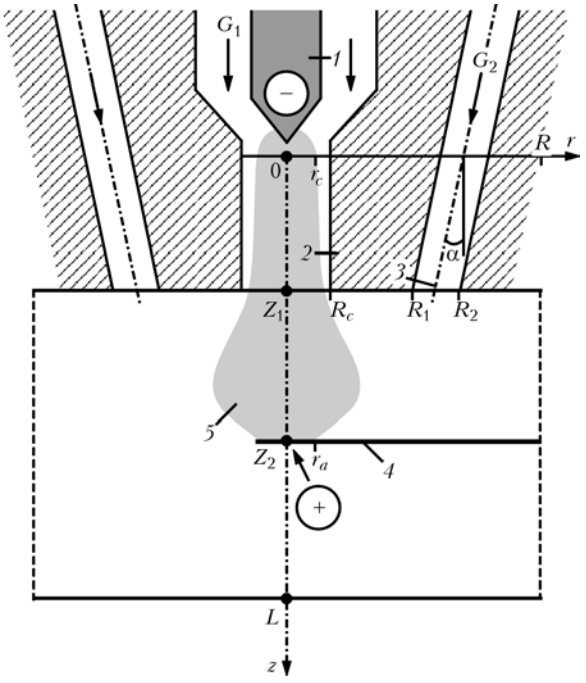

Figure 1. Schematic of the electric arc burning in plasmatron with external anode wire: *1* — refractory cathode; *2* — plasma-shaping nozzle; *3* — gas feeding channel; *4* — anode wire; *5* — arc column

Schematic of the DC arc being studied is shown in Figure 1. It burns in the plasma gas (argon) flow shaped by the plasmatron channel with radius R_c and length Z_1 between a refractory (tungsten) cathode and metal anode wire located after the exit section of a nozzle at distance Z_2 from the cathode tip. An exposed region of the arc discharge may be blown with a flow of a cold gas (argon, air) fed via an annular channel, which is located at angle α to the plasmatron axis and has internal, R_1, and external, R_2, radii. The calculation domain is limited by boundaries in radial, R, and axial, L, directions.

Gas-dynamic and thermal characteristics of the arc plasma generated by such a device can be described by a system of magnetic-gas-dynamic (MGD) equations in an approximation of a turbulent boundary layer [1]. For a more correct description of electromagnetic characteristics of the arc (with no assumption of smallness of the radial component of density of the electric current, compared with the axial one), we will use an equation of intensity of the magnetic field of the arc current [2]:

$$\frac{\partial}{\partial r}\left[\frac{1}{r\sigma}\frac{\partial (rH_\varphi)}{\partial r}\right] + \frac{\partial}{\partial z}\left[\frac{1}{\sigma}\frac{\partial H_\varphi}{\partial z}\right] = 0, \qquad (1)$$

where $\sigma[T(r, z)]$ is the temperature-dependent specific electric conductivity of the plasma; $H\varphi(r, z)$ is the azimuth component of intensity of the magnetic field related to the components of density of the electric current through the following equations [2]:

$$j_z = \frac{1}{r}\frac{\partial}{\partial r}(rH_\varphi); \quad j_r = -\frac{\partial H_\varphi}{\partial z}. \qquad (2)$$

Equations (1) and (2) can be complemented with a condition of conservation of the total current:

$$I = 2\pi \int_0^{R_\sigma(z)} j_z r dr, \tag{3}$$

where I is the arc current; and $R_\sigma(z)$ is the radius of the current-conducting region. Given that conductivity of the arc plasma is almost equal to zero outside this region, radius of the calculation domain can be used as an upper limit of integration in formula (3), i.e. it can be assumed that $R_\sigma(z) = R_c$ at $z \le Z_1$, and $R_\sigma(z) = R$ at $z > Z_1$ (see Figure 1). It should be noted that, as this model allows for both axial and radial components of density of the electric current, the Joulean source in energy equation [1] should be written down in the form of $(j_r^2 + j_z^2)/\sigma$.

Second-order differential equation (1) cannot be solved without setting the edge conditions for the entire contour of the calculation domain $\{0 \le r \le R_c$ at $0 \le z \le Z_1$, and $0 \le r \le R$ at $Z_1 < z \le Z_2\}$ (see Figure 1). To set the corresponding boundary conditions in the vicinity of the arc electrodes, i.e. at $z = 0$ and Z_2, we will use the experimental and calculation data from studies [3, 4] on densities of the current in the cathode and anode regions, assuming that

$$j_z(r, 0) = j_{0c} e^{-r/r_c}; \quad j_z(r, Z_2) = j_{0a} e^{-r^2/r_a^2}; \tag{4}$$

$$j_r(r, 0) = j_r(r, Z_2) = 0, \tag{5}$$

where j_{0c} and j_{0a} are the constants corresponding to the maximal values of density of the current in the cathode and anode regions; and r_c and r_a are the radii of the cathode and anode regions of fixation of the arc, respectively. In particular, at $I = 200$ A it is possible to use value $j_{0c} = 1.2 \cdot 10^8$ A/m^2 [3], and radius of the cathode region can be determined from total current conservation condition (3). An approximate radius of the anode wire is chosen as a radius of the anode region of arc fixation, and value j_{0a} is calculated from condition (3).

By substituting relationships (4) to the first equation of (2), we find:

$$H_\varphi(r, 0) = \frac{j_{0c} r_c^2}{r}\left[1 - e^{-r/r_c}\left(1 + \frac{r}{r_c}\right)\right];$$

$$H_\varphi(r, Z_2) = \frac{j_{0a} r_a^2}{2r}\left(1 - e^{-r^2/r_a^2}\right). \tag{6}$$

Then we set the boundary condition on axis of the system in the following form:

$$H_\varphi(0, z) = 0. \tag{7}$$

And assume the following at the external boundary of the calculation domain:

$$H_\varphi(R_c, z) = \frac{I}{2\pi R_c} \text{ at } 0 \le z \le Z_1;$$

$$H_\varphi(R, z) = \frac{I}{2\pi R_c} \text{ at } Z_1 < z \le Z_2. \tag{8}$$

Finally, at $z = Z_1$ and $R_c \le r \le R$, we have

$$H_\varphi(r, Z_1) = \frac{I}{2\pi r}. \tag{9}$$

Equations (1) and (2), together with boundary conditions (6) through (9), make up the basis of the refined mathematical model of electromagnetic processes for the arc burning in the plasmatron with an external current-conducting anode wire. These equations should be solved together with the MGD equations of a turbulent boundary layer [1], which determine spatial distributions of gas-dynamic and thermal characteristics of the arc plasma.

The complete system of equations was solved by the numerical finite difference method using global iterations with respect to intensity of the magnetic field (the procedure used to numerically solve the boundary layer equations is described in detail in [1]). The values of intensity of the magnetic field were updated at each new step of global iteration by numerically solving equation (1). This was done using the five-point implicit difference scheme by the sweep method [5]. The solution procedure was stopped when all characteristics of the plasma (at all points of the calculation domain) at two neighbouring iterations differed not more than by a preset low value of θ.

Analyse now the results of numerical modelling of electromagnetic, thermal and gas-dynamic characteristics of the arc plasma in the plasmatron under consideration by using approximation $j_r << j_z$ and the refined model of electromagnetic processes. The calculations were made for the plasmatron having a nozzle with length $Z_1 = 3$ mm and radius $R_c = 1.5$ mm, and an anode wire with a diameter of 1.4 mm located at a distance of 6.3 mm from the exit section of the nozzle ($Z_2 = 9.3$ mm). It was assumed that an external region of the plasma flow was blown with an argon flow going from the annular channel having radii $R_1 = 4.78$ mm and $R_2 = 7.22$ mm in the exit section, and inclined at angle $\alpha = 37.5°$ to the plasmatron symmetry axis (see Figure 1). The temperature of the cooled walls of the channels and ambient gas was assumed to be equal to 300 K. The following working mode was chosen for the plasmatron: arc current $I = 200$ A, plasma gas flow rate $G_1 = 1$ m^3/h, and blowing gas flow rate $G_2 = 20$ m^3/h.

Figure 2 shows the boundaries of regions $R_\gamma(z)$, within which the γ-fraction of the total arc current flows:

$$\frac{2\pi \int_0^{R_\gamma(z)} j_z r dr}{I} = \gamma = 0.1;\ 0.2;\ \ldots;\ 0.9, \tag{10}$$

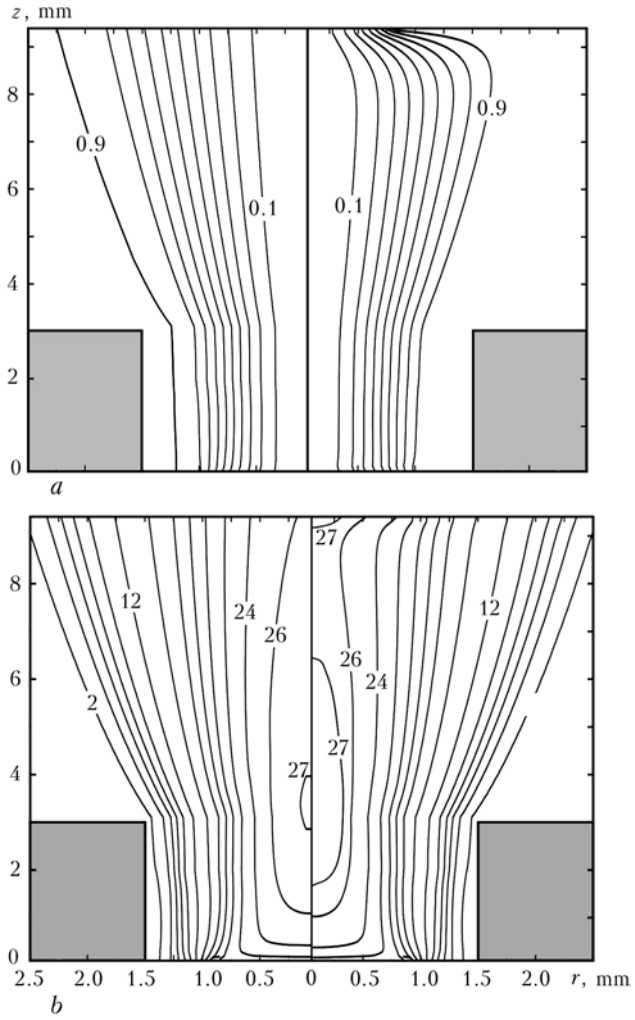

Figure 2. Isotherms of the electric current with a step of 0.1 (*a*) and isolines of temperature of the plasma with a step of T = 27, 26, 24 and then 2 kK (*b*) for the arc burning in plasmatron with an external anode wire for different methods of calculation of electromagnetic characteristics: *left* — approximation $j_r << j_z$; *right* — refined model

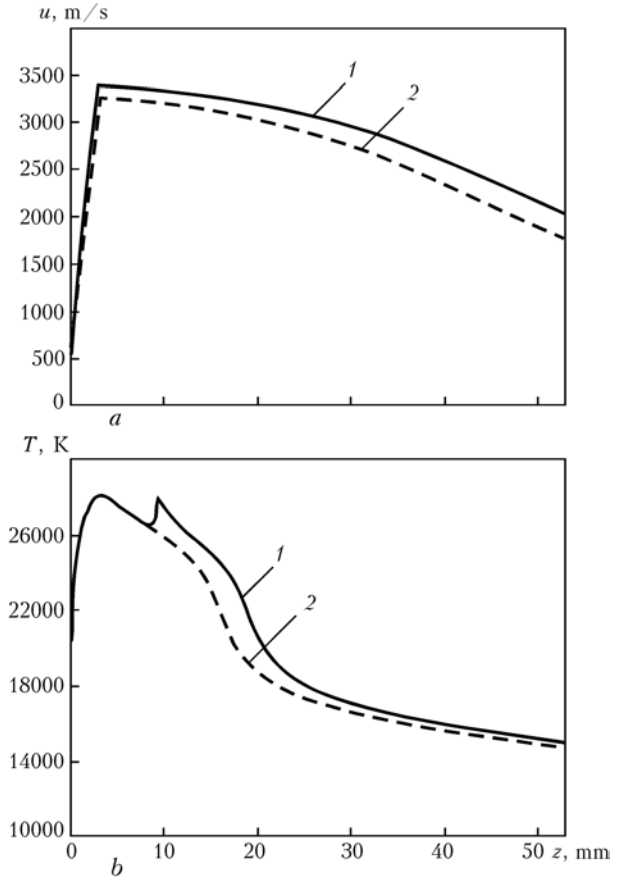

Figure 3. Distribution of axial velocity u (*a*) and temperature T of the arc plasma generated by the plasmatron with an external anode wire (*b*), determined by different methods of calculation of electromagnetic characteristics: *1* — refined model; *2* — boundary layer approximation ($j_r << j_z$)

which were calculated by using different calculation methods. As follows from this Figure, the use of approximation $j_r << j_z$ results in a current channel which gradually widens in an external region of the discharge (see Figure 2, *a*, *left*), and, in fact, coincides with a current-conducting region of the arc plasma (Figure 2, *b*, *left*). However, the solution of equation (1) showed qualitatively different results, especially in the exposed region of the arc, which is characterised by a substantial non-uniformity of the magnetic field along the length of the discharge and, accordingly, by higher values of the radial component of density of the electric current. As a result, the lines of the current, which diverge after leaving the plasma-shaping channel, converge towards the region of the anode fixation of the arc (Figure 2, *a*, *right*).

Figure 2, *b*, shows temperature fields corresponding to the chosen working mode of the plasmatron and calculated using different models of distribution of the current density in the arc. As can be seen from the isotherms shown in this Figure, differences in the calculated values of temperature turn out to be not as substantial as for the density of the electric current. However, we have to note an increase in the calculated temperature of the plasma near the region of the anode fixation of the arc when using the refined model of electromagnetic processes (see Figure 2, *b*, *right*). This is associated with the fact that the current channel determined within the framework of this model is markedly constricted in a region of the anode wire (see Figure 2, *a*, *right*), while the density of the current and, hence, Joulean heat sources is higher here and corresponds to a higher temperature. As to the gas-dynamic characteristics of the electric arc plasma in the plasmatron investigated, they hardly depend upon the method of calculation of its electromagnetic characteristics.

Consider now how thermal and gas-dynamic characteristics of the plasma flow change in a region of inertia movement of the plasma (after the anode wire) depending upon the model used to describe electromagnetic processes in the arc. The calculated distributions of axial values of the axial velocity and temperature of the plasma along the length of the jet are shown in Figure 3. With a variant of calculation involving the solution of equation (1), a higher temperature in the anode region of the arc leads to the fact that further on (in a no-current region of the flow) the temperature of the plasma will also be some-

what higher than with the calculation using simplifying approximation $j_r << j_z$. In the anode wire region the values of temperature at the discharge axis differ approximately by 14 %, further on they become almost identical, the difference being only 2–3 % (see Figure 3, *b*). The difference in the values of velocity of the plasma flow near the jet axis, on the contrary, grows with increase in the values of z: at z = 50 mm it amounts to 13 %.

CONCLUSIONS

1. The mathematical model of a turbulent flow of the arc plasma generated by the plasmatron with an external anode wire has been upgraded by refining the model of electromagnetic processes of the arc burning in such a device.

2. Spatial distribution of the electric arc current in the plasmatron with an external current-conducting anode wire has a non-uniform structure. The current lines diverge upon leaving the plasma-shaping channel, and converge with distance to the anode region, where the current density amounts to rather high values (over $1.5 \cdot 10^8$ A/m^2), thus providing an increased release of energy in the plasma. Ignoring the said peculiarities in numerical estimation of thermal and gas-dynamic characteristics of the generated plasma may lead to errors amounting to 14 % or more, depending upon the design parameters and working conditions of the plasmatron.

1. Kharlamov, M.Yu., Krivtsun, I.V., Korzhik, V.N. et al. (2007) Mathematical model of arc plasma generated by plasmatron with anode wire. *The Paton Welding J.*, **12**, 9–14.
2. Engelsht, V.S., Gurovich, V.Ts., Desyatkov, G.A. et al. (1990) *High-temperature plasma*: Vol. 1: Theory of electric arc column. Novosibirsk: Nauka.
3. Zhukov, M.F., Kozlov, N.P., Pustogarov, A.V. et al. (1982) *Near-electrode processes in arc discharges*. Novosibirsk: Nauka.
4. Hu, J., Tsai, H.L. (2007) Heat and mass transfer in gas metal arc welding. Pt 1: The arc. *Int. J. Heat and Mass Transfer*, **50**, 833–846.
5. Anderson, D., Tannehill, J., Pletcher, R. (1990) *Computational hydromechanics and heat exchange*. Vol. 1. Moscow: Mir.

NEW BOOKS

B.E. Paton. Selected works. — Ed. of the E.O. Paton Electric Welding Institute, NAS of Ukraine). — Kiev, 2008. — 894 p.

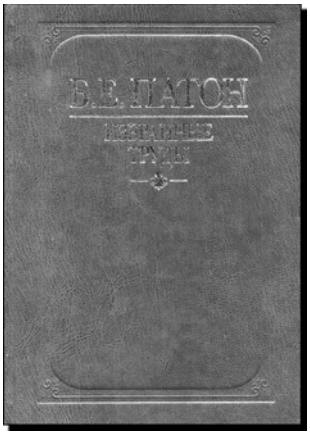

The collection is devoted to 90th anniversary of academician of NAS of Ukraine B.E. Paton — the prominent Ukrainian scientist in the field of welding, special electrometallurgy and materials science. The collection consists of seven sections which cover such directions of activity of B.E. Paton as fusion welding, pressure welding, arc welding metallurgy, special electrometallurgy, welded structures, space technologies and application of welding in medicine. Each section includes review of the works, the bibliography, and selection of the most important publications in which results of the works carried for the first time in the worl parctice are presented that had revolutionizing effect on development of leading bracnches of industry.

The work is intended for scientific and engineering-technical workers, professors, post-graduate students, and students of higher educational institutions.

B.E. Paton. — Introduction by I.K. Pokhodnya. — Kiev: Naukova Dumka, 2008. — 620 p.

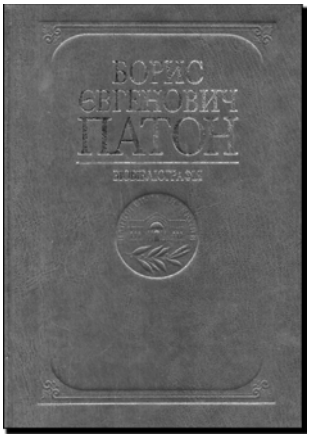

The book describes main stages of life, scientific-organizational and public activity of the prominent scientist in the field of welding, metallurgy and technology of metals and materials science, the prominent public figure and the talented organizer of science — the academician of the National Academy of Sciences of Ukraine, Russian Academy of Sciences, professor, honored figure of science and technology of Ukr. SSR, twice Hero of Socialist Labor of the USSR, Hero of Ukraine, participant of Great Patriotic war, mitigation worker at Chernobyl NPP Boris E. Paton.

Index of the published works familiarizes a reader with scientific works of the scientist. The book is intended for scientific workers and all those who are interested in history of national science and technology.

HARD-FACING BAY FOR REPAIR OF HYDROPOWER EQUIPMENT PARTS IN COMPANY «SAKENERGOREMONTI»

Yu.M. KUSKOV[1], **I.A. RYABTSEV**[1], **Yu.V. DEMCHENKO**[1], **A.M. DENISENKO**[1], **Z.Z. DZHAVELIDZE**[2], **Kh.N. KBILTSETSKLASHVILI**[2] and **A.A. KHUTSISHVILI**[2]
[1]E.O. Paton Electric Welding Institute, NASU, Kiev, Ukraine
[2]Company «Sakenergoremonti», Tbilisi, Georgia

The experience of establishing a hard-facing bay in company «Sakenergoremonti» is described, and design and technological peculiarities of performing in this bay repair of a shaft of the water turbine of 250 mW capacity are considered.

Keywords: *arc hard-facing, water turbine shaft, hard-facing technology, hard-facing materials, hard-facing equipment*

Hydropower is rather well developed in Georgia which is connected with its geographical position. At present in this country have been operating for a long time more than 20 big hydroelectric power stations of more than 1 mW capacity and dozens of smaller ones, that's why special-purpose units and parts of hydroelectric power stations require for repair or replacement, for example, of shafts and blades of the turbines that are subjected in process of operation to cavitation and hydroabrasive wear and corrosion.

In this work experience of establishment of the hard-facing bay in «Sakenergoremonti» is presented and design and technological peculiarities of performing in this bay repair of a shaft of the water turbine of 250 mW capacity are considered.

Shaft of the Kaplan turbine of mentioned capacity is one of its main units (Figure 1, *a*). It is manufactured from the 20G steel and has diameter 1 m, length 4.5 m and mass about 12 t. In process of operation occurs corrosive, cavitation and hydroabrasive wear of the shaft journal located under the bearings and the glands. Subject to renovation a worn part of the journal is located under internal surface of the bearing, the design of which envisages use of water flow for its lubrication and cooling (Figure 1, *b*).

Up till now the water turbine shafts were mainly renovated using method of shrouding. The shroud is manufactured from sheets of the 12Kh18N10T stain-

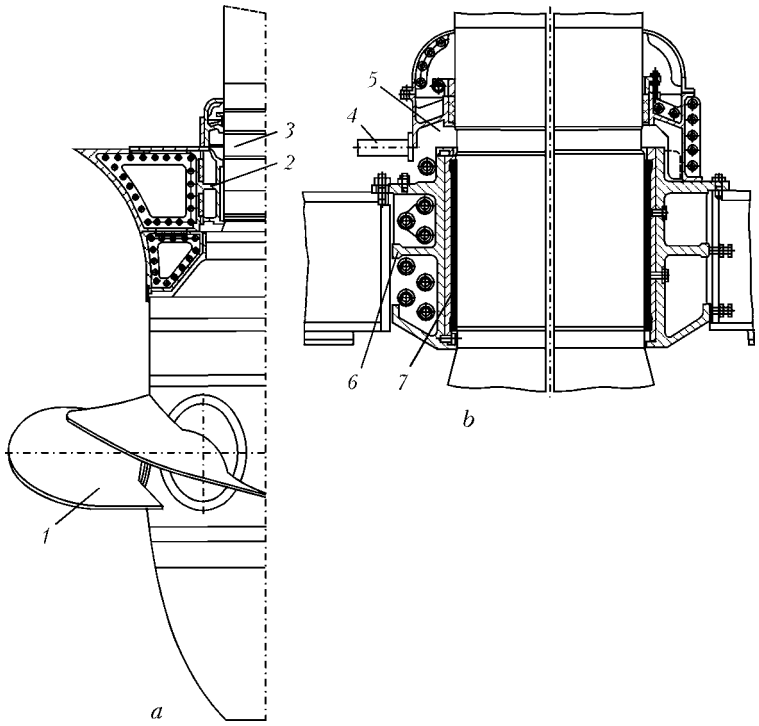

Figure 1. Scheme of shaft of Kaplan water turbine of 250 mW capacity (*a*) and guide bearing (*b*): *1* — impeller; *2* — guide bearing; *3* — turbine shaft; *4* — pipeline for bringing water; *5* — receiving vessel for water; *6* — guide bearing housing; *7* — rubber-coated collar step

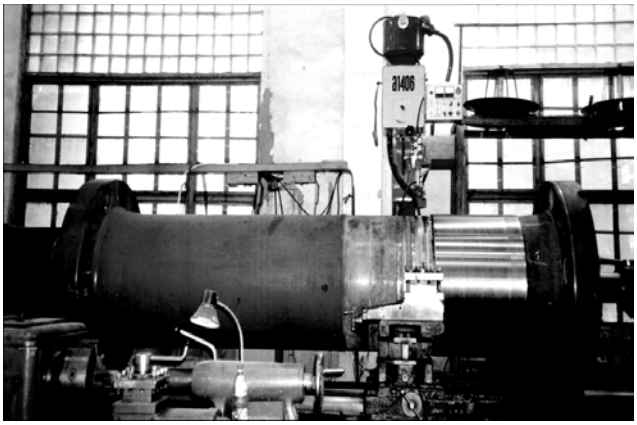

Figure 2. Upgraded installation developed on basis of PT-166 thread-cutting lathe for hard-facing and subsequent machining of water turbine shafts

Figure 3. Appearance of deposited on water turbine shaft corrosion-resistant layer

less steel of 10–12 mm thickness according to a complex technology that includes forge-rolling of the sheets, their cutting, welding, and machining. The time needed for shrouding of the water turbine journal of about 1 m diameter is 2–3 weeks.

Specialists of the E.O. Paton EWI suggested technology for renovation of a worn journal zone using hard-facing. The following technological scheme for renovation of the shaft was developed: visual examination and fault detection; machining for hard-facing; ultrasonic testing; automatic submerged arc hard-facing of a corrosion-resistant layer; turning; ultrasonic testing; grinding.

For hard-facing of the water turbine parts, specialists of STC «E.O. Paton EWI» upgraded at «Sakenergoremonti» enterprise the PT-166 thread-cutting lathe (of the DIP-500) type, and on its basis the hard-facing bay was established. Upgrading consisted in the following: on carriage of the lathe the A1406 hard-facing automatic machine was installed and then tailstock and reduction gear of the lathe were lifted by 160 mm (Figure 2). Electrical scheme of the lathe was supplemented with a frequency converter of the «Lenze» company (Germany) which ensured necessary for hard-facing speed of the water turbine shaft rotation. The VS-600 rectifier was used as a power source. Due to the upgrading it became possible not just to hard-face, but also to machine after hard-facing water turbine shafts of 400–1050 mm diameter, length up to 4500 mm and mass up to 12 t and perform hard-facing of flat surfaces, in particular turbine blades.

In addition to mentioned installation, the bay for repair of the parts comprises a furnace for calcination of the hard-facing materials in which, when it is necessary, heating of the parts before hard-facing and their slowed cooling after it are performed.

Visual examination of the worn water turbine shaft showed that length of the shaft area subject to renovation equaled about 710 mm and depth about 10 mm. On its worn surface defects in the form of cavities, caverns, laminations, etc. were detected. For their removal turning was used after which the remained defects were removed by means of scarfing using abrasive wheels. The machined for hard-facing surface of the shaft was checked for presence of defects using ultrasonic testing.

After machining diameter of the shaft equaled 1000 mm, and nominal diameter of the renovated shaft in this area was 1020 mm. At significant wear of the shaft first deposition of the sub-layer was performed using solid wire of the Sv-08 type and AN-348 flux (diameter of the shaft with the deposited sub-layer equaled approximately 1018 mm). Then on the installation for hard-facing turning of the deposited surface was performed up to diameter 1010 mm and afterwards ultrasonic testing was carried out.

Due to careful observance of all technological operations and technology of hard-facing defects in the deposited sub-layer did not form. External surface of the deposited layer was well formed, difference of height of the adjacent deposited beads did not exceed 0.5 mm.

Automatic multilayer submerged arc hard-facing using the AN-26P flux of the layer of corrosion-resistant stainless steel was performed with application of the Sv-08Kh20N9G7T wire. Diameter of the shaft after deposition of the corrosion-resistant layer was about 1028 mm (Figure 3).

The deposited surface of the shaft was turned down up to diameter 1020 mm, and then ultrasonic testing was performed. In the basic deposited layer as well as in the sub-layer defects were not detected.

As far as diameter of the shaft journal has strict tolerances, the deposited surface was treated by grinding.

All together on the worn surface of the shaft 320 kg of metal were deposited; general machine time of the hard-facing equaled 60 h. Suggested technology of hard-facing ensures significant saving of time and monetary means in repair of the water turbine parts in comparison with shrouding.

Restored water turbine shaft was shipped to the customer, and it will be installed at Inguri Hydropower Station (Georgia) for exploitation.

NEWS

NKMZ DETERMINED THE SIZE ON INVESTMENTS FOR TECHNICAL RE-EQUIPMENT OF THE ENTERPRISE FOR 2009

In 2008 the Novokramatorsk Machine-Building Plant (NKMZ company, Kramatorsk, Donetsk reg.) invested 120 mln USD into technical re-equipment. The main object of funding in 2008 was construction of the complex of 50 t steel-melting furnace. 200 mln UAH were invested into this project, 16 km of high-pressure gas pipeline, automated gas-distribution station, 110 kW power electric line, recycling water supply system, two oxygen plants and modern gas-cleaning system were built.

Before the end of the year 29 NC machine tools, machining centers and diverse auxiliary equipment for 50 mln UAH will be mounted in NKMZ shops.

The program of enterprise development for 2009 includes establishing forging shop #3 with automated forging complex for 5000 t. Upgrading FLTs-1, into which the plant is investing more than 40 mln UAH will become an important milestone. In addition to the available one, two more units for the so-called alpha-set-process will be purchased. Upgrading will result in a cardinal change of the technological processes, founders will switch completely to furane mixtures, which provide an entirely new quality of casting.

Fabrication of metal structures is expanded and for this purpose a new shop of 18,000 m^2 area will be established.

Contracts for purchase of 40 NC machines tool and machining centers have already been signed. Next year it is planned to construct eight thermal furnaces and six heating furnace of a new type, which will allow a 2 times reduction of gas consumption, ensure a high quality and accuracy of heating and will provide a practically unmanned operation schematic due to automation.

The expenditures for technical re-equipment in 2009 at NKMZ are planned in the amount of up to 600 mln UAH.

MACHINE FOR THERMAL CUTTING OF METAL

Plant of High-Technology Equipment of OJSC «Zont» (Odessa) is a well-known developer and manufacturer of machines for thermal cutting of metals. One of its most recent developments is ASSh-70 machine. It is designed for shaped cutting of parts of low-carbon steel of 5 to 150 mm thickness by three cutters with automatic tracing by a steel template 6–8 mm thick. Range of machine speeds allows using it also for plasma cutting of metal sheets of 3 to 50 mm thickness.

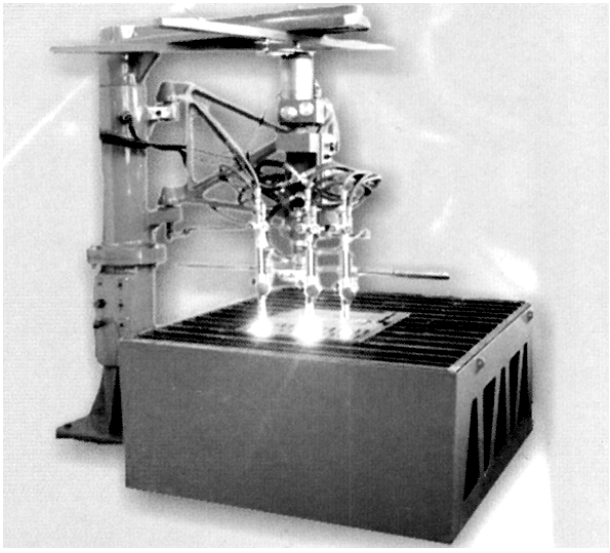

The machine can be successfully used for cutting out finished parts of the type of flanges, gussets, straps, etc.

Specification

Working zone, mm	1500 × 800
Range of cut thicknesses at cutting by one cutter, mm	5–150
Number of simultaneously working cutters	1 (3)
Cutter displacement speed, mm/min	100–2000
Maximum gas flow, m^3/h:	
natural gas	3.5
oxygen	38
propane	1.3
Gas pressure at machine inlet, atm:	
combustible gas	0.3
oxygen	10
Machine overall dimensions (with extended frames), mm	1810 × 1500 × 1750
Weight (without table), kg	390

BRANCH MEETING-CONFERENCE OF «GAZPROM» SPECIALISTS

On 10–14 of October 2008 in All-Russia Research-Scientific Institute of Natural Gases and Gas Technologies (VNIIGAZ) was held branch meeting-conference on State and Main Directions of OJSC «Gazprom» Welding Production Development. In the conference took part main welders of the «Gazprom-Transgaz» Ltd., regional units and representatives of production and scientific-research organizations, which ensure construction and operation of main pipelines (MP) in territory of Russia, and representatives of scientific centers and supplier-companies of welding equipment ---- all together more than 400 persons.

The conference was opened by report of the OJSC «Gazprom» representative *S.V. Alimov* who presented information about state and prospects of development of MP, networks of distribution gas pipelines, and gas storages. He noted that main efforts of «Gazprom» are directed at increasing efficiency of made design, technical and managerial decision. State-of-the-art systems of the GTS control assume orientation at servicing «according to the designation» i.e. a targeted long-term planning of diagnostics, overhaul repair, and reconstruction of the GTS objects allowing for expected load, needs in increase of the gas supply productivity, and forecast of the technical state change.

Representative of «Gazprom» *V.V. Salyukov* noted in his report that welding in overhaul repair of gas pipelines is one of main technological operations which ensures reliability and safety of the GTS operation.

E.M. Vyshemirsky informed about the state and technical level of welding production in «Gazprom» which has lately significantly improved, in particular in construction, operation, and repair of the MP objects. In addition, he informed about start of construction of a unique object of MP «Bovarenkovo-Ukhta» where pipes of new generation with internal coating of the K65 strength class are used.

In joint reports of the VNIIGAZ and the «Gazprom» representatives technical requirements to pipes and connection parts of MP from high-strength steels used for construction under Yamal conditions and other promising prospects of the «Gazprom» were presented.

In report of professor *O.I. Steklov* (the I.M. Gubkin RSU for Oil-and-Gas) the weldability criteria of structural materials were formulated. Results of investigations in the field of weldability of steels of the crude oil assortment were presented, and comprehensive assessment of service properties of welded joints was made. His colleagues *L.A. Efimenko, O.Yu. Elagina* jointly with representative of «Gazprom» Vyshemirsky E.M. considered issues of influence of carried out welding operations (welding at negative temperatures) on parameters of thermal cycles, structure and properties of welded joints.

In report of *V.A. Danilson* («Institute VNIIST» Ltd.) and *D.G. Budrevich* (VNIIGAZ Ltd.) the CRC-Evans AW welding complex for automatic two-sided welding of position circumferential butt joints of pipes of ∅ 1219 × 27 mm on a pipe-laying barge NRTS-De-

fender, used for laying underwater passage through Bajdaratskaya inlet of MP «Bovarenkovo–Ukhta», was considered.

O.E. Kapustin (the I.M. Gubkin RSU for Oil-and-Gas) dwelled upon training of the welding production specialists for enterprises which build and operate gas pipelines and perform diagnostics and repair of oil-and-gas structures.

On second plenary day the work was organized in two sections. In section A issues connected with development of welding production in subsidiary companies of «Gazprom» were considered, in particular issues of quality assurance of welding works in construction and repair of MP, main directions of development of non-destructive testing, normative support of non-destructive testing, and diagnostics of welded joints. Information of VNIIGAZ was presented about carried out scientific-research works and rendered engineering services in the field of welding production.

At the workshop also reports from Ukraine were presented.

V.Ya. Kononenko (SE «Ekotekhnologiya») and *V.V. Paskhin* («Podvodservis» Ltd.) dwelled upon application of wet underwater welding in repair of underwater passages of gas pipelines through water obstacles. Issues of weldability of pipe steels of oil assortment when using wet methods of welding were considered and videomaterials about application of dry welding in repair of an extended defect in the pipeline of 1200 mm diameter at depth 10 m were presented. In report of *S.Yu. Maksimov* and *Yu.Ya. Gretsky* (E.O. Paton EWI, NAS of Ukraine) it was informed about lately developed in PWI principally

new electrode materials and equipment for underwater wet welding. New electrode materials designed for welding of pipes from low-carbon and low-alloy steels ensure production of equal in strength welded joints. The welding may be performed at depth up to 20 m at speed up to 0.2 m/s and visibility not more than 0.25 m.

Of big interest were reports presented by *B.L. Getskin* (SPE «Tekhnotron» Ltd.), *A.A. Latyshev* (OJSC «Krasnodargazstroj») and *A.A. Latyshev* (VNIIGAZ Ltd.) about new sources of welding current of inverter type for MAW, TIG and MIG/MAG processes, mechanisms for feeding welding wire for mechanized processes of welding and welding heads for automatic welding produced by «Tekhnotron». Equipment for mechanized and automatic welding passed qualification tests within volume of the research certification of technologies for welding pipes of up to ∅ 1420 × 32 mm at production facilities of «Krasnodargazstroj».

In report of *Yu.B. Ezdakov* (CJSC «Uraltermosvar»), *V.I. Bespalov* and *D.G. Budrevich* (VNIIGAZ) a new welding equipment produced at CJSC «Uraltermosvar», its main characteristics, designation and possibilities of its application were presented. Joint project with VNIIGAZ and the POLYSOUDE company (France) for development of the complex for automatic orbital welding of position joints of pipes for construction and repair of MP was considered.

In a number of other reports also information was given about development of a new generation of inverters for MAW, TIG and MIG/MAG processes and feeding mechanisms and welding heads for orbital welding produced by WELDTEK Ltd., KEMPPI Ltd. and FSUE «Ryazan Instrument Plant».

INTRATUL Ltd. produces equipment for preparation works on pipelines of any thickness of walls of up to 3 m diameter. Proposed equipment and technologies increase quality of the welding-assembly works due to achievement of necessary conformity of geometric parameters of the units being welded with the normative documentation.

CJSC «Gazpriboravtomatikaservis» developed and produces the USMT-1M device for local demagnetization of the pipe joints. The device is air-tight, it consumes ~ 200 W power, can be easily installed into the zone where the works are performed, and by means of filling of the groove it is moved over the pipe butt by a welder. Mass of the device is 18 kg.

«Magnit Plus» Ltd. has developed and serially produces a compensation regulated constant magnet of 6 kg mass which allows compensating magnetic blow up to 2400 Gs.

In section B main direction of the welding production development were considered in construction of the MP systems from high-strength pipes of big diameter for long-distance transportation of gas.

In reports of V.I. Khomenko et al. (OJSC «Strojtransgaz») and *S.I. Kuchuk-Yatsenko* et al. (the E.O. Paton EWI) main problems of automatic methods of

welding of high-strength pipes of big diameter were considered. Suggestions were made to use high-productivity combined methods of welding with application for a thickened weld root of the resistance flash butt welding, and for the filling welds performed by automatic submerged arc welding, automatic gas-shielded welding, laser beam welding and semi-automatic welding using flux-cored wire.

A number of leading world producers of welding equipment and consumable materials, such as CRC-Evans AW (USA), Serimax (France), Saturnax, Autoweld Systems Ltd. (Great Britain), ESAB and a group of the ITS and the «Tekhnotron» Ltd. companies presented papers about their new developments in the field of equipment and technologies for automatic welding of position butt joints of pipes of up to 1420 mm diameter.

In report of *A.S. Tsiryuk* and *I.G. Samorodov* (CJSC «Baltijsky Steel Rolling Plant») it was informed about production at the enterprise of new seamless flux-cored wires and low-alloy solid wires for welding of pipe steels of the K65 strength class.

All together more than 65 papers were presented at the conference.

The conference demonstrated high interest of scientists and specialists in sharing on regular basis information on vital issues of welding in gas industry. At the same time one has to state that nowadays in construction of MP, as a rule, technologies, equipment, and consumable materials developed and produced abroad are used.

V.Ya. Kononenko
SE «Ekotekhnologiya» of the E.O. Paton EWI STC

SUBSCRIPTION
FOR «THE PATON WELDING JOURNAL»

If You are interested in making subscription directly via Editorial Board, fill, please, the coupon and send application by fax or e-mail.

The cost of annual subscription via Editorial Board is $324.

Telephones and faxes of Editorial Board of «The Paton Welding Journal»:

Tel.: (38044) 287 6302, 271 2403, 529 2623

Fax: (38044) 528 3484, 528 0486, 529 2623.

«The Paton Welding Journal» can be also subscribed worldwide from catalogues of subscription agency EBSCO.

SUBSCRIPTION COUPON
Address for journal delivery

Term of subscription since _____ **200** **till** _____ **200**
Name, initials _____
Affiliation _____
Position _____
Tel., Fax, E-mail _____

ADVERTISEMENT IN «THE PATON WELDING JOURNAL»
(DISTRIBUTED ALL OVER THE WORLD)

«AVTOMATICHESKAYA SVARKA»
RUSSIAN VERSION OF «THE PATON WELDING JOURNAL»
(DISTRIBUTED IN UKRAINE, RUSSIA AND OTHER CIS COUNTRIES)

External cover, fully-colored:
First page of cover (190×190 mm) – $700
Second page of cover (200×290 mm) – $550
Third page of cover (200×290 mm) – $500
Fourth page of cover (200×290 mm) – $600

Internal cover, fully-colored:
First page of cover (200×290 mm) – $400
Second page of cover (200×290 mm) – $400
Third page of cover (200×290 mm) – $400
Fourth page of cover (200×290 mm) – $400

Internal insert:
Fully-colored (200×290 mm) – $340
Fully-colored (double page A3) (400×290 mm) – $570
Fully-colored (200×145 mm) – $170

- Article in the form of advertising is 50 % of the cost of advertising area
- When the sum of advertising contracts exceeds $1000, a flexible system of discounts is envisaged

Technical requirement for the advertising materials:
- Size of journal after cutting is 200×290 mm
- In advertising layouts, the texts, logotypes and other elements should be located 5 mm from the module edge to prevent the loss of a part of information

All files in format IBM PC:
- Corell Draw, version up to 10.0
- Adobe Photoshop, version up to 7.0
- Quark, version up to 5.0
- Representations in format TIFF, color model CMYK, resolution 300 dpi
- Files should be added with a printed copy (makeups in WORD for are not accepted)